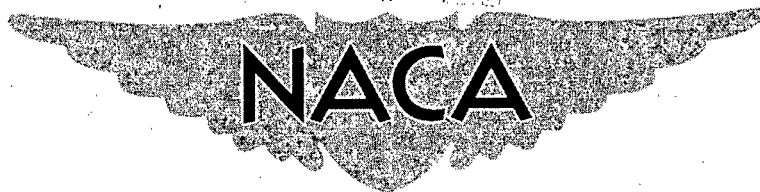


~~CONFIDENTIAL~~Copy  
RM L57K05

NACA RM L57K05



# RESEARCH MEMORANDUM

LONGITUDINAL STABILITY INVESTIGATION  
OF A VERTICAL-TAKE-OFF-AND-LANDING AIRPLANE  
CONFIGURATION WITH SIMULATED JET INTAKE AND EXHAUST  
AT MACH NUMBERS OF 1.61 AND 2.01

By Douglas R. Lord

Langley Aeronautical Laboratory  
Langley Field, Va.

**LIBRARY COPY**

JAN 30 1958

LANGLEY AERONAUTICAL LABORATORY  
LIBRARY, NACA  
LANGLEY FIELD, VIRGINIA

CLASSIFIED DOCUMENT

This material contains information affecting the National Defense of the United States within the meaning of the espionage laws, Title 18, U.S.C., Secs. 793 and 794, the transmission or revelation of which in any manner to an unauthorized person is prohibited by law.

## NATIONAL ADVISORY COMMITTEE FOR AERONAUTICS

WASHINGTON

January 30, 1958

~~CONFIDENTIAL~~



## NATIONAL ADVISORY COMMITTEE FOR AERONAUTICS

## RESEARCH MEMORANDUM

LONGITUDINAL STABILITY INVESTIGATION  
OF A VERTICAL-TAKE-OFF-AND-LANDING AIRPLANE  
CONFIGURATION WITH SIMULATED JET INTAKE AND EXHAUST  
AT MACH NUMBERS OF 1.61 AND 2.01

By Douglas R. Lord


## SUMMARY

An investigation has been made at Mach numbers of 1.61 and 2.01 and a Reynolds number of  $2.5 \times 10^6$ , based on the wing chord, of a semi-span model of a possible vertical-take-off-and-landing jet bomber configuration. The purpose of the investigation was to determine the effects of jet interference, horizontal-tail location, and canard controls on the longitudinal stability characteristics of the model. Tests were made for an angle-of-attack range from  $0^\circ$  to  $12^\circ$  and for a range of ratios of jet total pressure to stream static pressure from the jet-off condition to a maximum of 21.2.

In general, the jet-interference effects on longitudinal stability were of small magnitude except for a decrease in stability as the jet was first turned on for the high-tail configurations at a Mach number of 2.01. The horizontal tail located at the midpoint of the vertical tail caused severe pitch-up characteristics whereas the low horizontal-tail configuration exhibited generally favorable stability characteristics.

## INTRODUCTION

A coordinated program of research is under way at the Langley Laboratory on a possible vertical-take-off-and-landing jet bomber configuration which employs the tilt-wing concept for achieving its vertical-flight capabilities. The proposed aircraft would be capable of cruising at supersonic Mach numbers and therefore the side-by-side positioning of the six jet engines gives a plan-form area large enough that the required



wing area can be obtained by merely placing a fairing over the engines. Preliminary tests of two versions of the aircraft were conducted in the Langley 9-inch supersonic tunnel to determine whether practical lift-drag ratios could be obtained. These results were obtained without any attempt to simulate the jet flow and were reported in reference 1.

The purpose of the present report is to present the results of tests which were made in the Langley 4- by 4-foot supersonic pressure tunnel to determine the interference effects of the jet exhausts on the longitudinal stability of the aircraft. In addition, the effects of horizontal-tail size, location, and incidence, and the comparative effect of canard-type controls for longitudinal control will be presented.

The tests reported herein consisted of measuring the lift, drag, pitching moment, and rolling moment of the various configurations at Mach numbers of 1.61 and 2.01 at a Reynolds number of  $2.5 \times 10^6$ , based on the wing chord. The angle-of-attack range was from  $0^\circ$  to  $12^\circ$ , and the range of ratios of jet total pressure to stream static pressure was from the jet-off condition to maximums of 13.1 and 21.2 at Mach numbers of 1.61 and 2.01, respectively.

#### SYMBOLS

$C_L$	semispan model lift coefficient, $\frac{\text{Lift}}{qS}$
$C_D$	semispan model drag coefficient, $\frac{\text{Drag}}{qS}$
$C_m$	semispan model pitching-moment coefficient referred to 0.5c, $\frac{\text{Pitching moment}}{qSc}$
$C_{l,\text{gross}}$	semispan model rolling-moment coefficient, $\frac{\text{Rolling moment}}{2qSb}$
$C_l$	incremental rolling-moment coefficient
$C_{p,B}$	base pressure coefficient, $\frac{P_B - P}{q}$
$\frac{b}{2}$	wing semispan, 4.40 in.

$c$	wing chord, 8.18 in.
$p_{t,j}$	jet total pressure
$p_{t,j}/p$	ratio of jet total pressure to stream static pressure
$M$	stream Mach number
$p$	stream static pressure
$p_B$	base static pressure
$q$	stream dynamic pressure
$S$	semispan wing area, 36.0 sq in.
$S_H$	semispan horizontal-tail area
$\alpha$	model angle of attack
$\delta_c$	canard incidence
$\Delta$	prefix indicating increment in coefficient (horizontal tail on minus horizontal tail off or vertical tail on minus vertical tail off)
$i_t$	horizontal-tail incidence

## APPARATUS

### Wind Tunnel

This investigation was conducted in the Langley 4- by 4-foot supersonic pressure tunnel, which is a rectangular, closed-throat, single-return type of wind tunnel with provisions for the control of the pressure, temperature, and humidity of the enclosed air. Flexible nozzle walls were adjusted to give the desired test section Mach numbers of 1.61 and 2.01. During the tests, the dewpoint was kept below  $-20^{\circ}$  F at atmospheric pressure so that the effects of water condensation in the supersonic nozzle were negligible.



### Model

The basic model used in these tests consisted of a semispan wing-fuselage model with the nose and afterbody portions of the half fuselage removable. The removable portions of the fuselage consisted of the portions ahead of and behind the wing. Sketches of the model are shown in figure 1 and photographs of the model are presented in figure 2. Interchangeable fuselage noses were available with and without a canopy and with canard controls having incidences of  $-4^\circ$ ,  $-2^\circ$ ,  $0^\circ$ , and  $2^\circ$ . Fuselage afterbodies were available without any tail, with a vertical tail only, and with the vertical tail and five different horizontal tails. In general, the configuration used was a composite of the two configurations tested in reference 1. The model had a simulated inlet and exit to duplicate the external flow field of the proposed configuration. The inlet air was ducted out of the model to a vacuum pump and the exhaust air was brought in through a common plenum to exhaust through the three simulated engine exhaust nozzles.

Fuselage.- The basic fuselage was 30.00 inches in length and was developed from a circular-arc body of revolution having a fineness ratio of 13.8. Back of the midpoint, the fuselage was sheared upward so that the top meridian line of the fuselage was a straight line. The fuselage was constructed of stainless steel.

Wing.- The wing had a rectangular plan form of aspect ratio 1.08 and was located at the midpoint of the fuselage length flush with the top of the fuselage. The leading edge of the wing was drooped so as to fair over the two-dimensional inlet as shown in figures 1 and 2. The trailing edge of the wing was boattailed a minimum of  $5^\circ$  over the simulated jet-exhaust nozzles and a maximum of  $8^\circ$  between the jet-exhaust nozzles. Clearance was provided around the inlet and exhaust plenum chambers and the exhaust nozzles to separate them from the wing skin. (See fig. 1(b).) At the base of the wing, the wing skin filled in the spaces between the jet exhausts and was instrumented with four base-pressure orifices. The base of the wing between the inboard exhaust and the fuselage was left open. The wing skin was constructed of stainless steel and was machined integral with the center portion of the fuselage.

Inlet.- When the inlet for this model was designed, it was desirable to simulate the external aerodynamic shape of the variable geometry inlet which would be used on the aircraft at Mach numbers from 0 to 2.5. Because of the complexity of such a design and the small size of the model, it was decided to duplicate the external geometry of the proposed inlet as it would be set for  $M = 2.2$ . This Mach number is a compromise so that the model could be tested at  $M = 2.0$  in the present tests and at  $M = 2.5$ , if desired, at a later date. The inlet plenum was constructed of steel and was ducted to a 3-inch vacuum line.

Jet exit.- The exhausts of the three jet engines in the wing semi-span were simulated by cold air exhausting from the three circular nozzles shown in figures 1 and 2. The nozzle contours were chosen to duplicate the jet boundaries of ejector-type nozzles for the required jet engine operating at a stream Mach number of 2.0 with half-afterburning. In order that later tests could be made at  $M = 2.5$  with full afterburning, however, the wing-skin fairing around the nozzles was made large enough to accommodate the required nozzles. This condition, in turn, meant that fairly large regions of base area existed between the jet exits and the wing skin at the base. These regions were filled in by a solid annulus around the nozzle exits, and four base-pressure orifices were installed around the perimeter of each exit as shown in figure 1(b). The nozzles were made of brass and were press fitted into the steel exhaust plenum which, in turn, was ducted to a 2-inch high-pressure air line. A 13/64-inch-diameter hole was drilled in the plenum chamber just inboard of the most inboard nozzle to simulate the disposal of secondary air at the wing trailing edge along the fuselage.

Canopy.- The canopy was arbitrarily designed but was approximately the same as that used in reference 1. It was constructed of molded plastic.

Tails.- The vertical half-tail had an aspect ratio of 1.41 and a wedge-slab section of 7-percent half-thickness. The leading-edge half-wedge angle was  $10^\circ$  normal to the leading edge. The large thickness of the vertical tail was required for structural reasons but was not considered to be objectionable since at this station the vertical tail would be completely submerged in the boundary layer on the bypass plate.

The horizontal tails had 5-percent-thick circular-arc sections, the four large tails each having an aspect ratio of 2.86 and the small tail having an aspect ratio of 1.71. Three of the large tails had  $0^\circ$  incidence and were located at the bottom, middle, and top of the vertical tail. The fourth large tail had  $-3^\circ$  incidence and was located at the top of the vertical tail. The center line of rotation of the tails was at the trailing edge. The small tail had  $0^\circ$  incidence and was also located at the top of the vertical tail. All the horizontal tails and the vertical tail were constructed of heat-treated steel.

Canard controls.- The four canard controls were identical to the small horizontal tail and had an aspect ratio of 1.71 and 5-percent-thick circular-arc sections. The center line of rotation of the canard controls was at the midpoint of the root chord. The canard controls were constructed of stainless steel.

### Model Mounting

The semispan model was mounted from a four-component strain-gage balance located in the turntable of a boundary-layer bypass plate which, in turn, was located  $10\frac{3}{4}$  inches from the tunnel side wall. (See fig. 2(c).) Pressure and vacuum ducts to the exhaust and inlet plenum chambers passed through a hole in the center of the balance. The ducts and plenum chambers were not attached to the balance. The model and wing skin therefore were free to float around the inlet scoop and exhaust nozzles. The minimum clearance was 0.020 inch (see fig. 1(b)) and fouling was avoided by designing the balance with minimum deflections. An electrical system for indicating fouling was incorporated in the model.

### TESTS

#### Preliminary Jet Calibration

Before the model was installed in the tunnel, bench tests were made of the exhaust plenum and jet-exhaust nozzles. These tests consisted of total- and static-pressure surveys at the jet exits to ascertain whether the flow was uniform from the three exits. As a result of these tests, 1/32-inch-thick guide vanes were inserted in the exhaust plenum to improve the exit flow distributions. When the model was mounted in the tunnel, surveys were again made with and without the tunnel air flow. From these tests it was found that the flow from the three nozzles was almost identical, with an exit Mach number of 2.0.

#### Force Tests

The lift, drag, pitching moment, and rolling moment on fourteen configurations of the semispan model (listed in table I) were measured by the four-component strain-gage balance. The model angle of attack was changed by rotating the turntable in which the balance was located and the angle of attack was measured by a vernier located outside of the tunnel.

Throughout most of the tests, the valve in the 3-inch vacuum line was wide open to ensure that the inlet was started. Since the internal operation of the inlet had no significance in these tests, the starting of the inlet assured that the external-shock formations on the inlet would be approximately correct. The model and bypass plate were painted white for visual observation of a shadowgraph image of the two-dimensional-inlet shock formation. A few test points were made with the valve on the

vacuum line closed to examine the force and moment changes due to not simulating the inlet.

A valve in the 2-inch high-pressure air line was used to control the pressure in the exhaust plenum chamber from a minimum equal to the average base pressure with the valve closed to a maximum of 40 lb/sq in. abs.

Although this model was designed to be tested at  $M = 2.01$ , tests were also made at  $M = 1.61$ . Because of the fixed geometry of the exit and the inlet, neither the exit nor the inlet simulation is ideal for this aircraft at the lower Mach number; however, the results are considered to be of interest from the standpoint of the basic jet-interference research problem.

The tunnel stagnation pressure was set at 15.0 and 13.0 lb/sq in. abs. at the test Mach numbers of 2.01 and 1.61, respectively, corresponding to a Reynolds number of  $2.5 \times 10^6$ , based on the wing chord. The tests were made with natural transition; however, the boundary layer over the model is believed to be primarily turbulent because of the small effect which was found to be due to fixing transition in the lower Reynolds number tests of reference 1. The model angle-of-attack range was from  $0^\circ$  to  $12^\circ$  in increments of  $3^\circ$ .

#### PRECISION

The mean Mach numbers in the region occupied by the model were estimated from calibration to be 1.61 and 2.01 with local variations smaller than  $\pm 0.02$ . There was no evidence of significant flow angularity. The estimated accuracy of the balance measurements and other pertinent quantities is as follows:

$\alpha$ , deg . . . . .	$\pm 0.05$
$C_L$ . . . . .	$\pm 0.005$
$C_D$ . . . . .	$\pm 0.001$
$C_m$ . . . . .	$\pm 0.001$
$C_{l, \text{gross}}$ . . . . .	$\pm 0.001$
$C_{p, B}$ . . . . .	$\pm 0.01$
$p_{t, j}/p$ . . . . .	$\pm 0.1$

## RESULTS AND DISCUSSION

## Presentation of Results

The four-component balance measurements and base-pressure measurements are presented in figures 3 to 17 in coefficient form as follows:

	Figure
Stability and drag . . . . .	3 and 4
Effect of jet pressure on -	
$C_L$ . . . . .	5
$C_D$ . . . . .	6
$C_m$ . . . . .	7
$C_{l, gross}$ . . . . .	8
Increments due to -	
Horizontal tail . . . . .	9 and 10
Vertical tail . . . . .	11
Comparison of canard controls and tails . . . . .	12
Canard-control effectiveness . . . . .	13
Tail effectiveness . . . . .	14
Effect of tail size . . . . .	15
Effect of inlet simulation . . . . .	16
Base-pressure variations . . . . .	17

## Basic Coefficients

The basic curves of the variation of semispan model angle of attack, pitching-moment coefficient, rolling-moment coefficient, and drag coefficient with lift coefficient are presented in figures 3 and 4. Curves are shown for jet-off, maximum jet-pressure ratio, and an intermediate jet-pressure ratio for each of the 14 test configurations at  $M = 2.01$  in figure 3 and for the 12 configurations tested at  $M = 1.61$  in figure 4. (Two of the canard configurations were not tested at  $M = 1.61$ .)

In general, the variations of angle of attack and rolling-moment coefficient with lift coefficient for all the configurations are linear at all jet pressures and at both Mach numbers. The variations in drag coefficient show the minimum drag occurring near zero lift coefficient and the curves for the various jet pressures are very similar. Because of the difficulty in simulating the flow through jet engines by the method used herein, certain forces are imposed on the model by the internal flow at the inlet and by the air leaking around the plenum chambers. An attempt was made to find correction factors for these effects which primarily affect the drag but, because of the numerous assumptions and

simplifications required, they are not included herein. These correction factors would undoubtedly have a large effect on the gross-drag measurements; however, the incremental drag values due to jet or tail changes may be assumed to be approximately correct.

The only basic curves (figs. 3 and 4) which exhibit any unusual trends are those of the pitching-moment coefficient with lift coefficient which are very nonlinear for the midtail and high-tail configurations (figs. 3(d), 3(e), 3(f), 3(g), 3(n), 4(d), 4(e), 4(f), 4(g), and 4(l)). The midtail configuration shows strong pitch-up above a lift coefficient of about 0.3, particularly at  $M = 1.61$ . The high-tail configurations tend to pitch up to a lesser degree at both Mach numbers; however, at  $M = 2.01$  increasing the jet pressure causes a decrease in stability and an increase in the linearity of the pitching-moment curves. The pitching-moment curves are approximately linear for the canard-control, tail-off, and low-tail configurations. The pitching-moment variations for the canard configurations are very unstable as would be expected for this model because it was not designed to be canard controlled. The tail-off configurations are unstable but are effectively stabilized by the addition of the low tail.

#### Effect of Jet Pressure

In the previous section, it was shown that the only configurations which exhibited any change in stability due to jet pressure were the high-tail configurations. Cross plots are therefore presented of the variation of lift coefficient, drag coefficient, pitching-moment coefficient, and rolling-moment coefficient with jet-pressure ratio in figures 5, 6, 7, and 8, respectively, for the high-tail configurations. Curves are presented therein for each of the four test configurations at angles of attack of  $0^\circ$ ,  $6^\circ$ , and  $12^\circ$ . In general, the curves of lift coefficient and rolling-moment coefficient show little, if any, change due to varying the jet pressure. The drag coefficient gradually decreases as the jet pressure is increased. This change in drag is similar for all the configurations and must therefore be caused by the effects of the jet on the wing or fuselage. The decrease in drag is in the direction that would be expected from the effect of the increased jet pressures acting on the negative slopes of the fuselage afterbody and wing base.

As was shown previously, the primary effect of jet interference was on the pitching-moment characteristics of the high-tail configurations at  $M = 2.01$ . In figure 7, the curves for the high-tail configurations at  $M = 2.01$  and  $\alpha = 0^\circ$  show large negative increases in pitching moment as the jet is first turned on. In an effort to understand this behavior, attempts were made to construct the shock pattern behind the wing with and without jet flow by using the simplifying assumption of a two-dimensional wing trailing edge and jet exit and applying the methods

described in references 2 and 3. The indications were that, at angles of attack, or with the jet on at  $\alpha = 0^\circ$  and  $M = 2.01$ , or for all conditions at  $M = 1.61$ , the trailing-edge shock is ahead of the high tails. For the no-flow condition at  $\alpha = 0^\circ$  and  $M = 2.01$ , however, the trailing-edge shock probably is impinging on the lower surface of the high tail. Then, as the jet is turned on, the movement of the shock forward on the high horizontal tail causes a greater portion of the tail to operate in a region of greater upwash and therefore produces a negative increment in pitching moment. At all other conditions of Mach number, angle of attack, and jet pressure, there is a general trend for a gradual positive increase in pitching moment with jet pressure.

#### Effect of the Tail

The incremental coefficients due to the addition of the various horizontal tails are presented at  $M = 2.01$  in figure 9 and at  $M = 1.61$  in figure 10 for jet off, maximum jet-pressure ratio, and an intermediate jet-pressure ratio. The lift, drag, and rolling-moment coefficient increments are roughly the same for the five horizontal-tail configurations, the large high tail at  $0^\circ$  incidence generally producing the largest increments. The changes in incremental pitching-moment coefficient with  $\alpha$  produced by the horizontal tails are much larger than the changes in increments of the other coefficients, as would be expected, because of the location of the horizontal tails with respect to the pitch center. As the tail height is increased, the slope of the low angle-of-attack pitching-moment contribution is increased. Giving the large high tail  $3^\circ$  of negative incidence merely shifts the pitching-moment curve in the positive direction at any jet-pressure setting. Decreasing the size of the horizontal tail reduces the pitching-moment-curve slope and increases the pitch-up tendency.

The incremental coefficients due to the addition of the vertical tail alone are presented in figure 11. The vertical tail caused only small changes in lift, pitching-moment, and rolling-moment coefficients and increments in drag coefficient from 0.006 to 0.009. In all cases the changes due to adding the vertical tail were relatively constant with changes in angle of attack.

#### Effect of the Canard

For effective use of a canard-type control, the basic wing-body must exhibit sufficient longitudinal stability to overcome the destabilizing effect of the canard. In the case of the present model at the cruising conditions investigated herein, this condition would require rearward movement of the wing, which in turn would require auxiliary control devices such as swiveling nozzles and nose reaction

jets for the vertical-take-off or landing conditions. Use of canard controls would, however, eliminate some of the problems inherent in placing a horizontal tail in the wake of the jet engines. In spite of the poor canard capabilities of the wing-body combination used in these tests, canard controls were tested in order to compare the pitching moments produced by a canard control with those produced by similar horizontal tails having the same moment arms but operating in a flow field downstream of a thick wing.

Curves of the incremental pitching-moment coefficient due to the canard control as compared with those for two of the horizontal tails at  $0^\circ$  incidence with angle of attack are presented in figure 12. At both test Mach numbers the slope of the pitching-moment-coefficient increments with angle of attack is about the same for the canard control as for the large low horizontal tail but of opposite sign. The high horizontal tail having the same geometry as the canard control produces a lower pitching-moment-curve slope and is considerably changed by jet pressure at Mach number 2.01.

Since there seems to be essentially no effect of jet pressure on the pitching moment produced by the canard control, the variation of model pitching-moment coefficient with canard deflection is presented in figure 13 for the jet-off condition. Indications are that the variations with canard deflection are linear.

It would be desirable to compare the pitching-moment coefficient due to canard deflection with the pitching-moment coefficient due to horizontal-tail inclination for a tail of equal size. Unfortunately, the small horizontal tail was not tested at incidences other than  $0^\circ$ . If it is assumed that the variation of the pitching-moment coefficient with tail incidence for the large tail in the jet-off condition is linear, as shown in figure 14, the pitching-moment coefficient per degree inclination is approximately  $-0.013$  at  $M = 2.01$  and  $-0.028$  at  $M = 1.61$ . Note the large change in slope with Mach number as compared with the corresponding change in slope for the canard (fig. 13) from  $0.010$  to  $0.012$ . Although the effectiveness with inclination of the large high tail is greater than that for the canard control, it appears that above a Mach number of 2 this advantage would soon be reversed.

Since a linear slope has been assumed in the curves of figure 14, it is now possible to estimate the pitching-moment effectiveness with incidence of the small high horizontal tail if the variation of pitching-moment coefficient with tail size is linear. That this is not the case can be seen in the curves of figure 15. Any further attempts at estimating the effectiveness of the small tail with incidence would be of questionable value.



### Effect of the Inlet

When the model for these tests was designed, some questions were raised as to the importance of the inlet simulation. In order to show the effect of not simulating the inlet flow, comparisons are made in figure 16 of the variation of the basic coefficients with jet-pressure ratio at three angles of attack for the large high-tail configuration at  $0^\circ$  incidence with and without the vacuum line open. In general, the differences are small with respect to the lift coefficient and rolling-moment coefficient. The changes in drag coefficient and pitching-moment coefficient are very large and decrease with increasing angle of attack. It therefore appears that simulation of the inlet is necessary insofar as duplicating the external flow field in order to obtain satisfactory data for performance estimates.

### Base-Pressure Measurements

The 16 base-pressure orifices have been divided into four groups designated by the letters A, B, C, and D. (See fig. 1(b).) In general, the pressures measured at all the orifices of a given letter were very nearly identical. For this reason, the variations of the average base pressure coefficient with jet-pressure ratio and angle of attack for the four groups of orifices are presented in figure 17. There was no effect on the base pressures of changing the configuration; thus, the curves shown are for a representative configuration.

The curves of figure 17(a) show that at  $M = 1.61$  and  $\alpha = 0^\circ$ , as the jet pressure was increased, the base pressures first decreased and then increased. The amount of this initial decrease in pressure was reduced by increasing either the Mach number or the angle of attack. The curves are dotted in the region between the jet-off condition and the lowest jet-pressure setting because previous tests (for example, ref. 4) have shown that, for very low jet-pressure ratios, the base pressure is increased above the pressure measured in the jet-off condition.

In general, the curves of figure 17(a) at an angle of attack of  $0^\circ$  exhibit identical variations. At an angle of attack of  $12^\circ$ , however, there is a very definite trend for the base pressures at the outboard orifices to be considerably lower than those at the inboard orifices. Attempts were again made to use the method shown in reference 2 for predicting the base pressures. The agreement between the predictions and experiment was very poor, as would be expected from the negligible changes in base pressures shown in figure 17(a) for the various vertical locations of the orifices.

The variations in base pressure coefficients with angle of attack, presented in figure 17(b), show that for the jet-off condition the base

pressures gradually decrease with increasing angle of attack and there is little effect of orifice location. At the maximum jet-pressure setting, the base pressures are more nearly constant with angle of attack except for the outboard orifices which exhibit a large decrease in base pressure with angle of attack.

### CONCLUSIONS

An investigation has been made at Mach numbers of 1.61 and 2.01 of a semispan model of a possible vertical-take-off-and-landing jet bomber configuration. The results of the tests indicate the following conclusions regarding the effects of jet interference, horizontal-tail position, and canard control effectiveness on the longitudinal stability characteristics of the model:

1. The jet-interference effects on longitudinal stability were generally of small magnitude except for a decrease in stability as the jet was first turned on for the high-tail configurations at a Mach number of 2.01.

2. The horizontal tail located at the midpoint of the vertical tail caused severe pitch-up characteristics.

3. The low horizontal-tail configuration exhibited generally favorable stability characteristics at all test conditions.

4. Although the proposed configuration was not intended to be canard controlled, the canard control produced as much pitching moment due to angle of attack as did a much larger horizontal tail. Indications are that at Mach numbers greater than 2.0 the pitching moment due to control incidence would also be greater for the canard control than for the larger horizontal tail.

Langley Aeronautical Laboratory,  
National Advisory Committee for Aeronautics,  
Langley Field, Va., October 21, 1957.

## REFERENCES

1. Jones, Robert A., and Rainey, Robert W.: Wind-Tunnel Investigation of Two Vertical-Take-Off-and-Landing Jet Bomber Airplanes at Mach Numbers of 1.94 and 2.40. NACA RM L56H22a, 1956.
2. Coletti, Donald E.: Measurements and Predictions of Flow Conditions on a Two-Dimensional Base Separating a Mach Number 3.36 Jet and a Mach Number 1.55 Outer Stream. NACA RM L54C08, 1954.
3. Love, Eugene S.: Base Pressure at Supersonic Speeds on Two-Dimensional Airfoils and on Bodies of Revolution With and Without Fins Having Turbulent Boundary Layers. NACA TN 3819, 1957. (Supersedes NACA RM L53C02.)
4. Fuller, L., and Reid, J.: Experiments on Two Dimensional Base Flow at  $M = 2.4$ . Rep. No. Aero. 2569, British R.A.E., Feb. 1956.

TABLE I

## CONFIGURATIONS TESTED

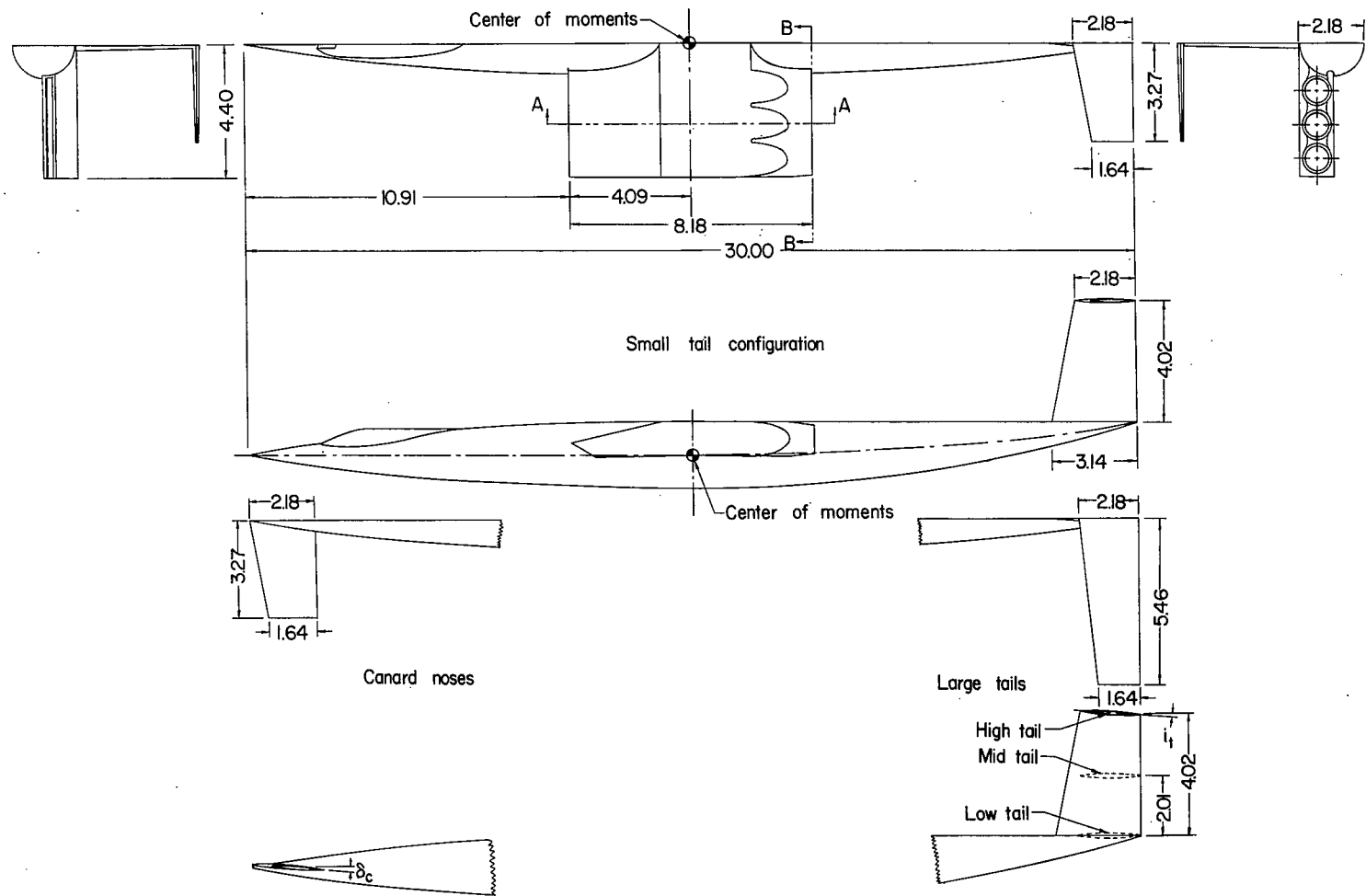
Configuration designation	Canard control (a)	Canopy (b)	Horizontal tail (c)	Vertical tail (d)
0100	None	On	None	Off
0101	None	On	None	On
0111	None	On	Low, 0° incidence	On
0121	None	On	Middle, 0° incidence	On
0131	None	On	High, large, 0° incidence	On
0141	None	On	High, large, -3° incidence	On
0151	None	On	High, small, 0° incidence	On
4001	-4°	Off	None	On
3001	-2°	Off	None	On
2001	0°	Off	None	On
1001	2°	Off	None	On
0001	None	Off	None	On
0011	None	Off	Low, 0° incidence	On
0051	None	Off	High, small, 0° incidence	On

(a) Condition of canard control indicated by first digit of configuration designation.

(b) Presence of canopy indicated by second digit of configuration designation.

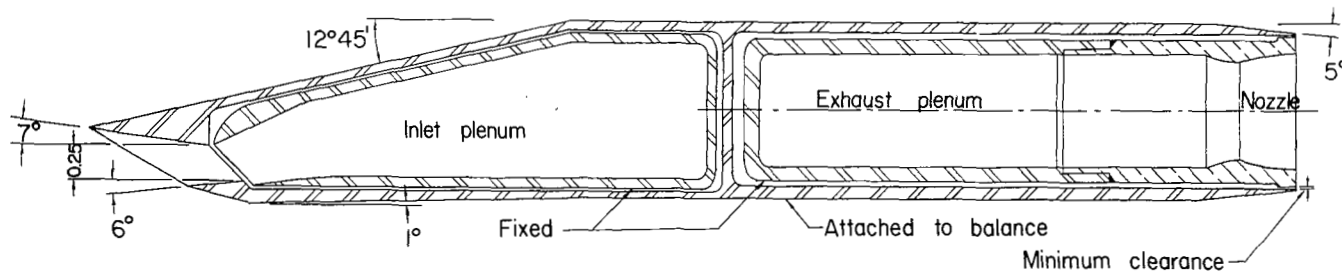
(c) Type of horizontal tail indicated by third digit of configuration designation.

(d) Presence of vertical tail indicated by fourth digit of configuration designation.

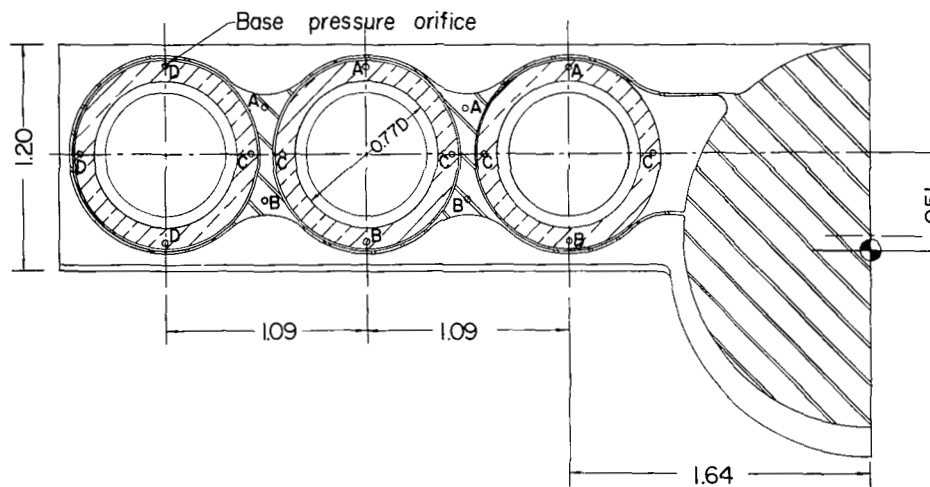


(a) General configurations.

Figure 1.- Sketches of the model configurations. All dimensions are in inches.



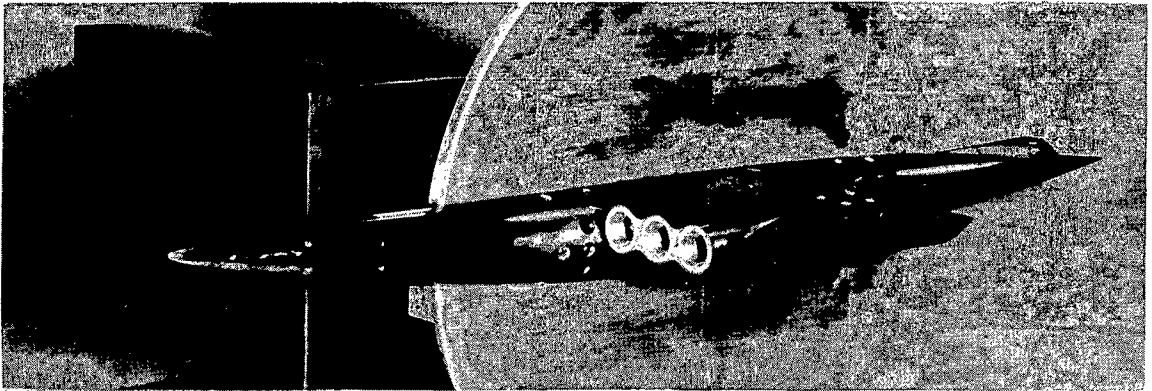
Section A-A (from figure 1-(a))



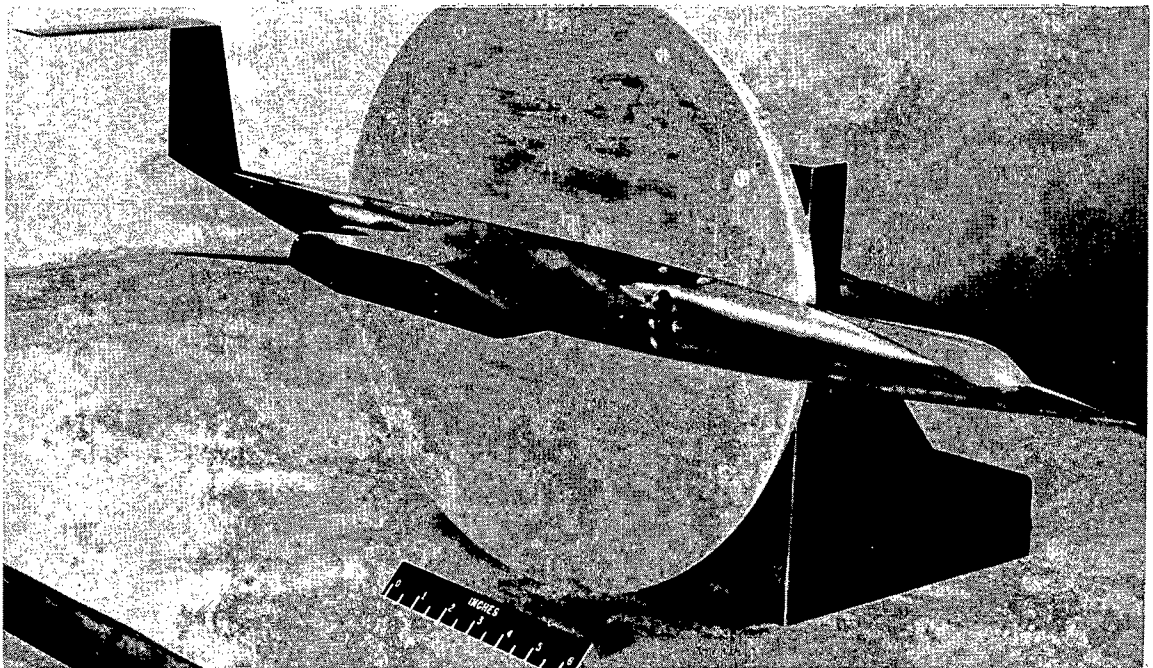
Section B-B (from figure 1-(a))

(b) Wing cross-section and trailing-edge details.

Figure 1.- Concluded.

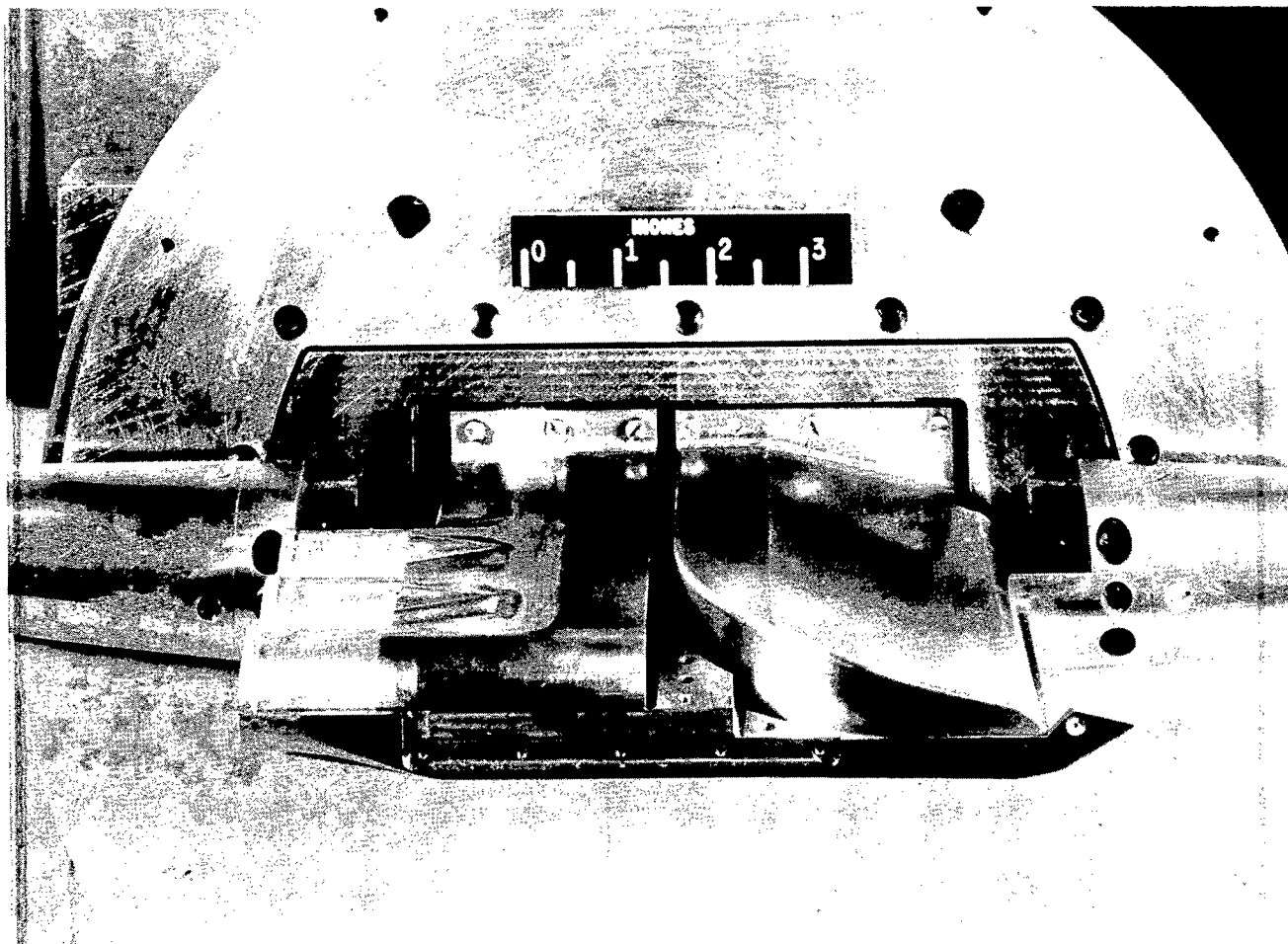


L-57-388



(a) Bench setup of the large high-tail configuration. L-57-387

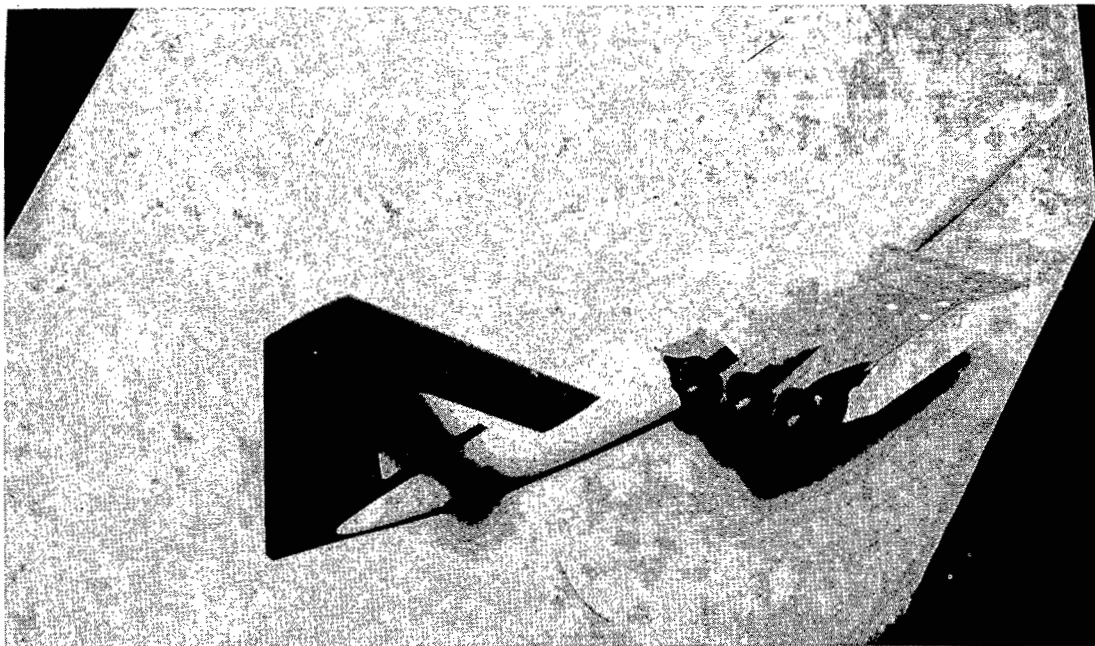
Figure 2.- Photographs of the model.



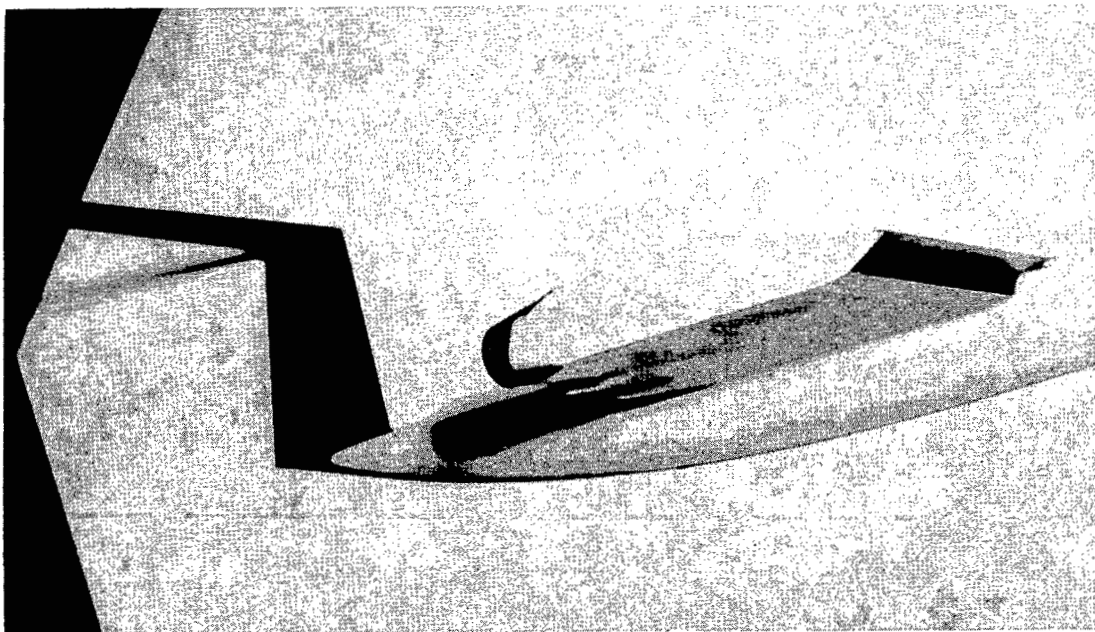
(b) Closeup of inlet- and exit-plenum chambers with wing upper surface removed. L-57-389

Figure 2.- Continued.





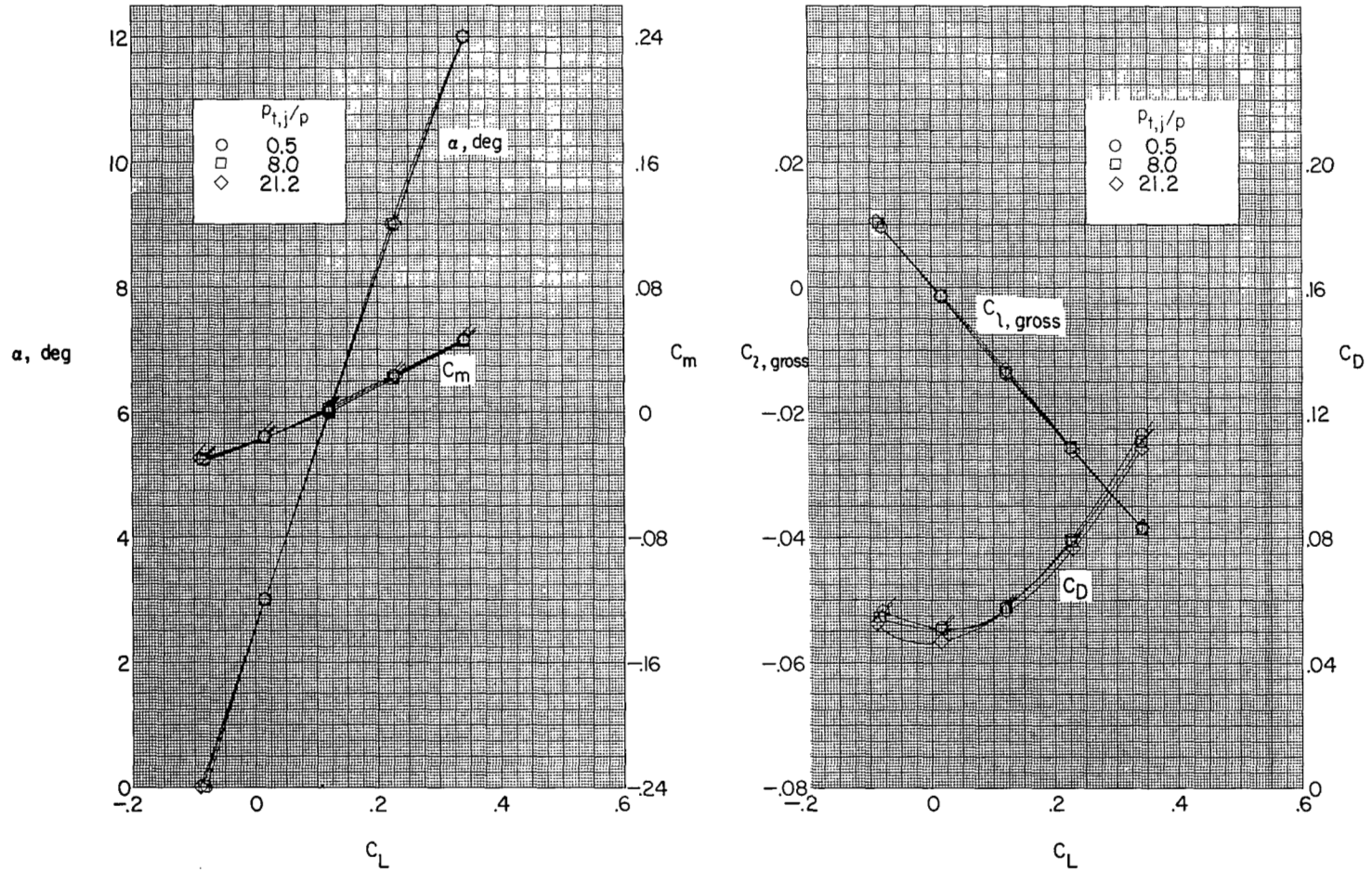
L-57-965



L-57-966

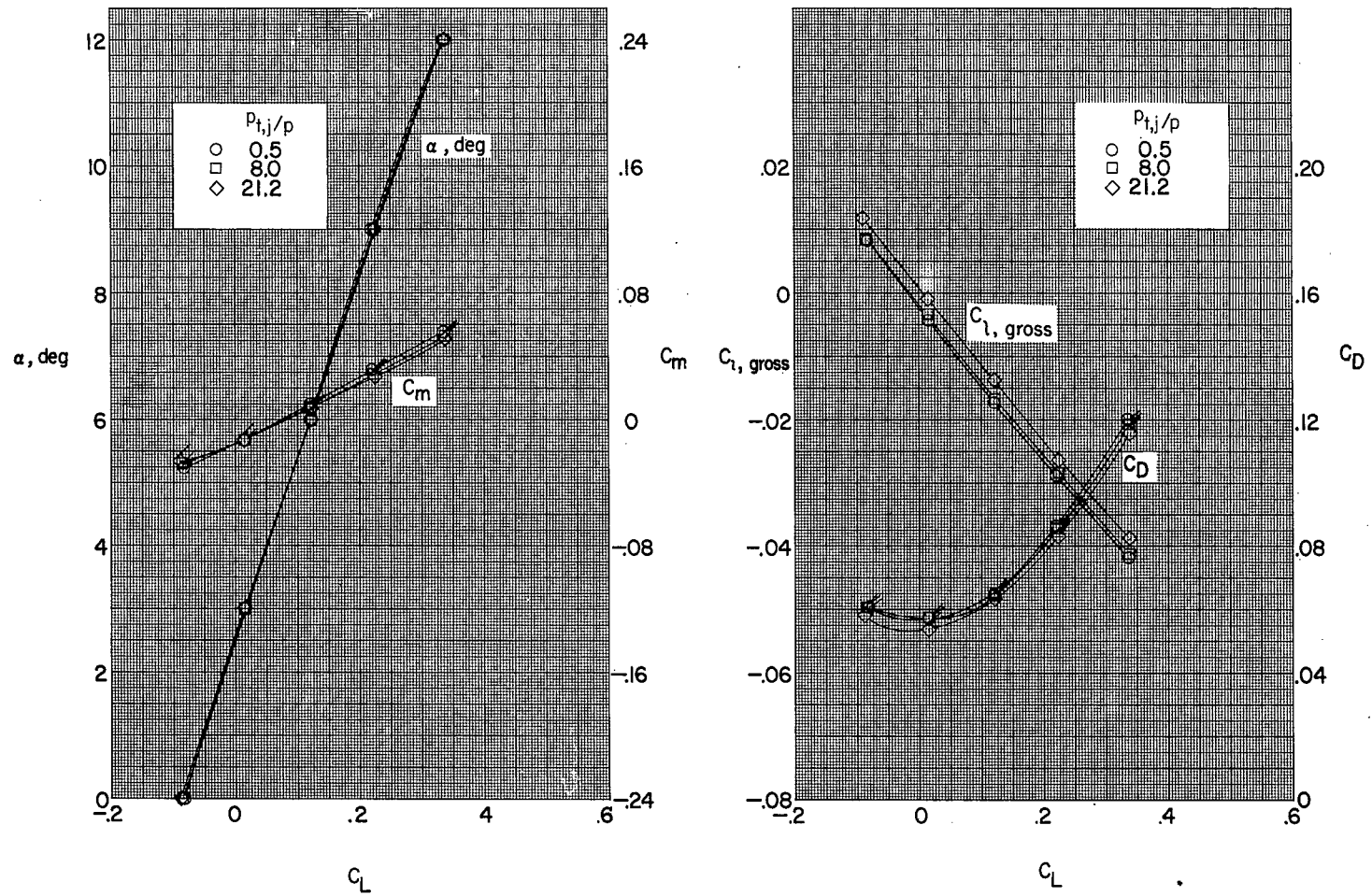
(c) Large high-tail configuration mounted on bypass plate for testing.

Figure 2.- Concluded.



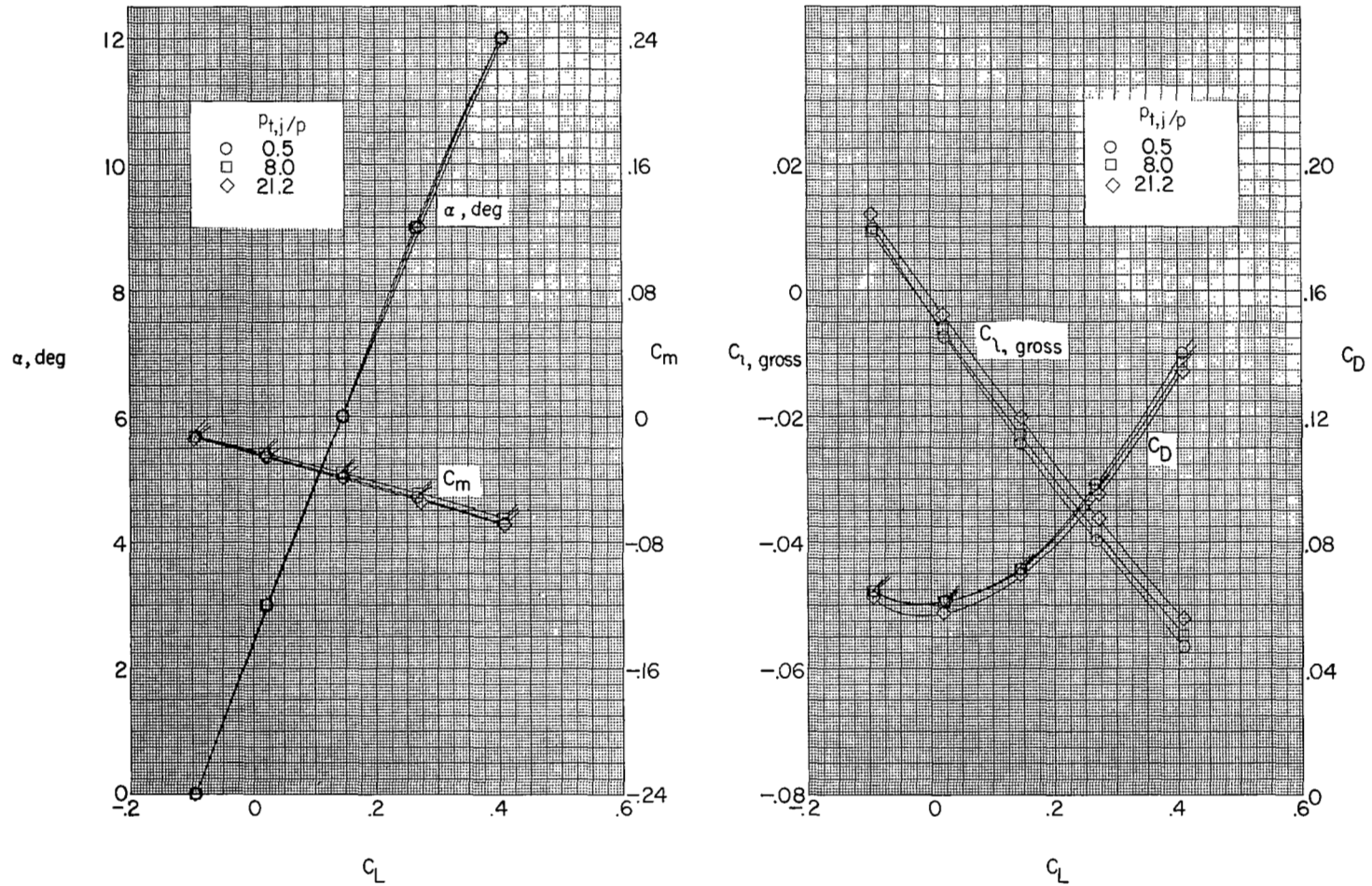
(a) Configuration 0100; no horizontal tail; no vertical tail.

Figure 3.- Basic variations of the four-component balance measurements for the 14 configurations tested at  $M = 2.01$ . Flagged symbols indicate pitching-moment or drag coefficient.



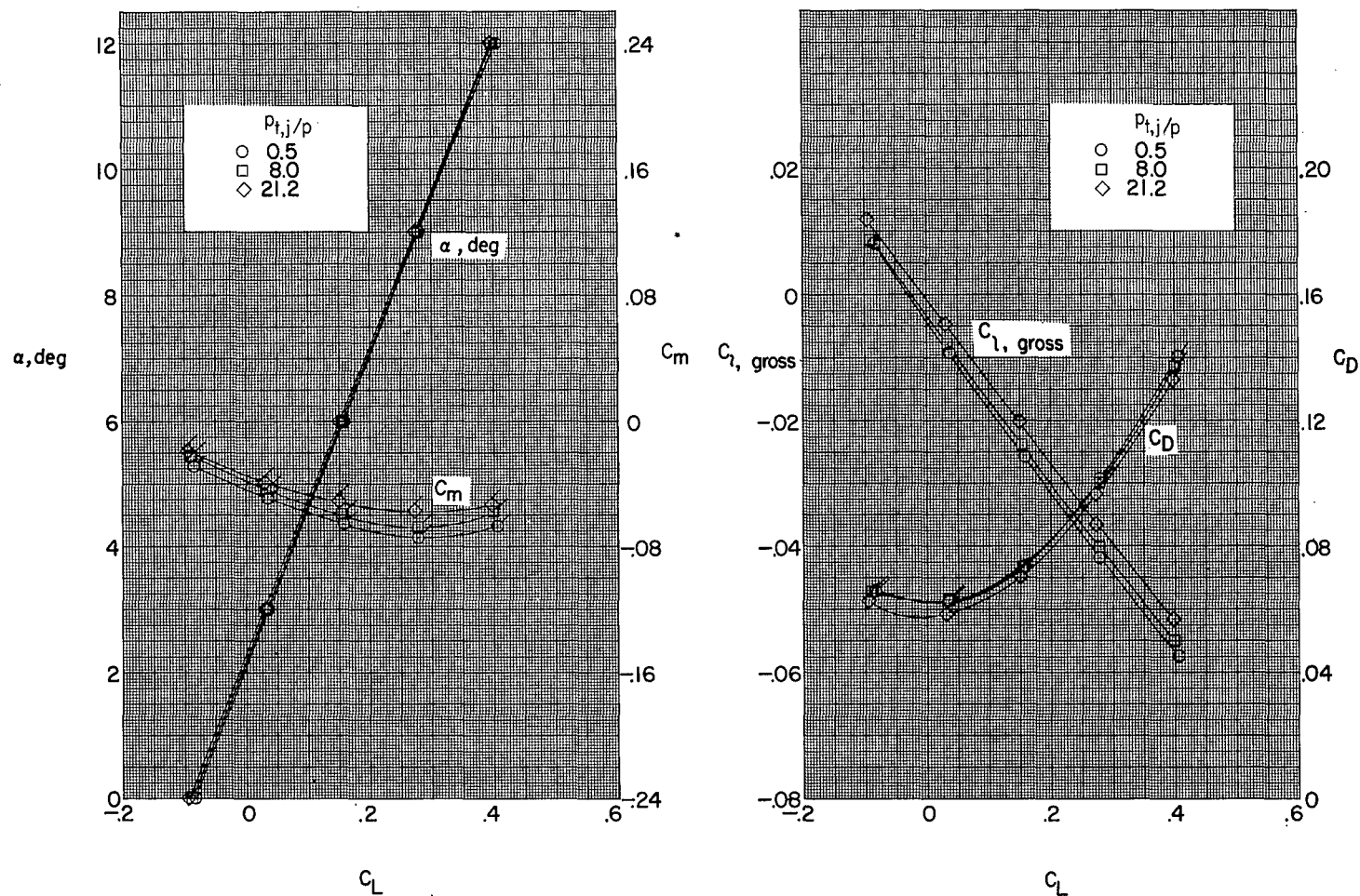
(b) Configuration 0101; no horizontal tail.

Figure 3.- Continued.



(c) Configuration 0111; low tail.

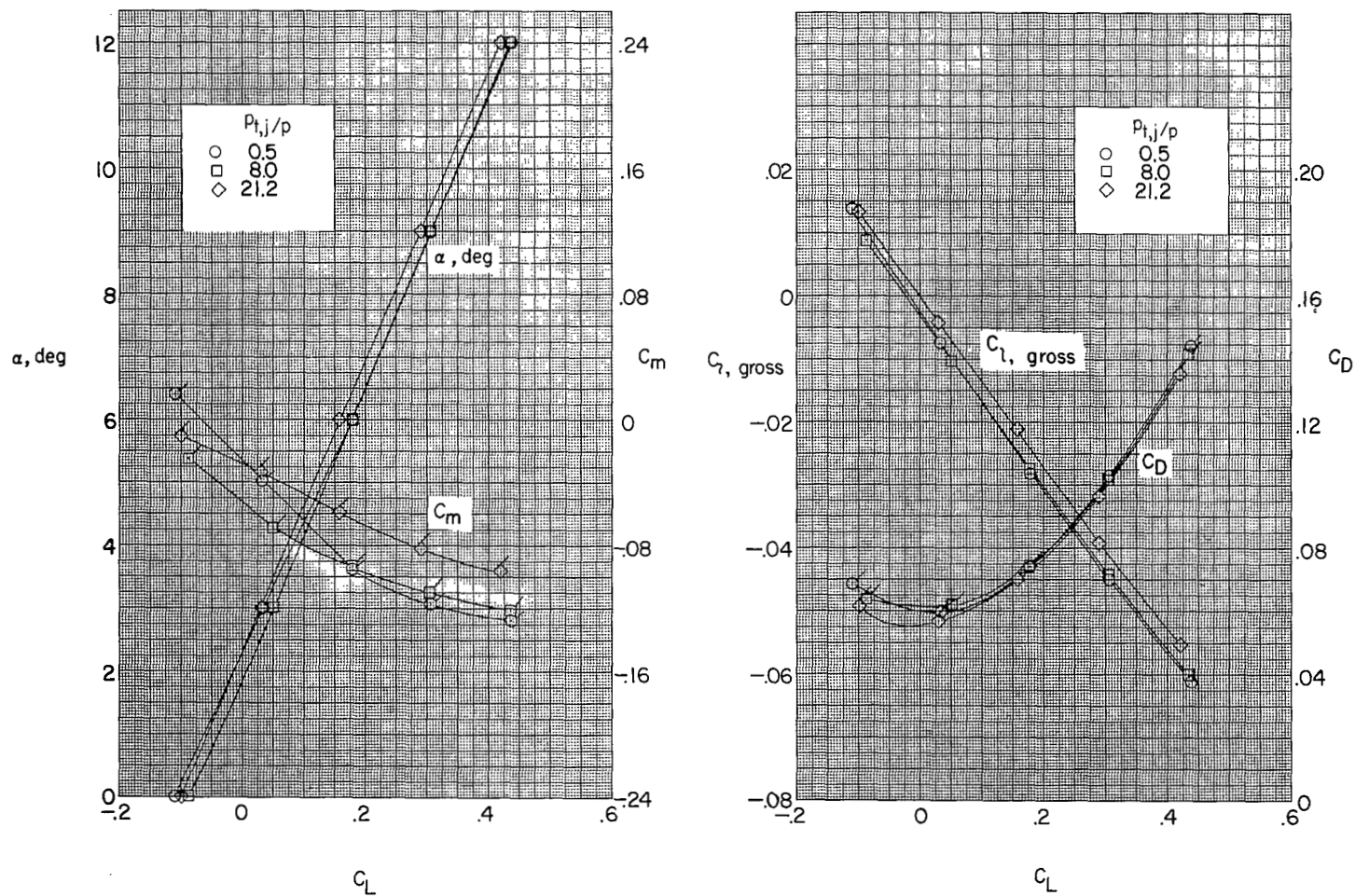
Figure 3.- Continued.



(d) Configuration 0121; midtail.

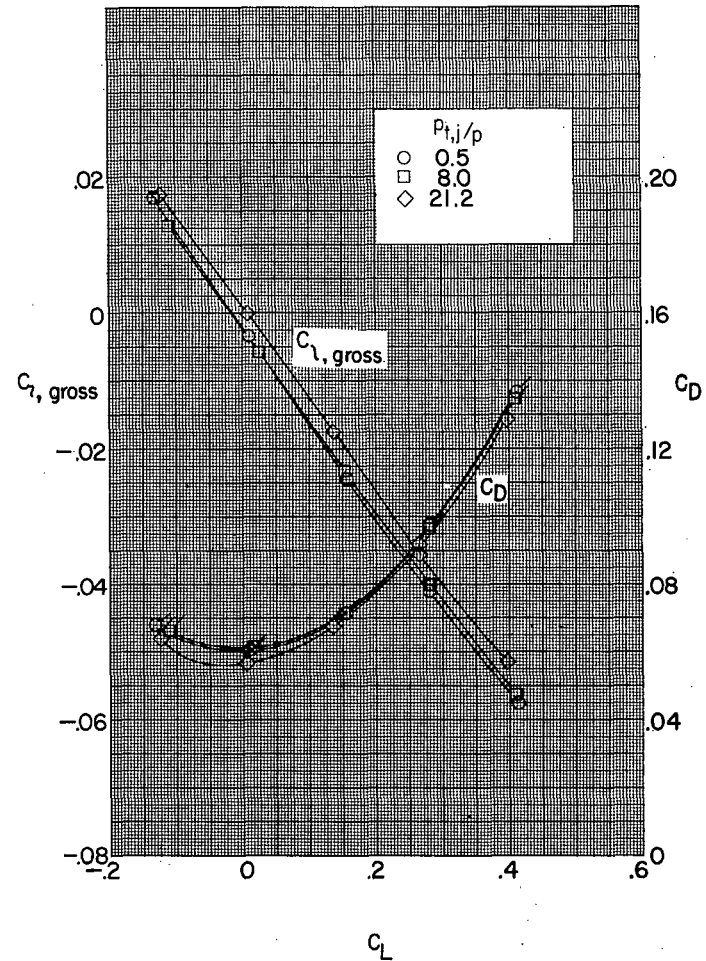
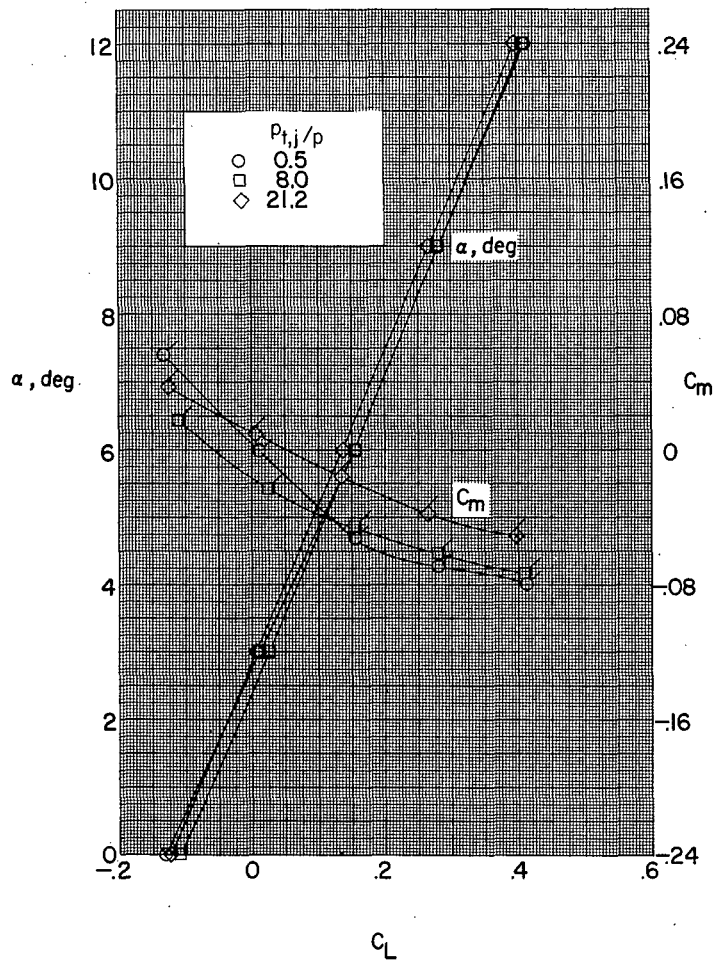
Figure 3.- Continued.





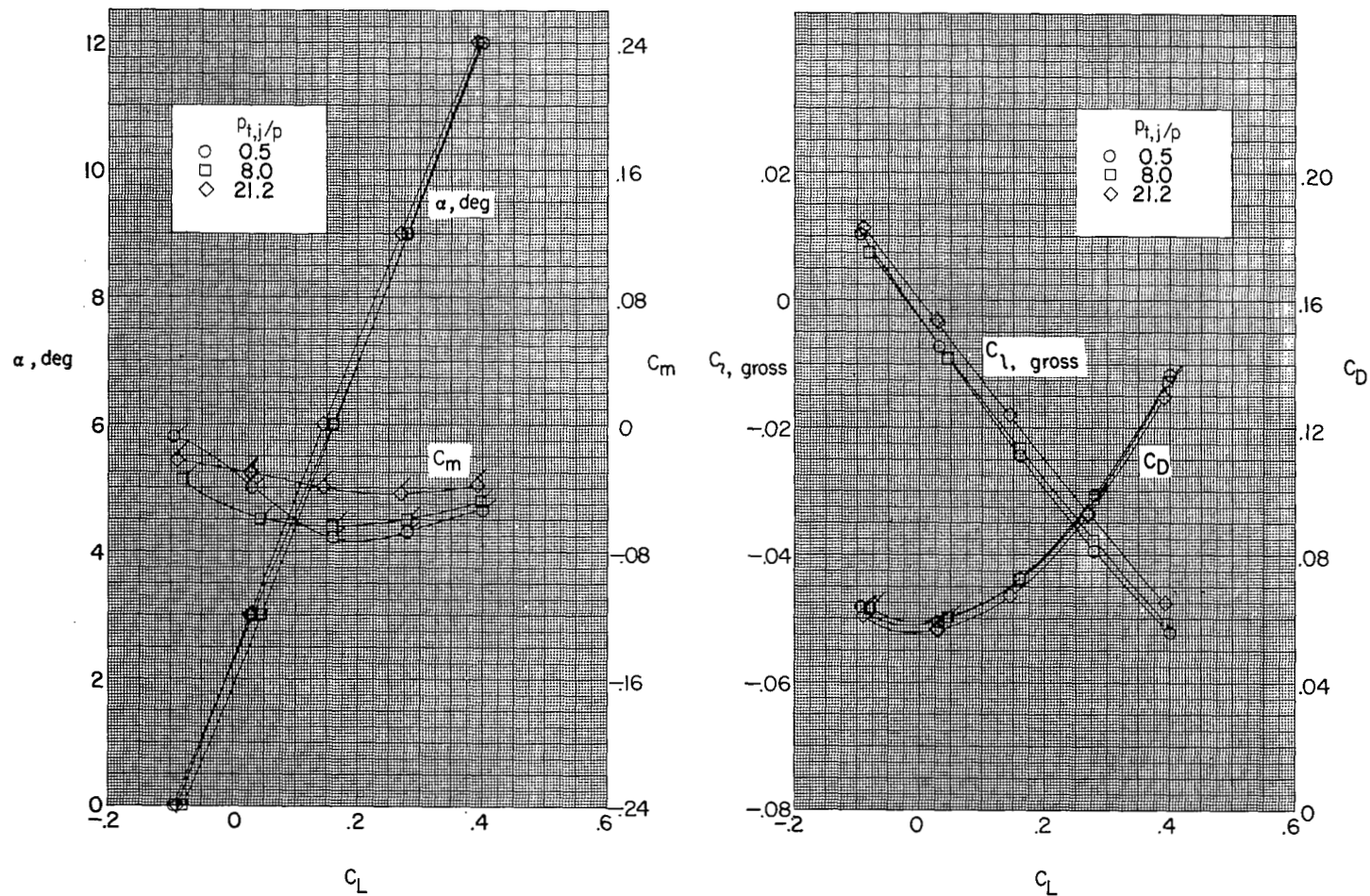
(e) Configuration 0131; large high tail;  $i_t = 0^\circ$ .

Figure 3.- Continued.



(f) Configuration 0141; large high tail;  $i_t = -3^\circ$ .

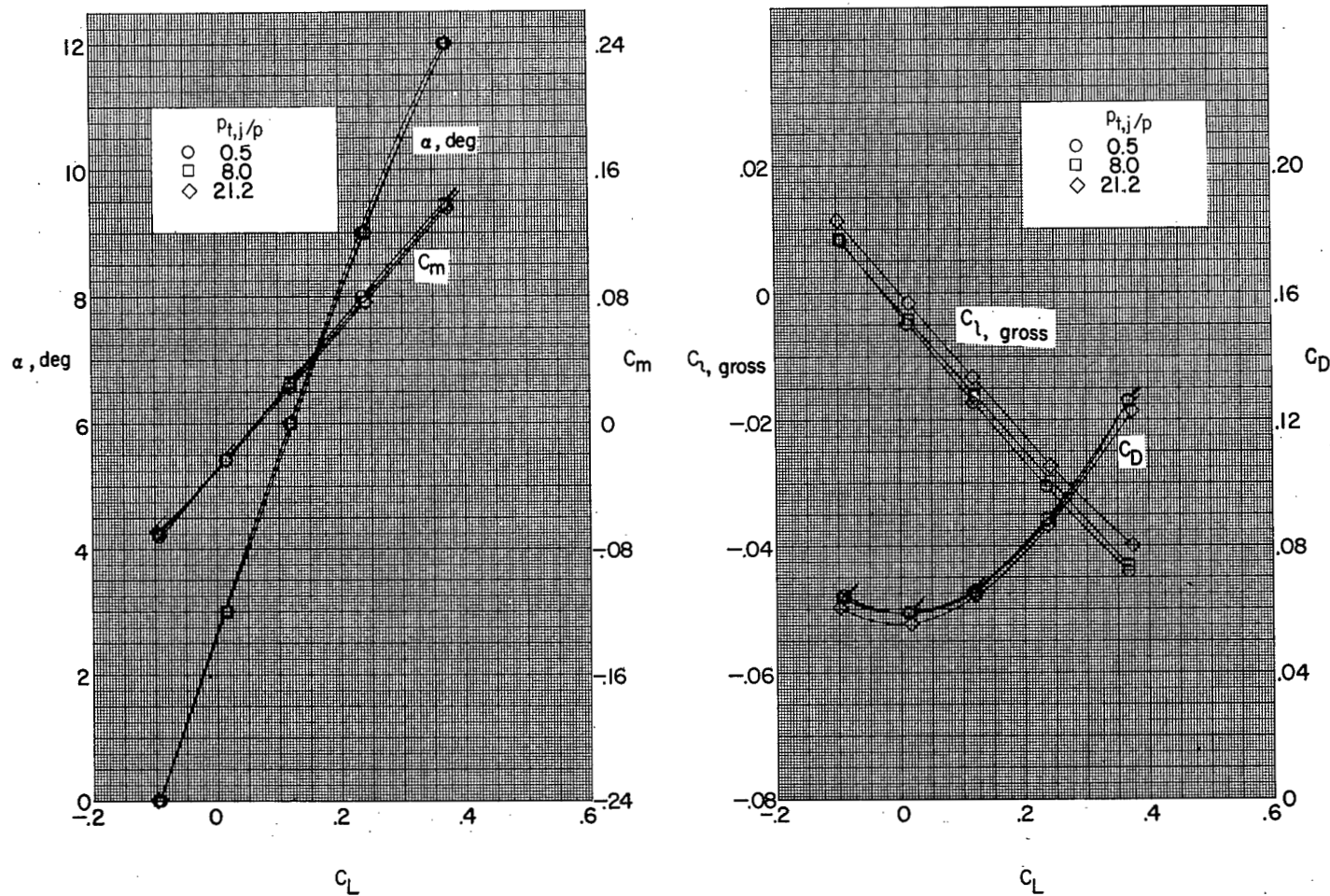
Figure 3.- Continued.



(g) Configuration 0151; small high tail.

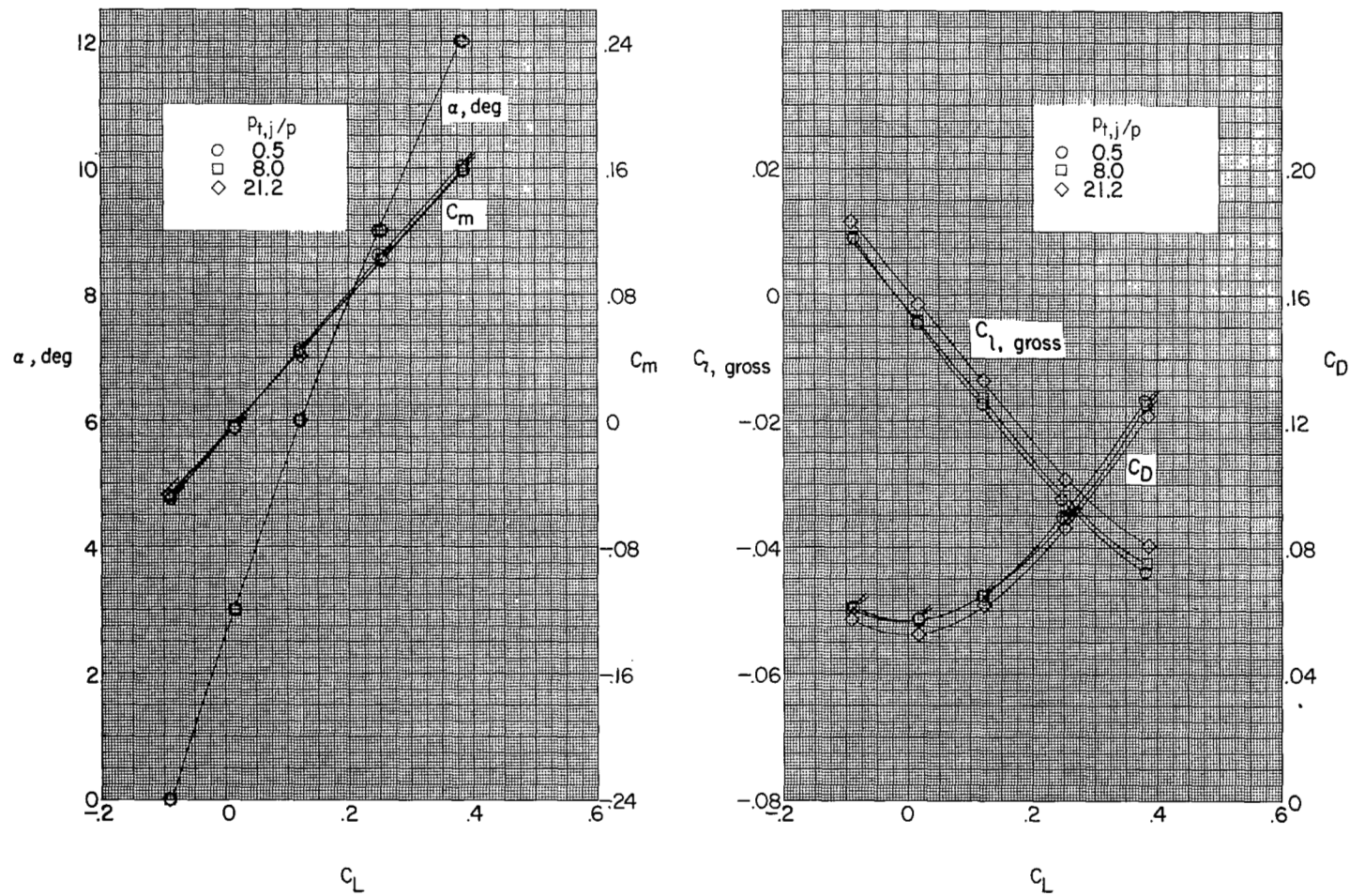
Figure 3.- Continued.





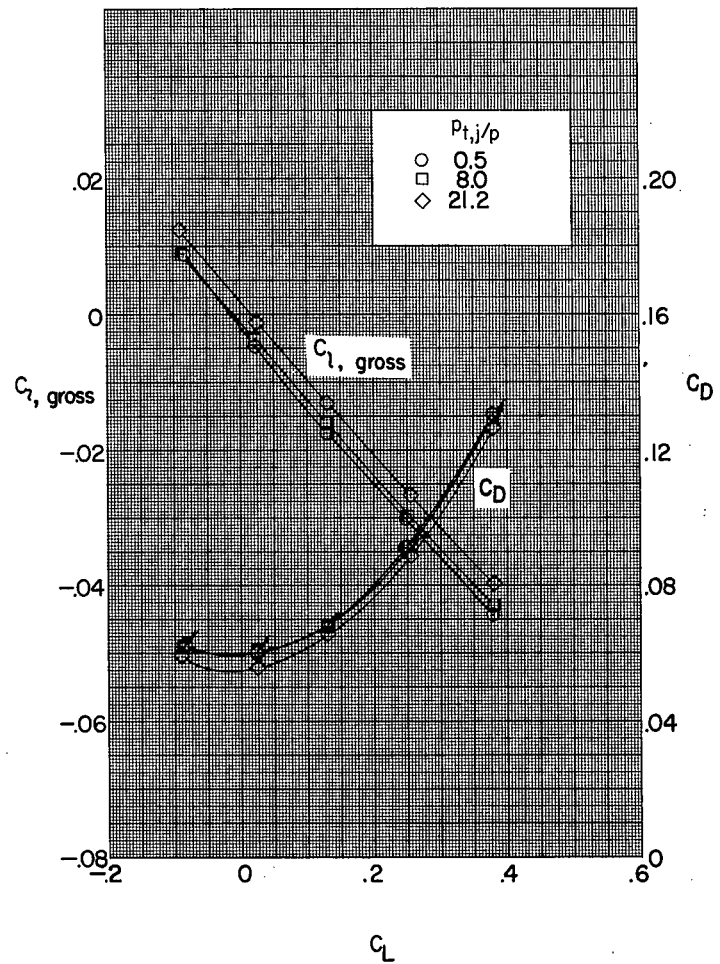
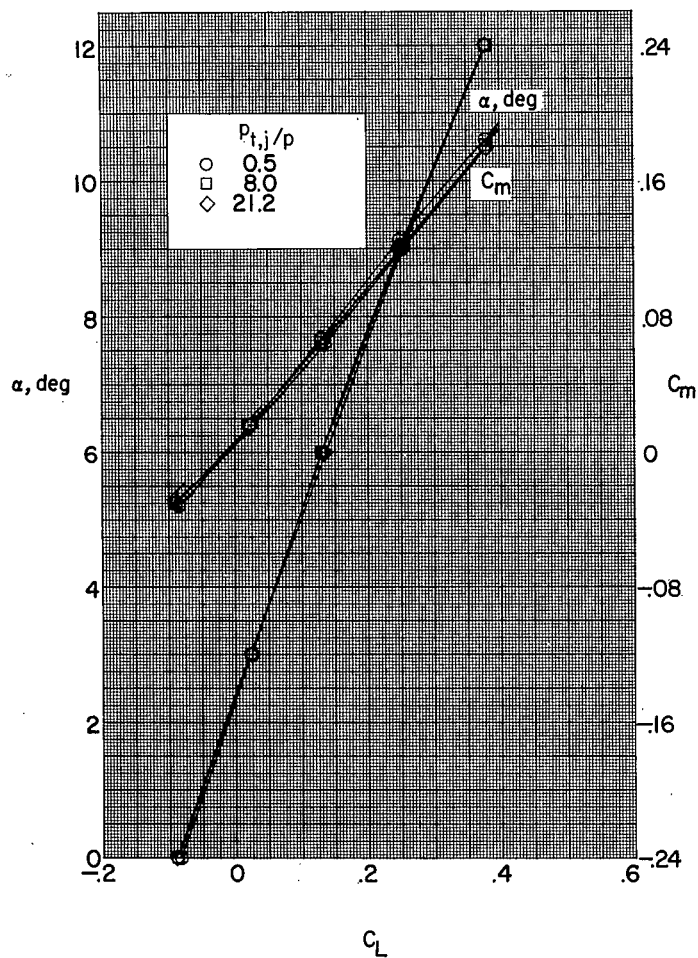
(h) Configuration 4001; no canopy; no horizontal tail;  $-4^\circ$  canard control.

Figure 3.- Continued.



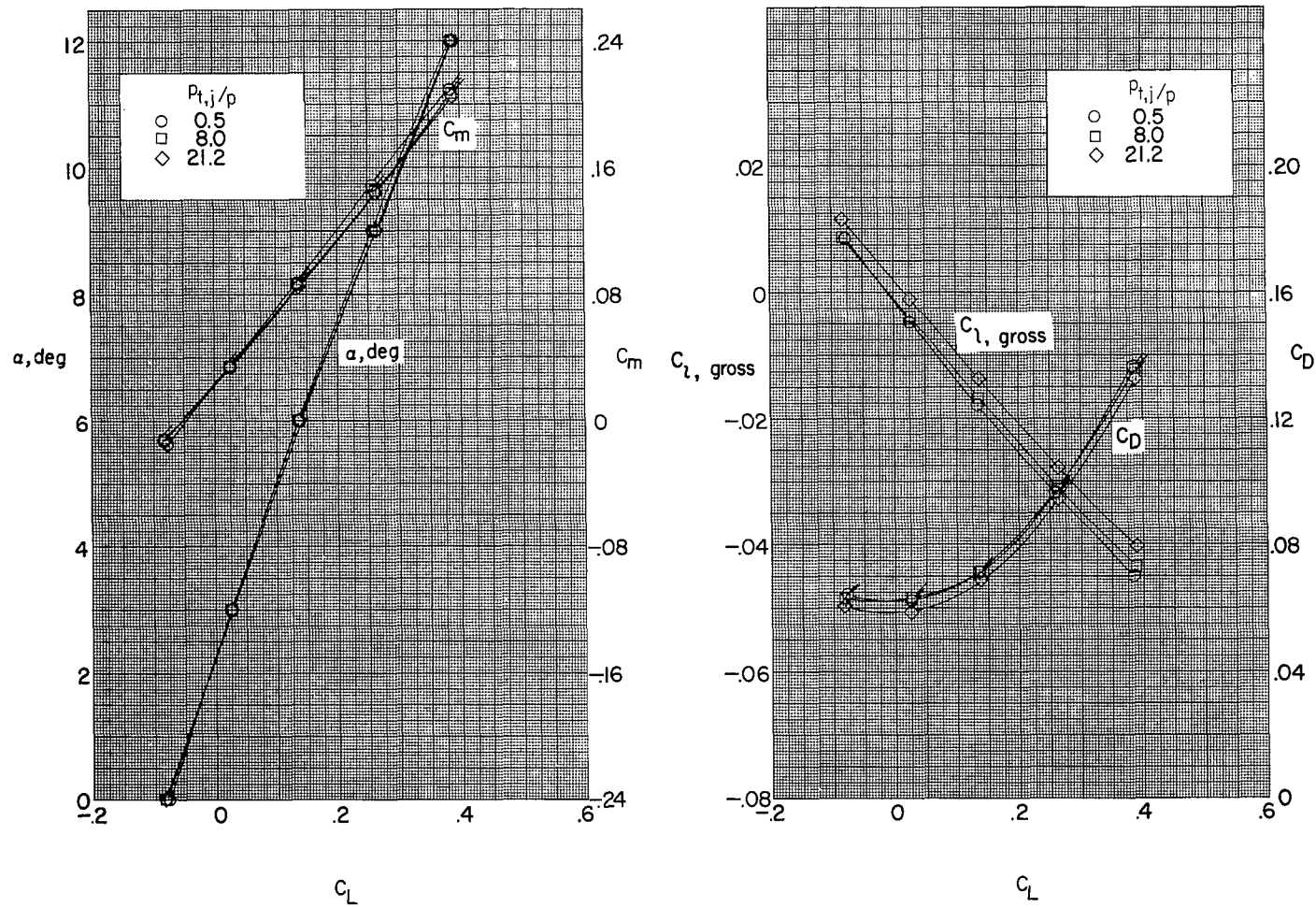
(i) Configuration 3001; no canopy; no horizontal tail;  $-2^\circ$  canard control.

Figure 3.- Continued.



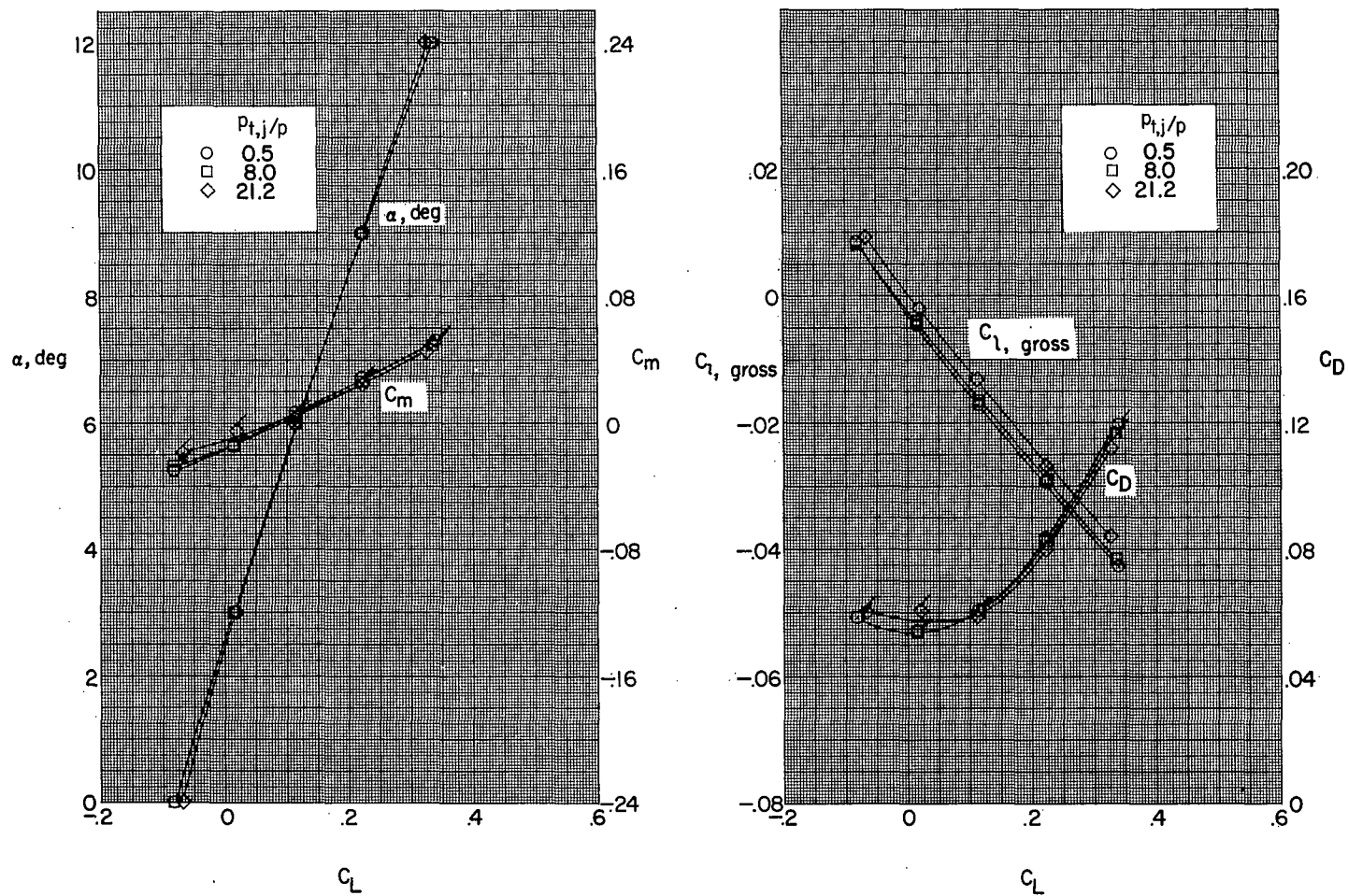
(j) Configuration 2001; no canopy; no horizontal tail;  $0^\circ$  canard control.

Figure 3.- Continued.



(k) Configuration 1001; no canopy; no horizontal tail;  $2^\circ$  canard control.

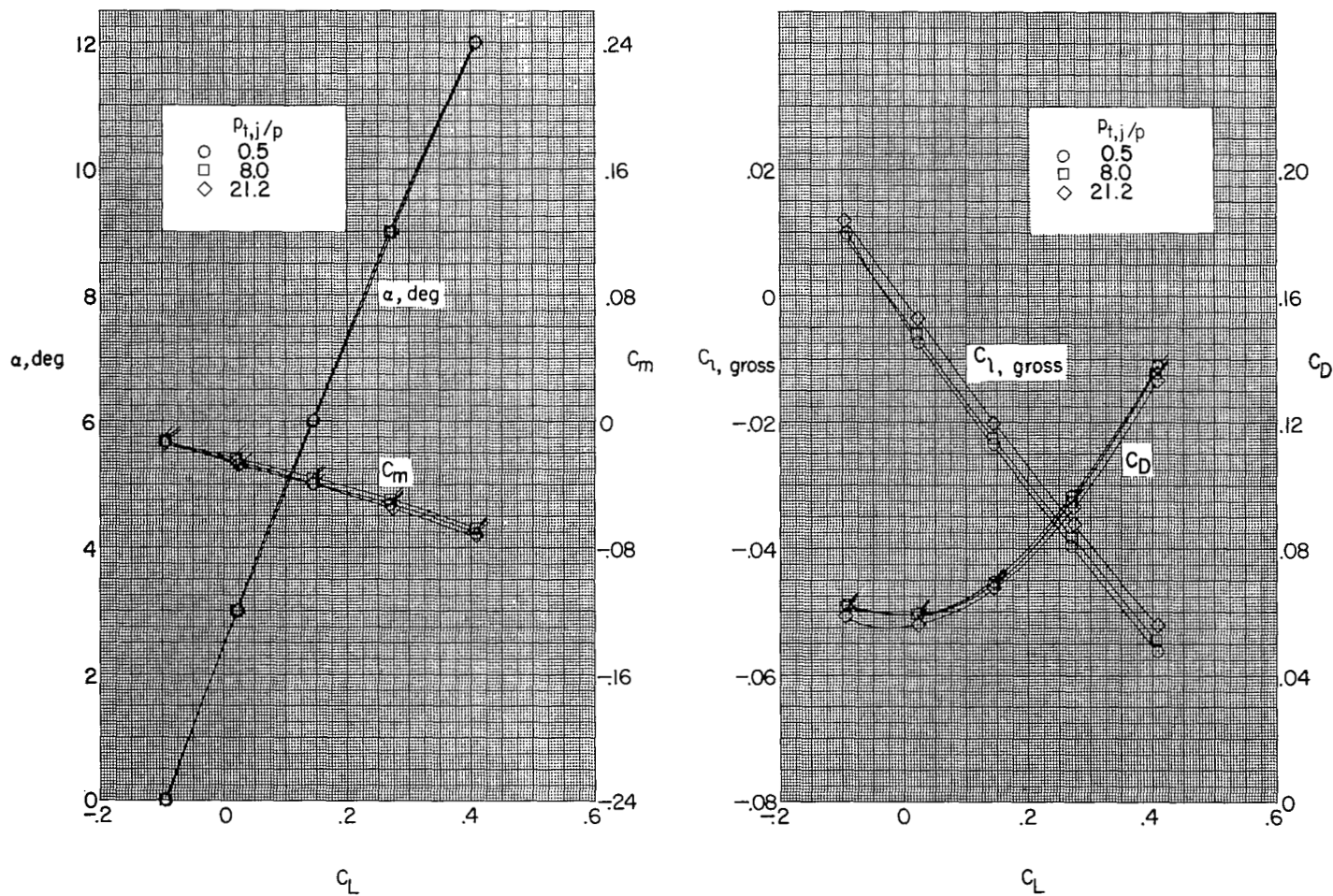
Figure 3.- Continued.



(1) Configuration 0001; no canopy; no horizontal tail.

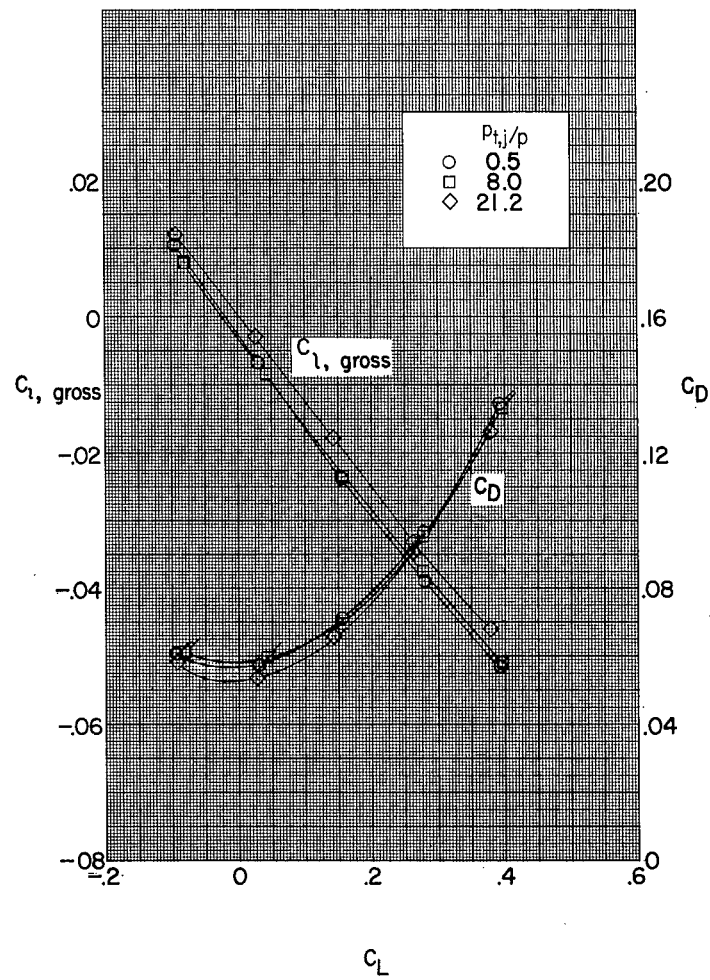
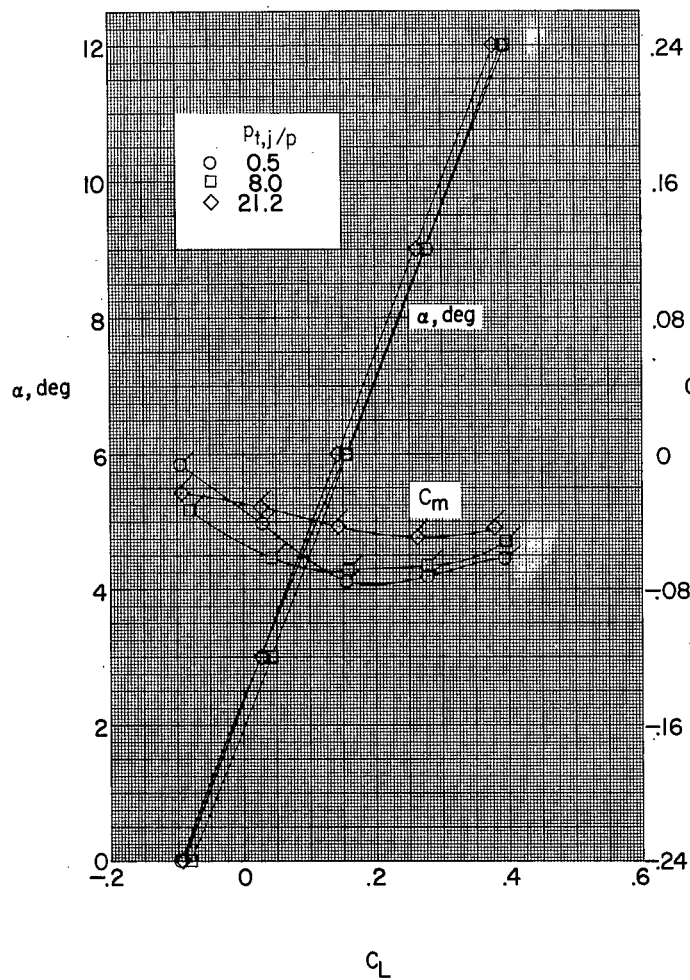
Figure 3.- Continued.





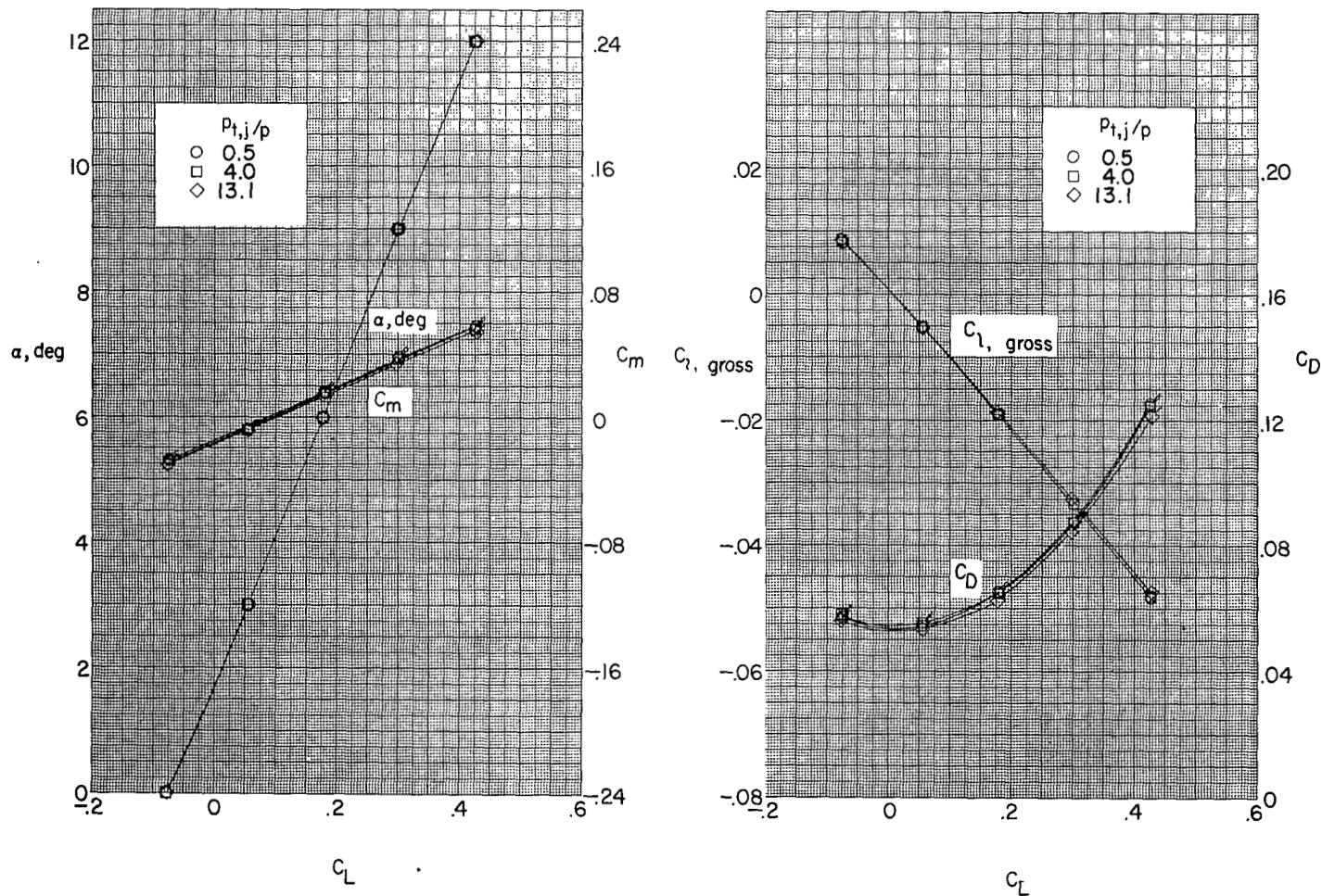
(m) Configuration 0011; no canopy; low tail.

Figure 3.- Continued.



(n) Configuration 0051; no canopy; small high tail.

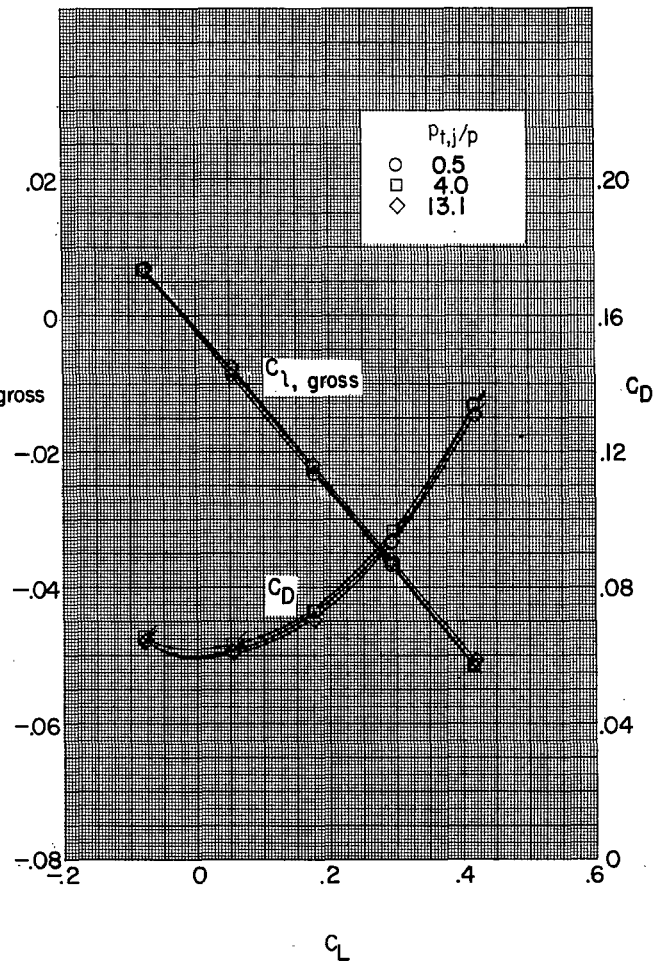
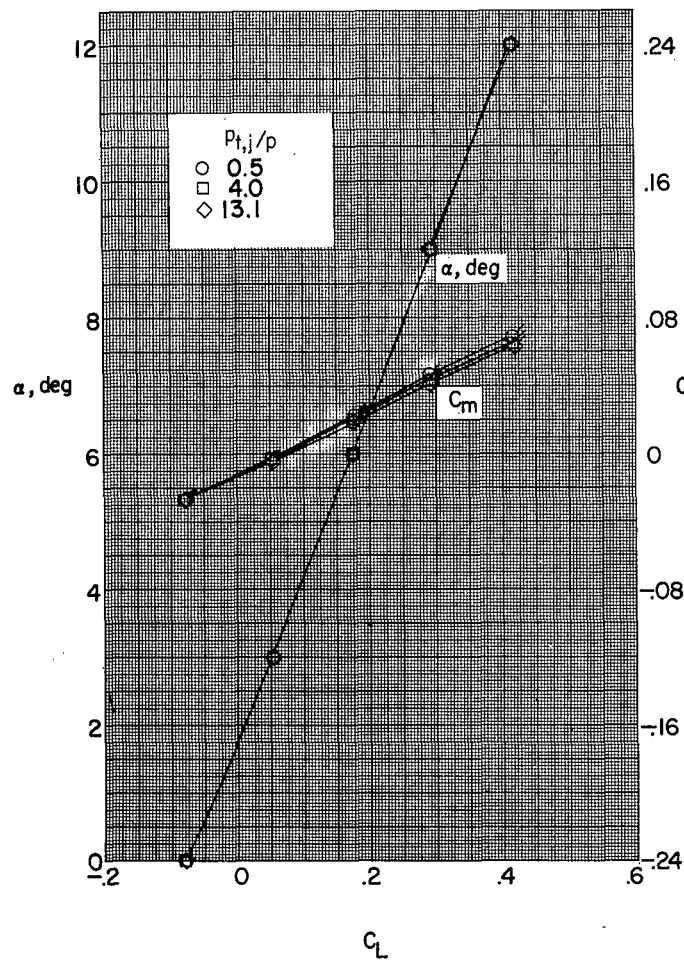
Figure 3.- Concluded.



(a) Configuration 0100; no horizontal tail; no vertical tail.

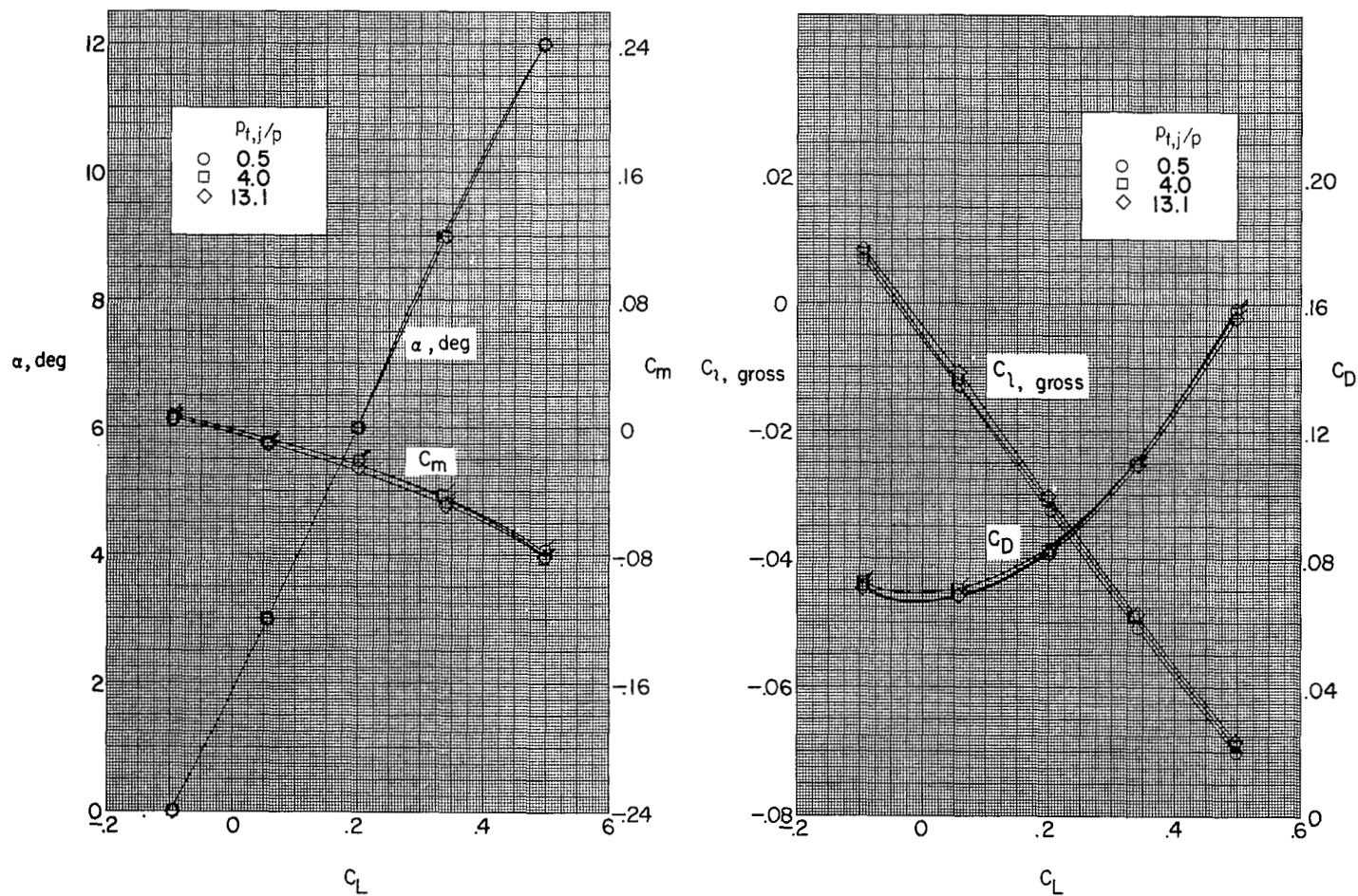
Figure 4.- Basic variations of the four-component balance measurements for the 12 configurations tested at  $M = 1.61$ . Flagged symbols indicate pitching-moment or drag coefficient.





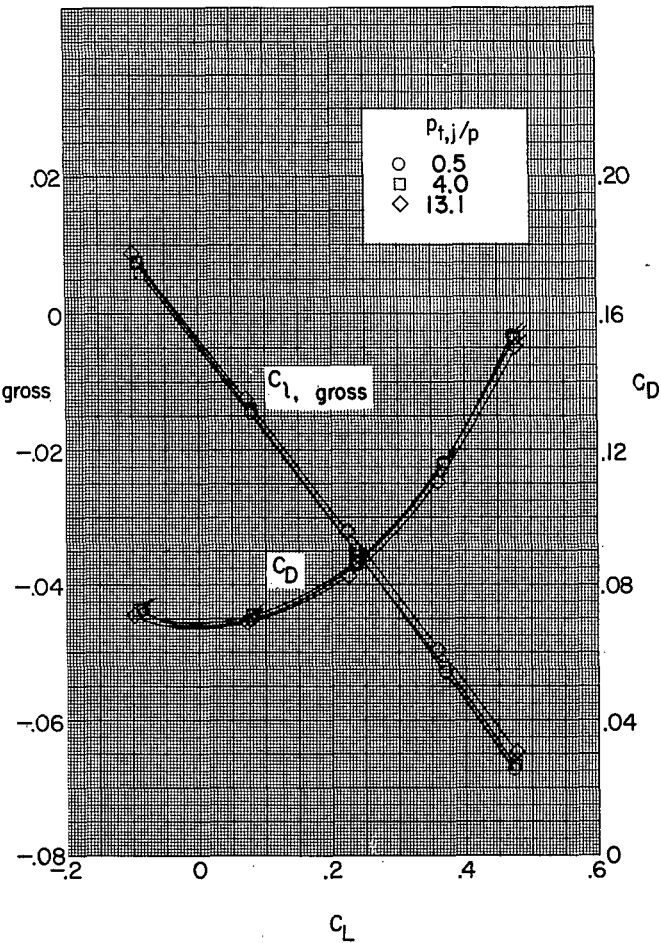
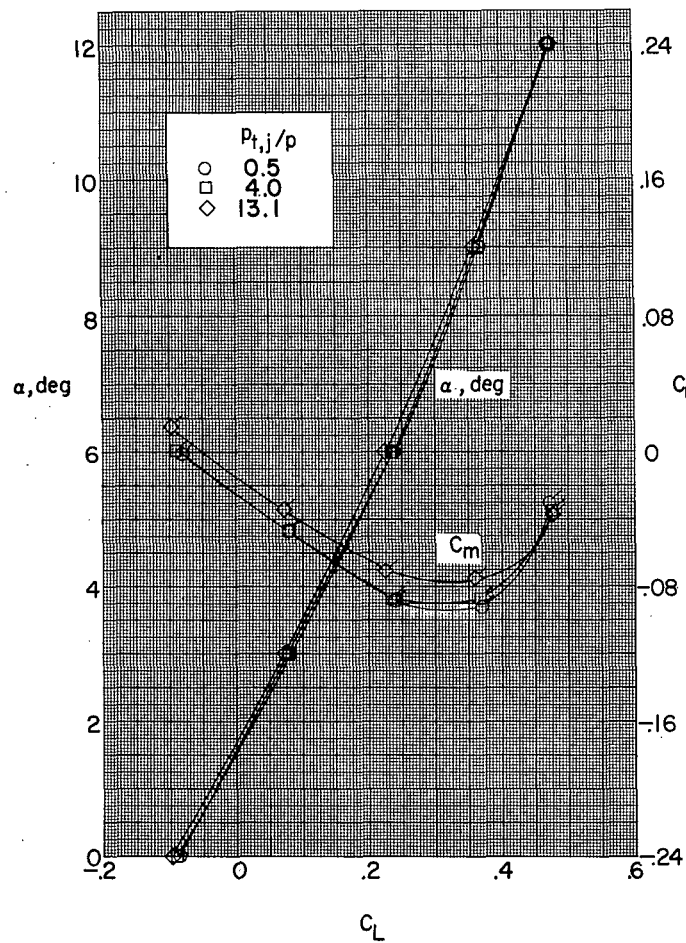
(b) Configuration 0101; no horizontal tail.

Figure 4.- Continued.



(c) Configuration 0111; low tail.

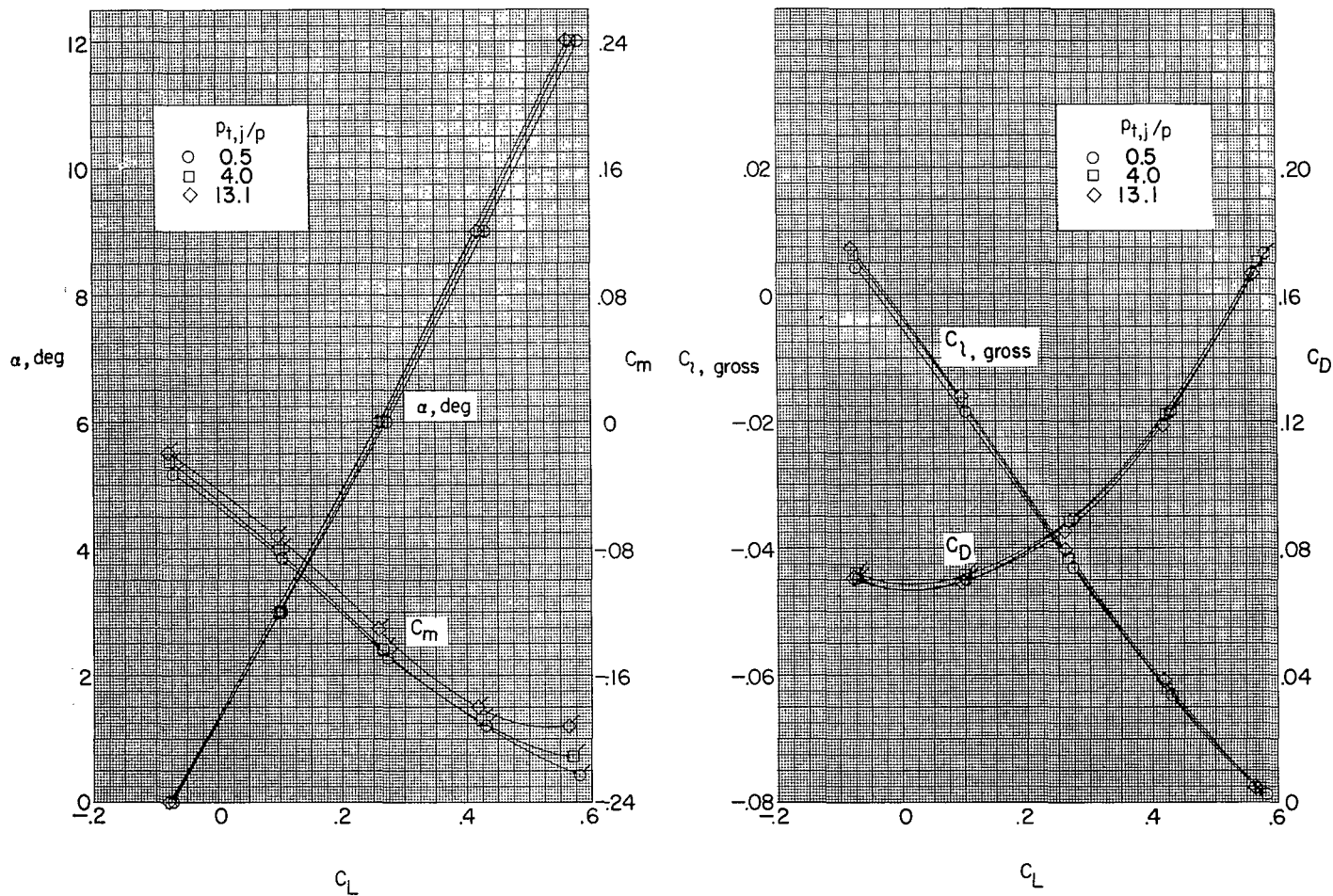
Figure 4.- Continued.



(d) Configuration 0121; midtail.

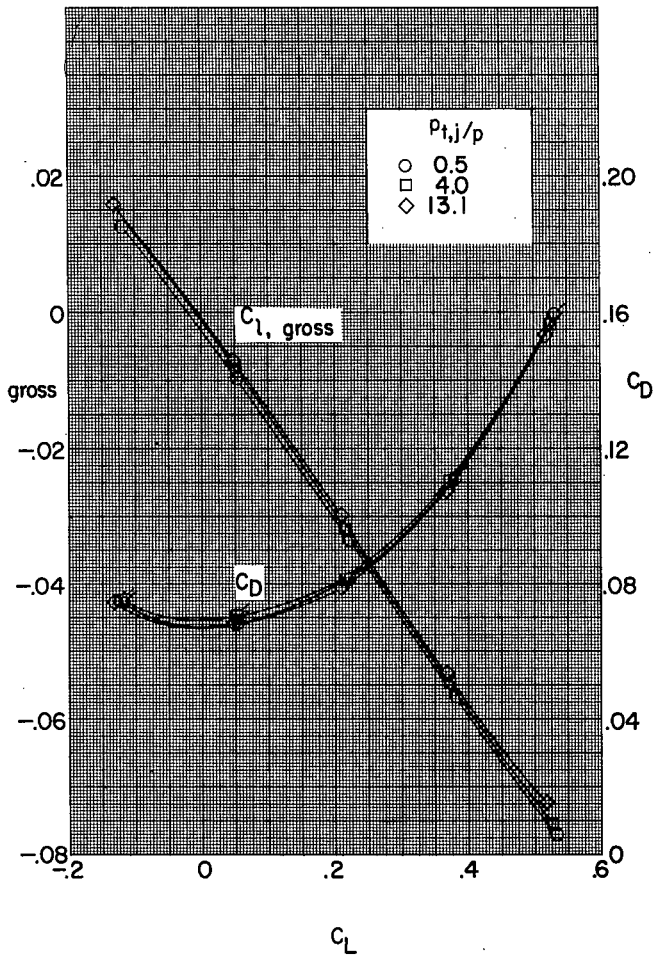
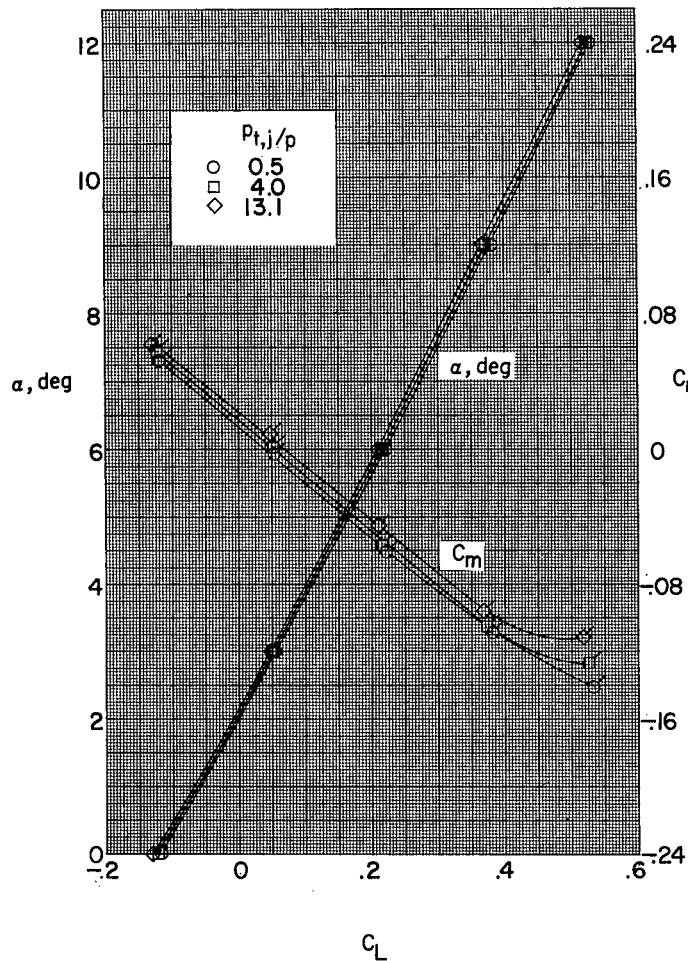
Figure 4.- Continued.

CONFIDENTIAL



(e) Configuration 0131; large high tail;  $i_t = 0^\circ$ .

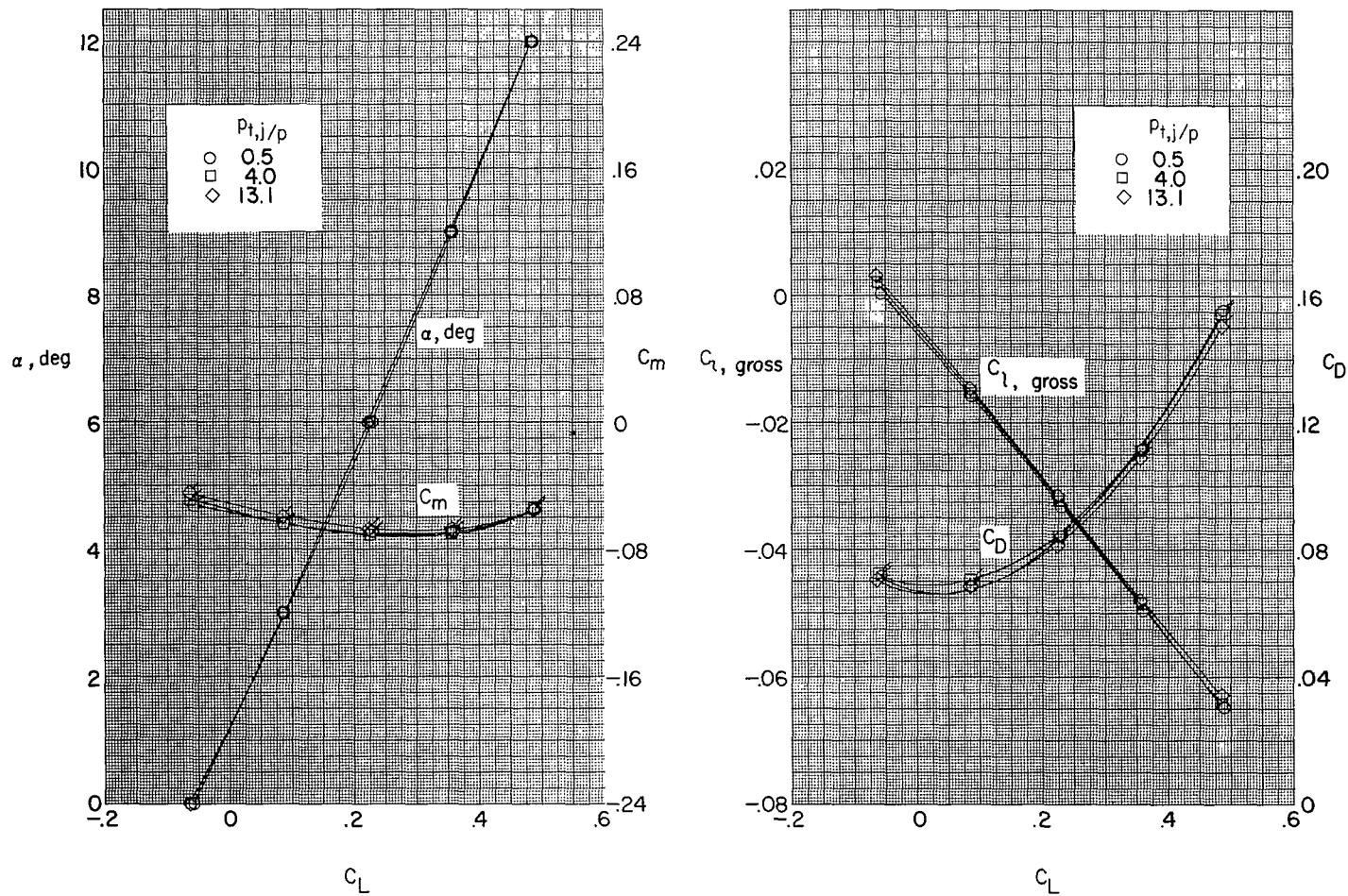
Figure 4.- Continued.



(f) Configuration 0141; large high tail;  $i_t = -3^\circ$ .

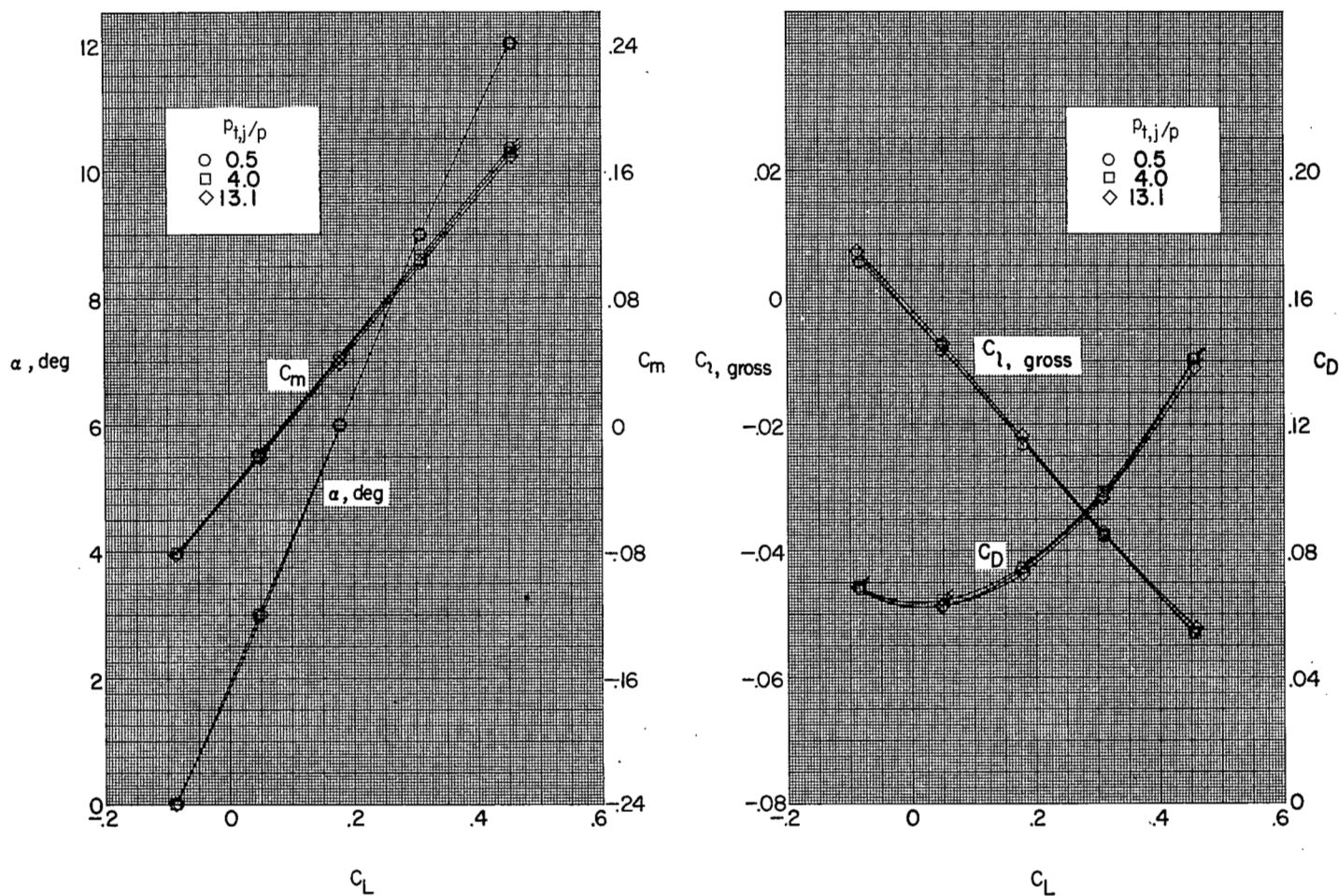
Figure 4.- Continued.





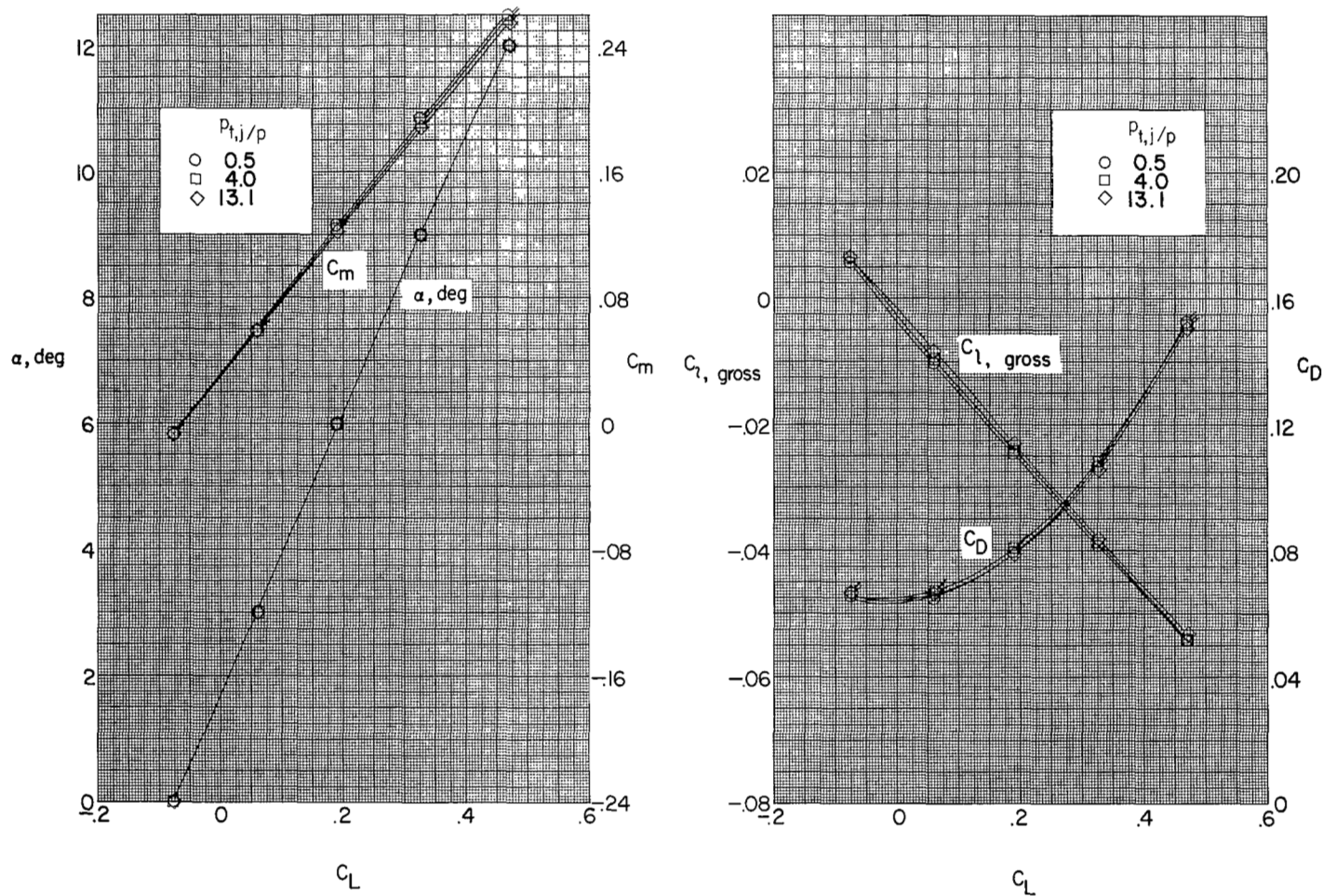
(g) Configuration 0151; small high tail.

Figure 4.- Continued.



(h) Configuration 4001; no canopy; no horizontal tail;  $-4^\circ$  canard control.

Figure 4.- Continued.

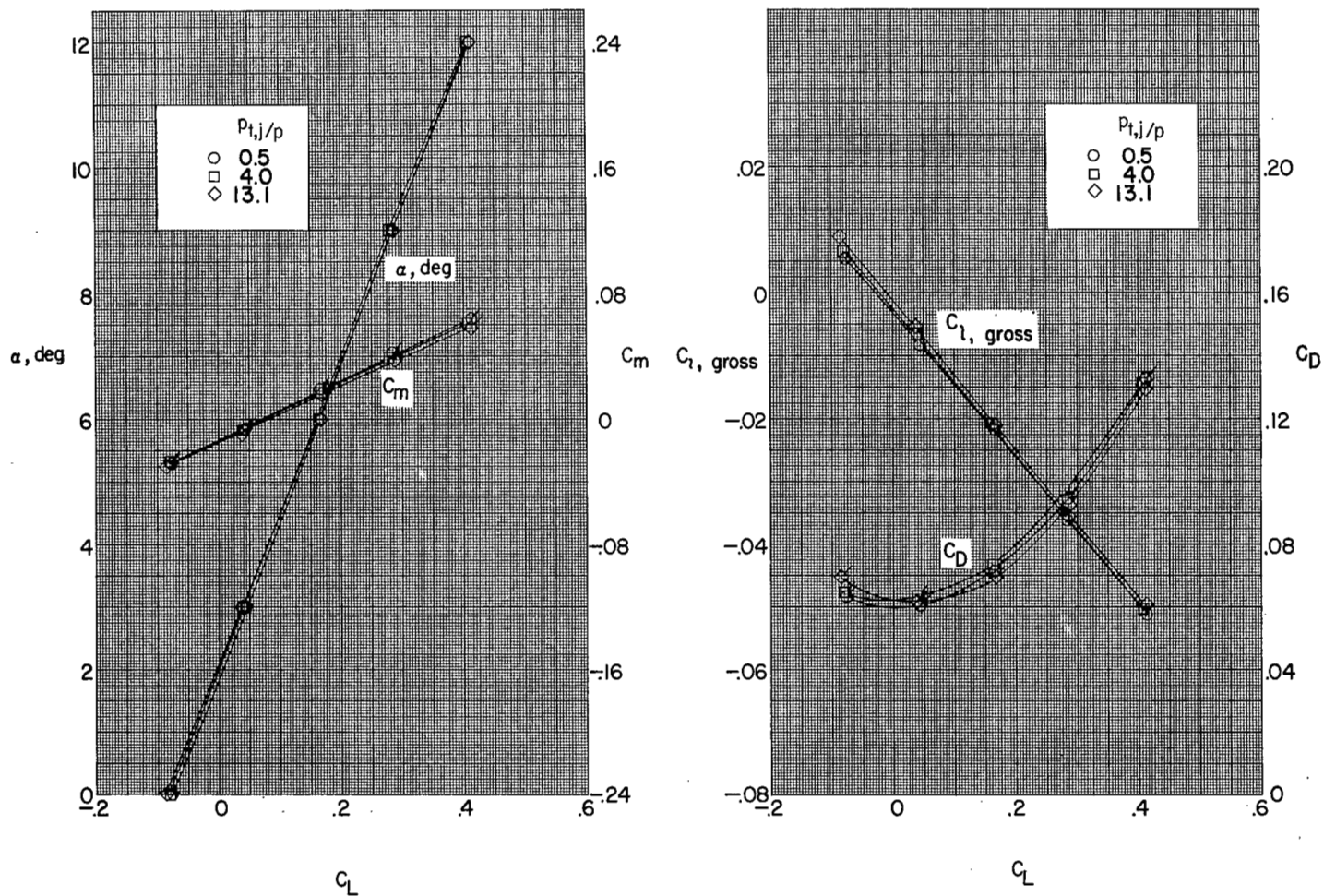


(i) Configuration 1001; no canopy; no horizontal tail;  $2^\circ$  canard control.

Figure 4.- Continued.

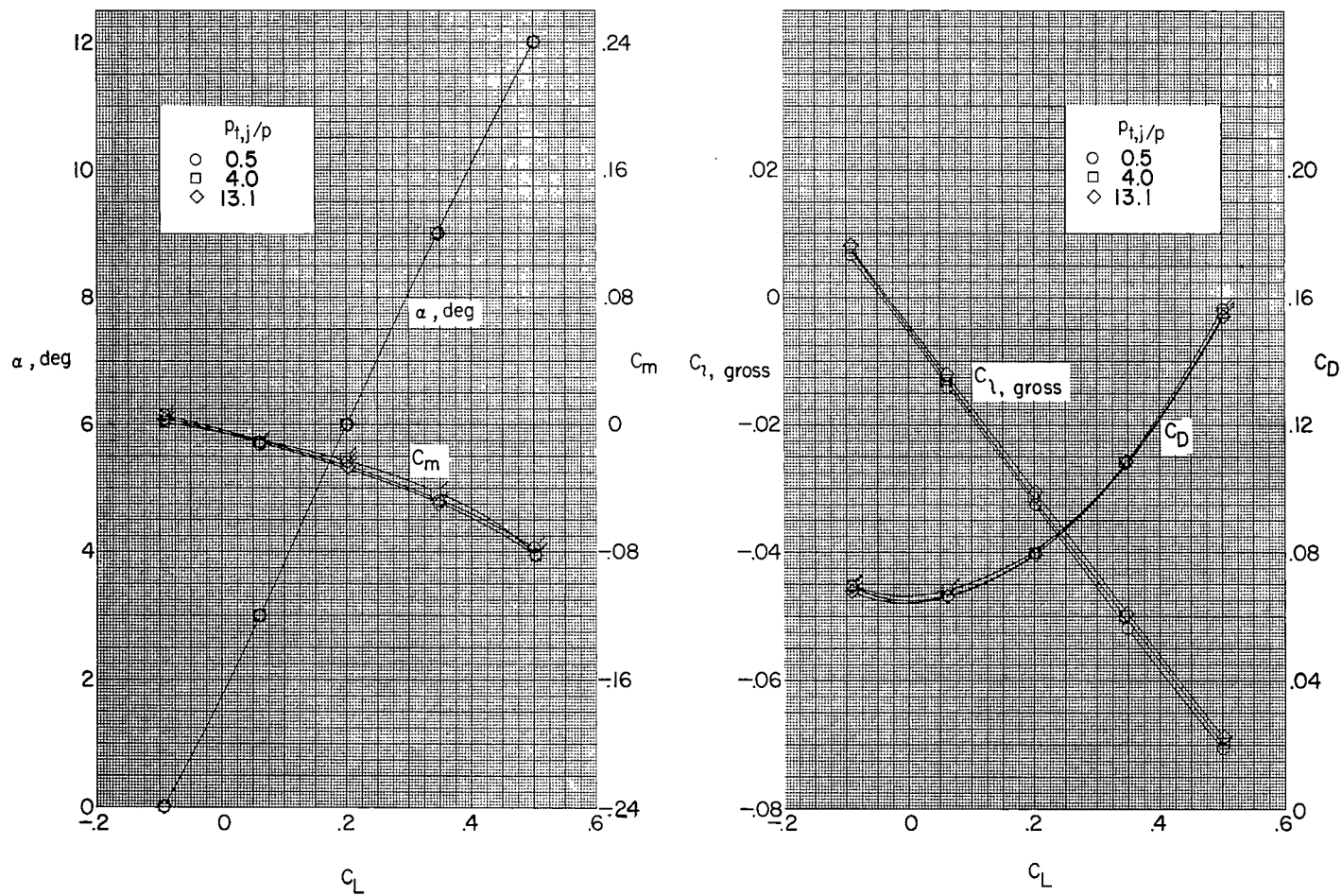


CONFIDENTIAL



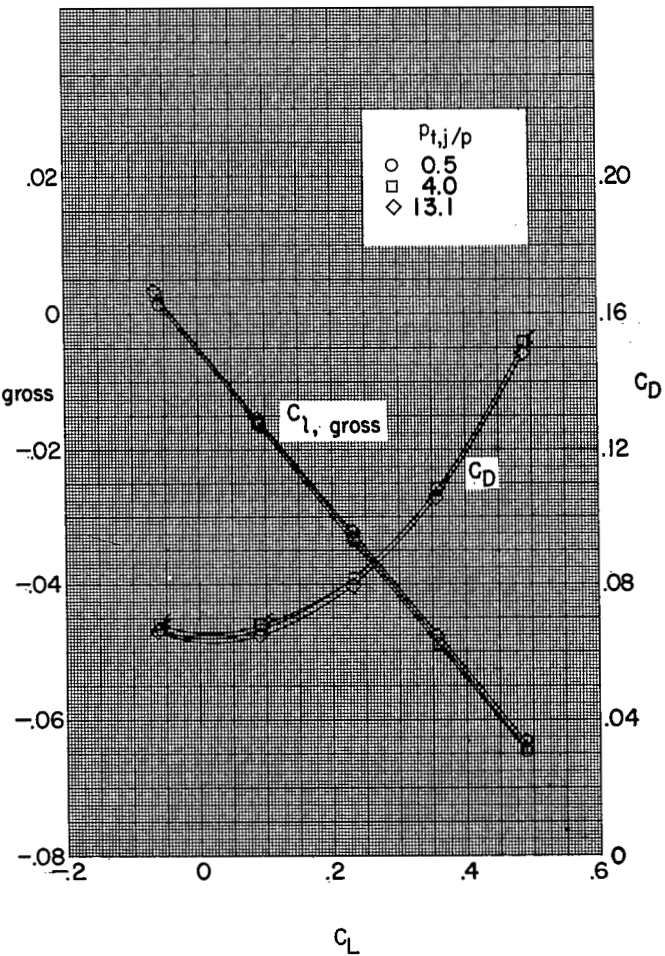
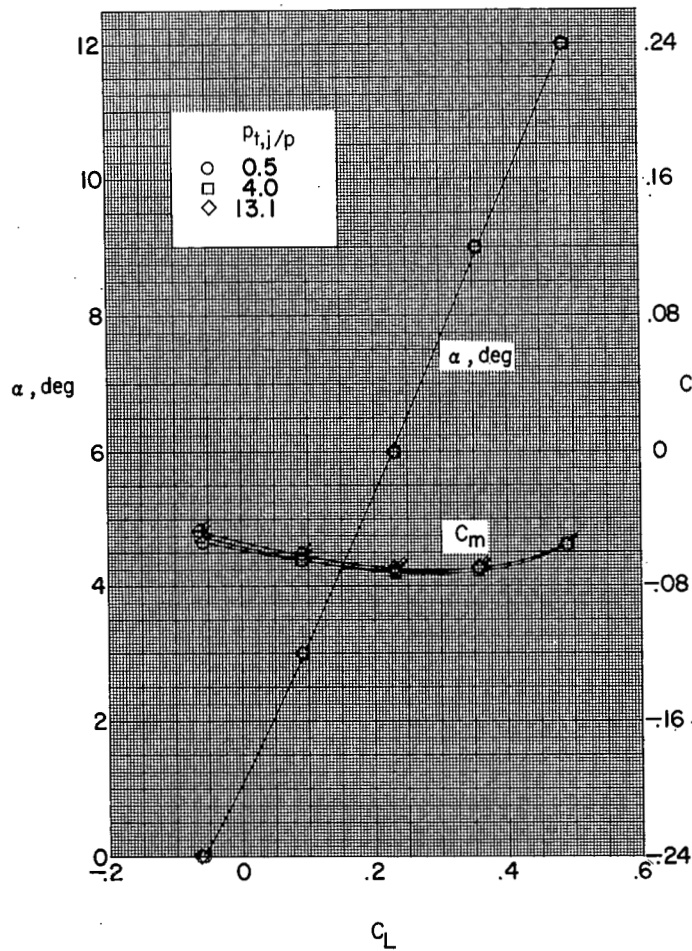
(j) Configuration 0001; no canopy; no horizontal tail.

Figure 4.- Continued.



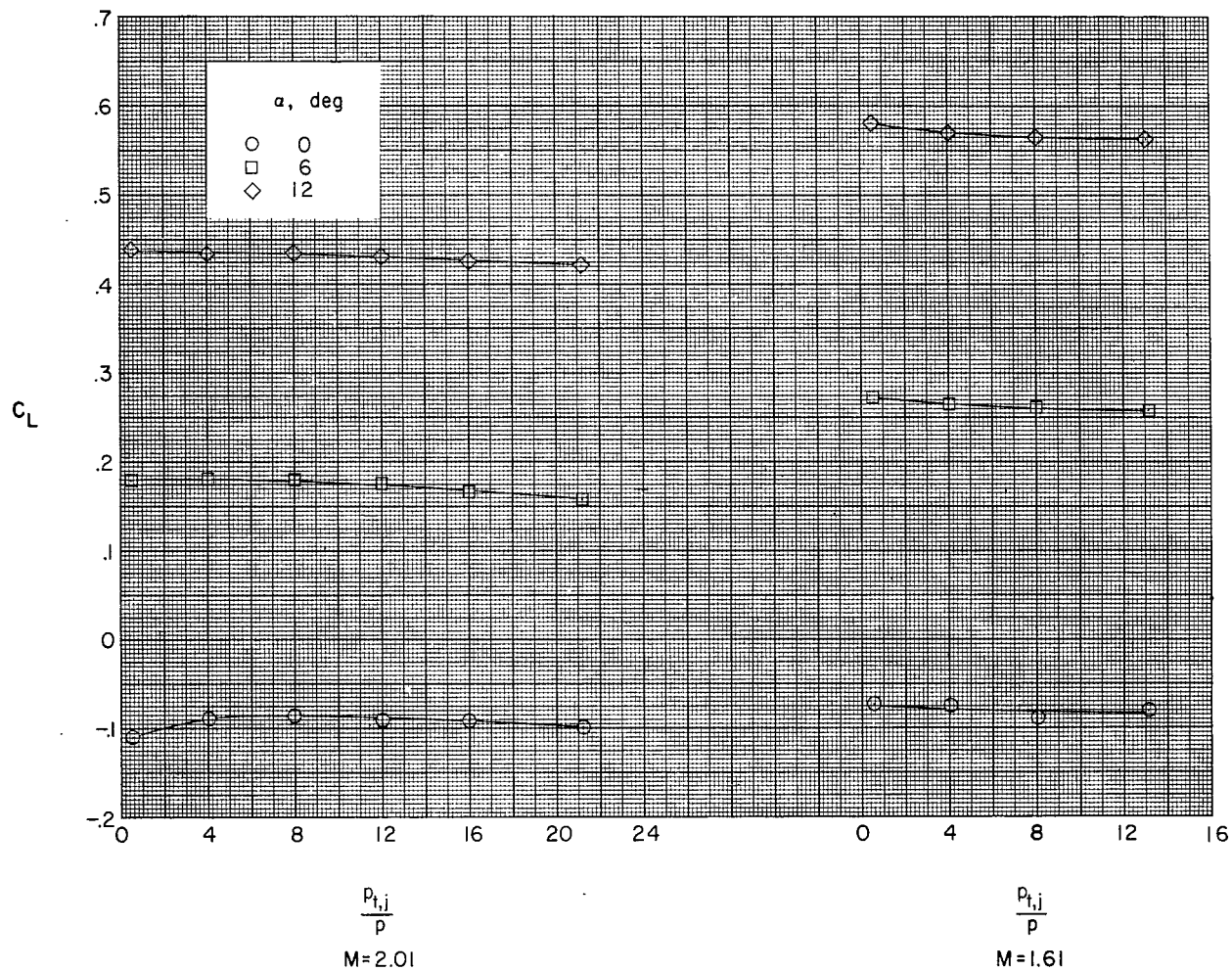
(k) Configuration 0011; no canopy; low tail.

Figure 4.- Continued.



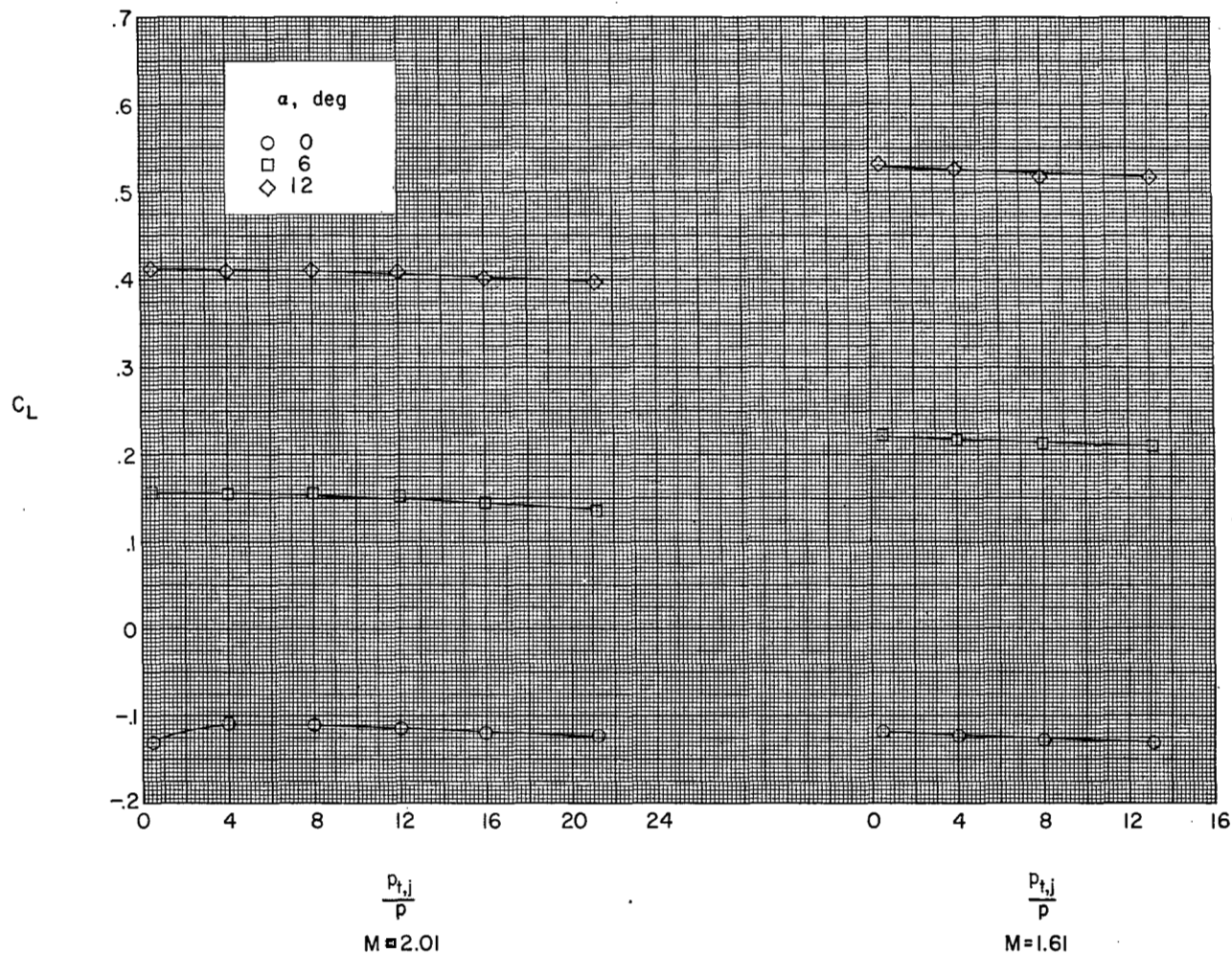
(2) Configuration 0051; no canopy; small high tail.

Figure 4.- Concluded.



(a) Configuration 0131; large high tail;  $i_t = 0^\circ$ .

Figure 5.- Variations of the semispan model lift coefficient with jet-pressure ratio.

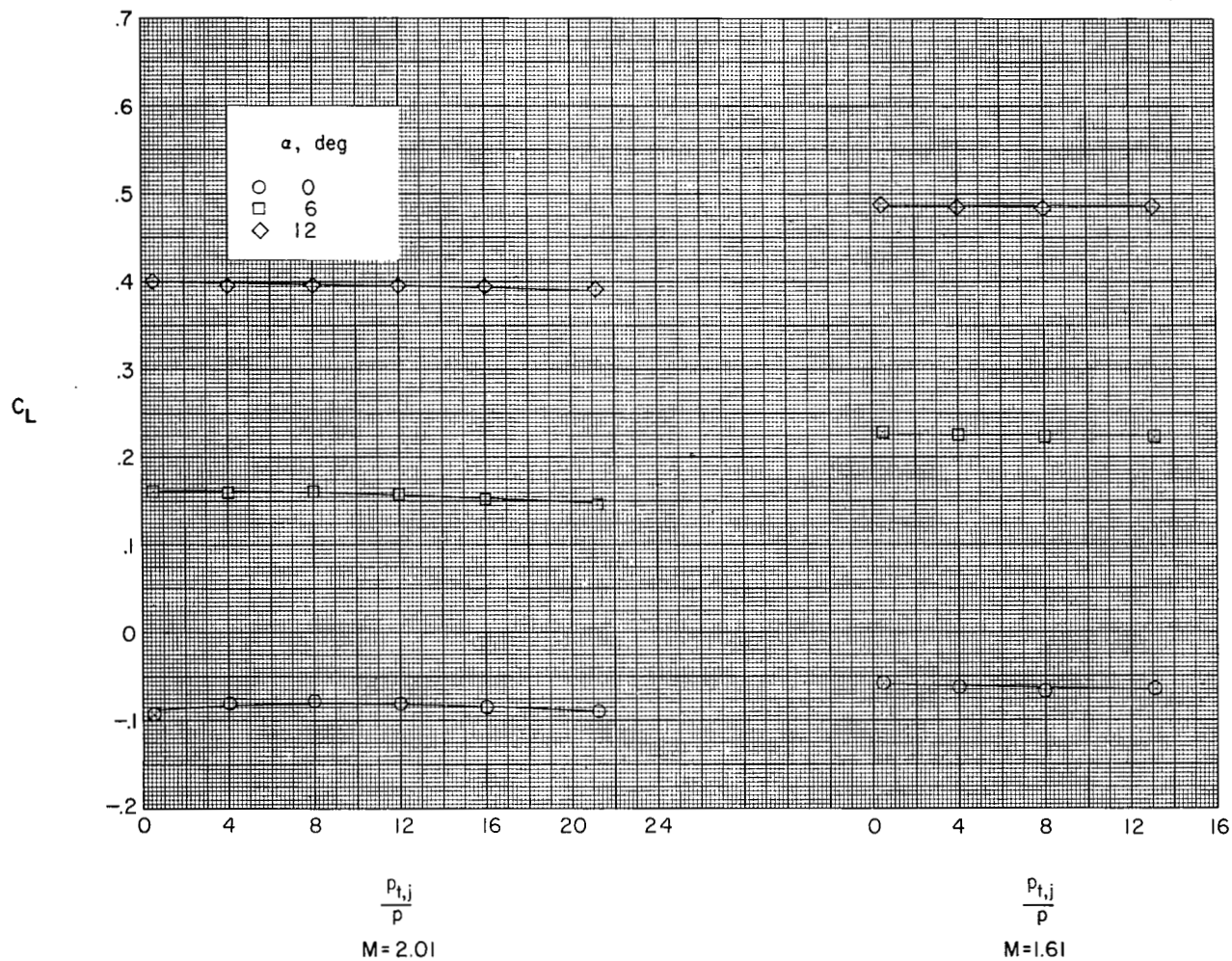


(b) Configuration 0141; large high tail;  $i_t = -3^\circ$ .

Figure 5.- Continued.

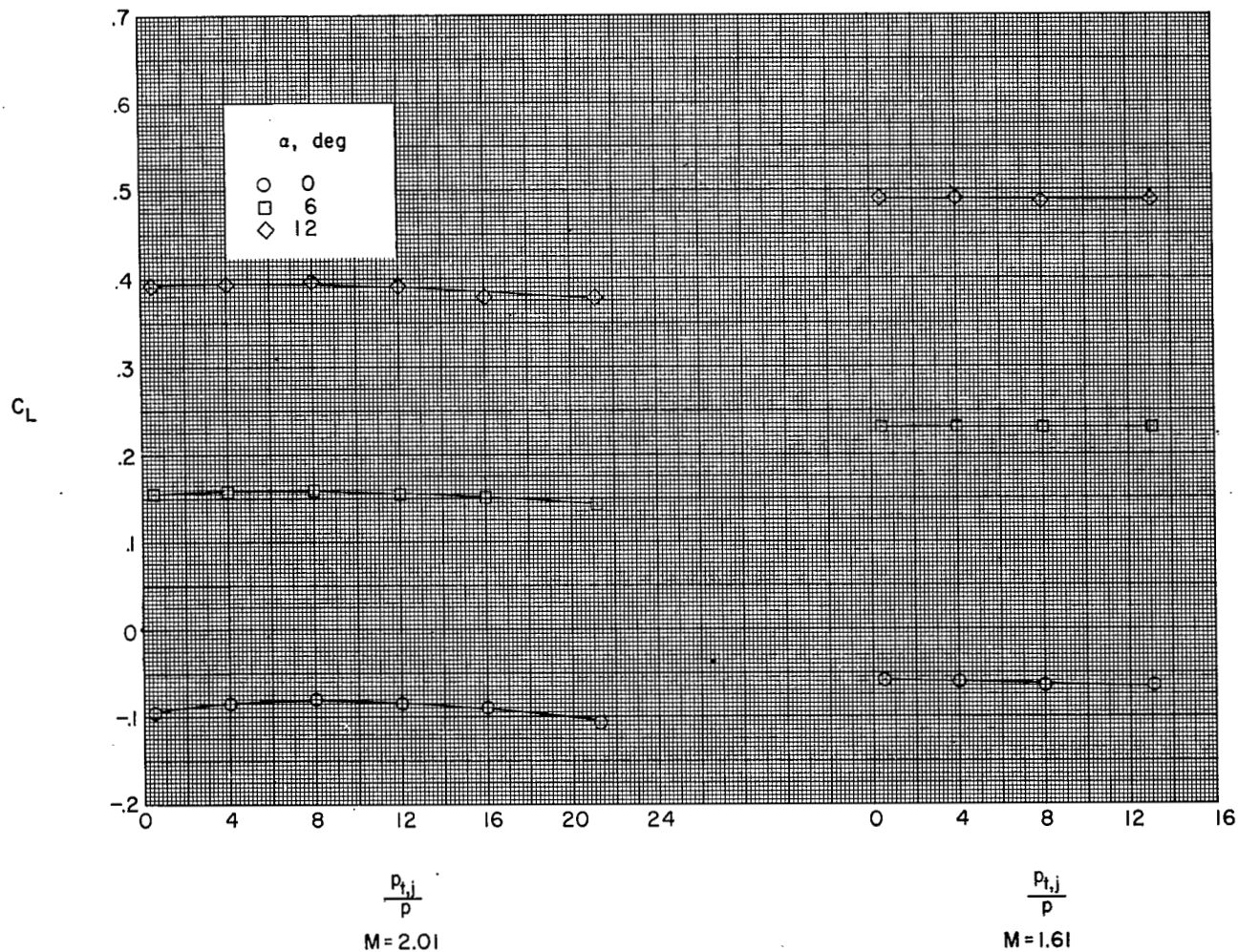


~~CONFIDENTIAL~~



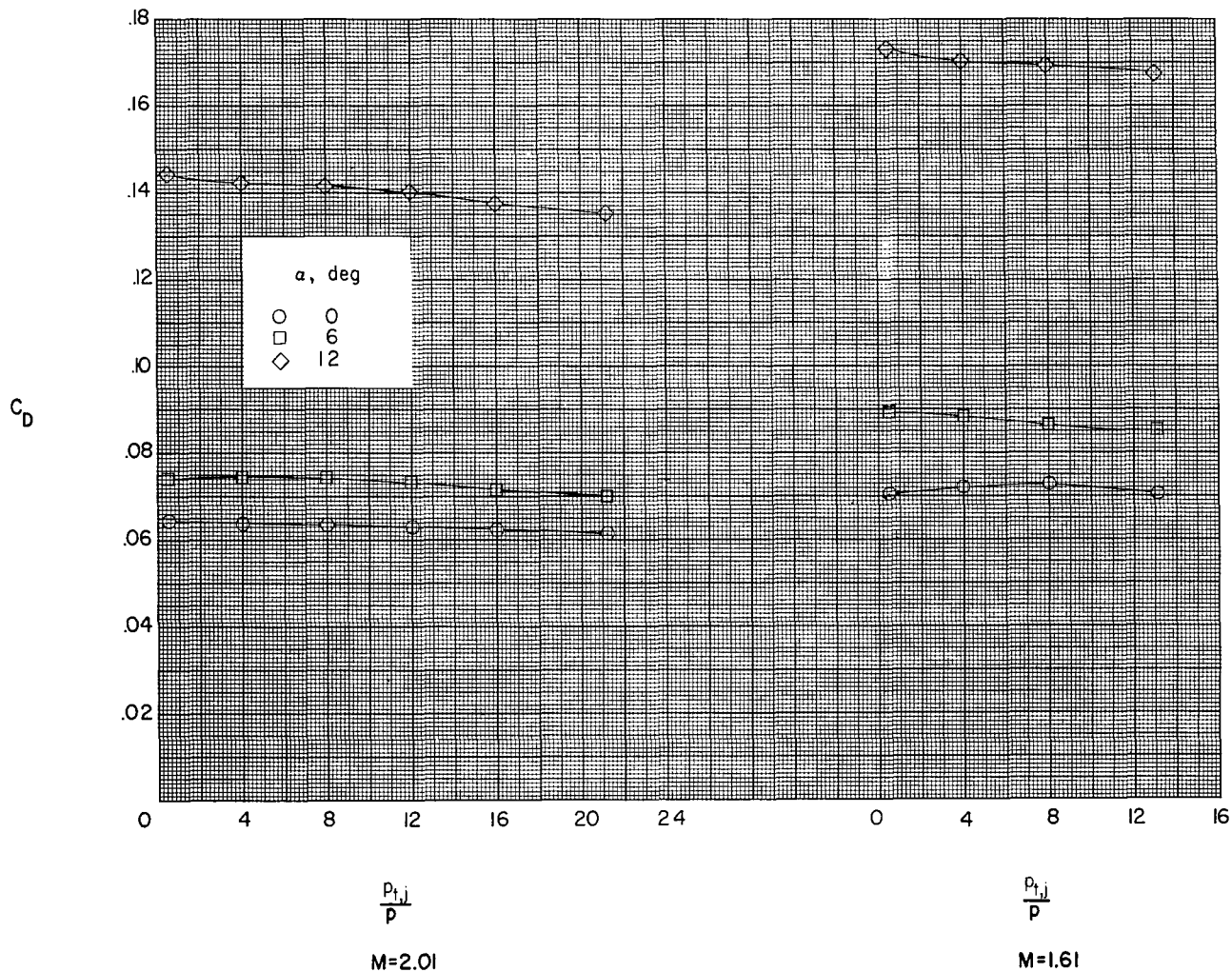
(c) Configuration 0151; small high tail.

Figure 5.- Continued.



(d) Configuration 0051; no canopy; small high tail.

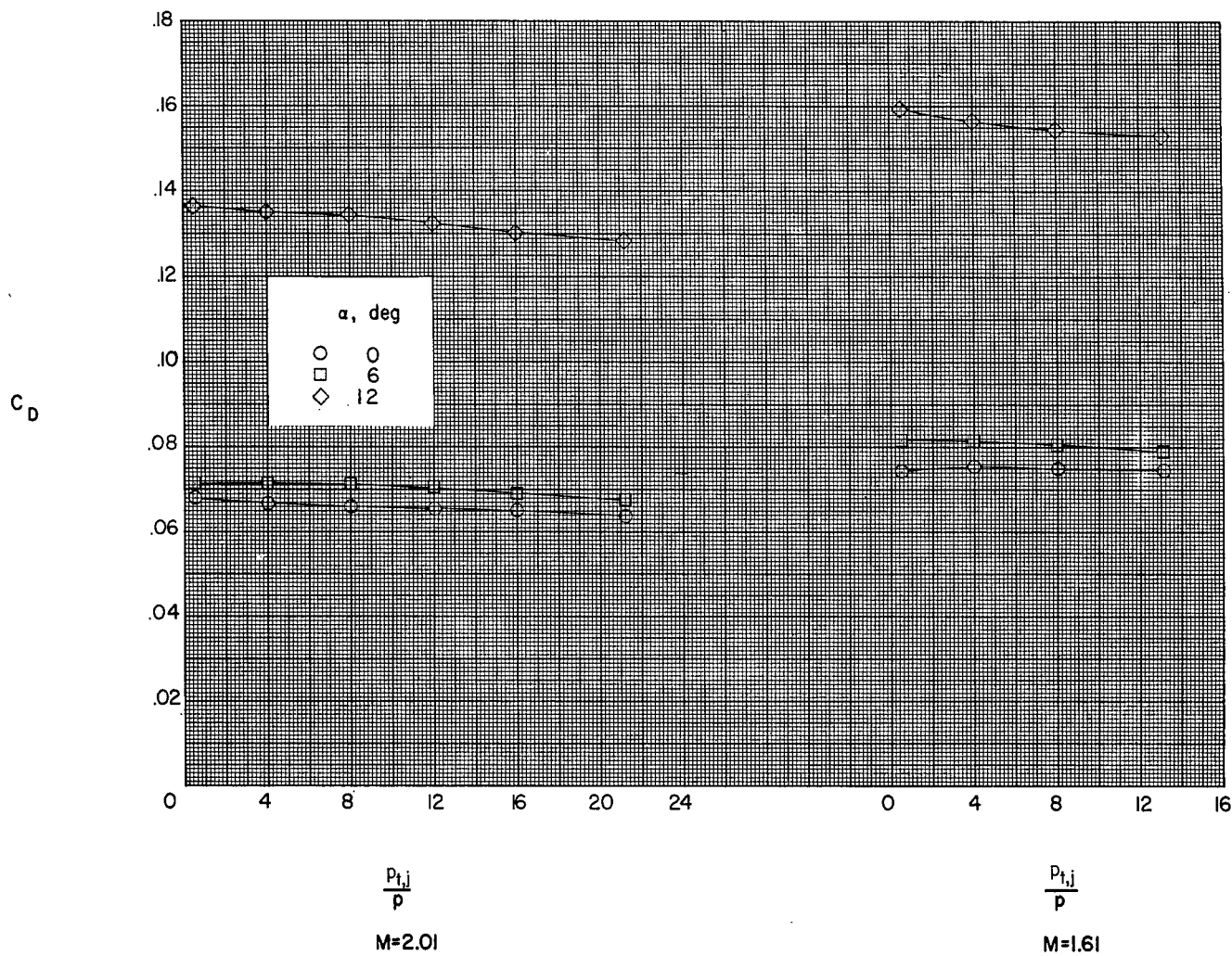
Figure 5.- Concluded.



(a) Configuration 0131; large high tail;  $i_t = 0^\circ$ .

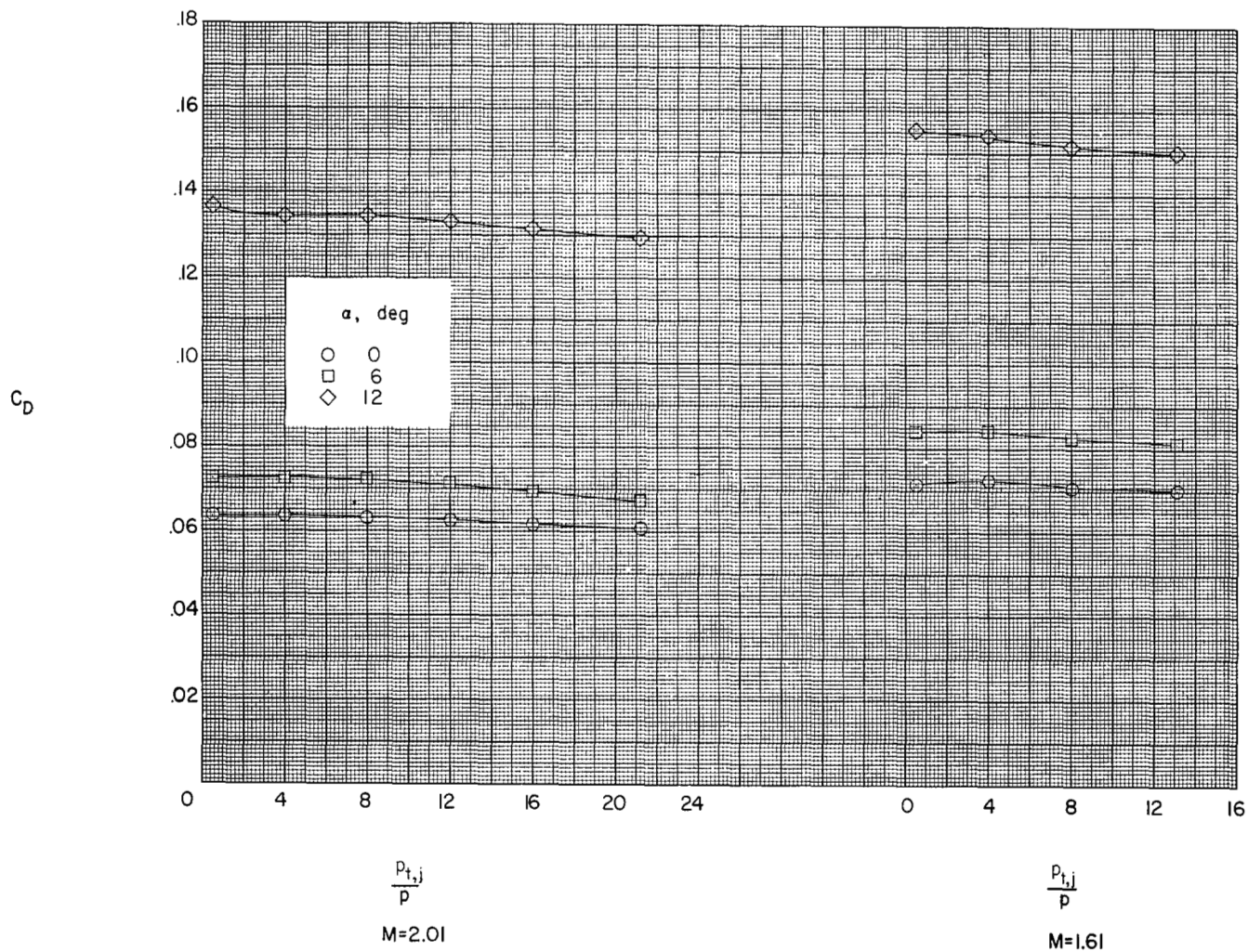
Figure 6.- Variations of the semispan model drag coefficient with jet-pressure ratio.





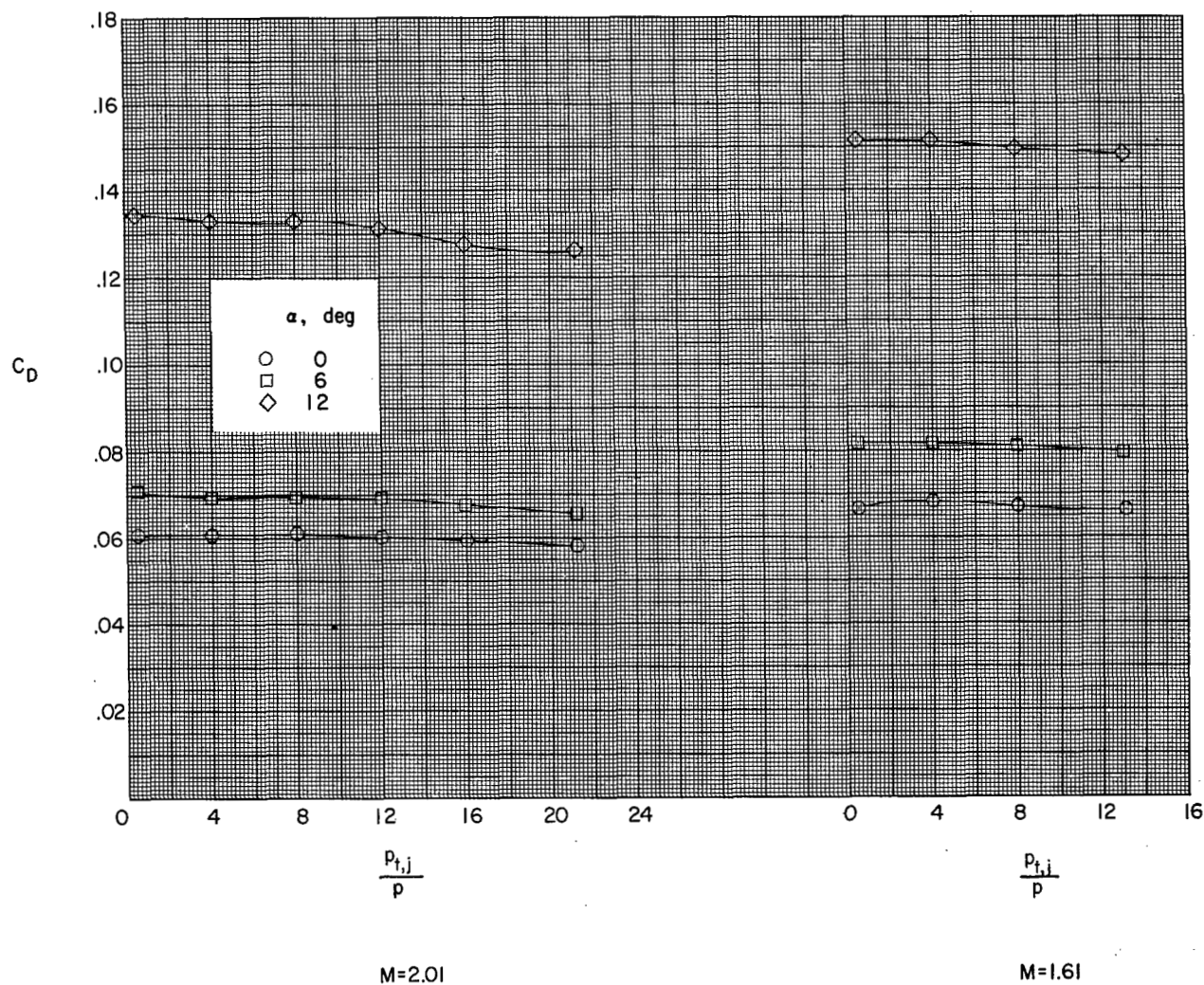
(b) Configuration 0141; large high tail;  $i_t = -3^\circ$ .

Figure 6.- Continued.



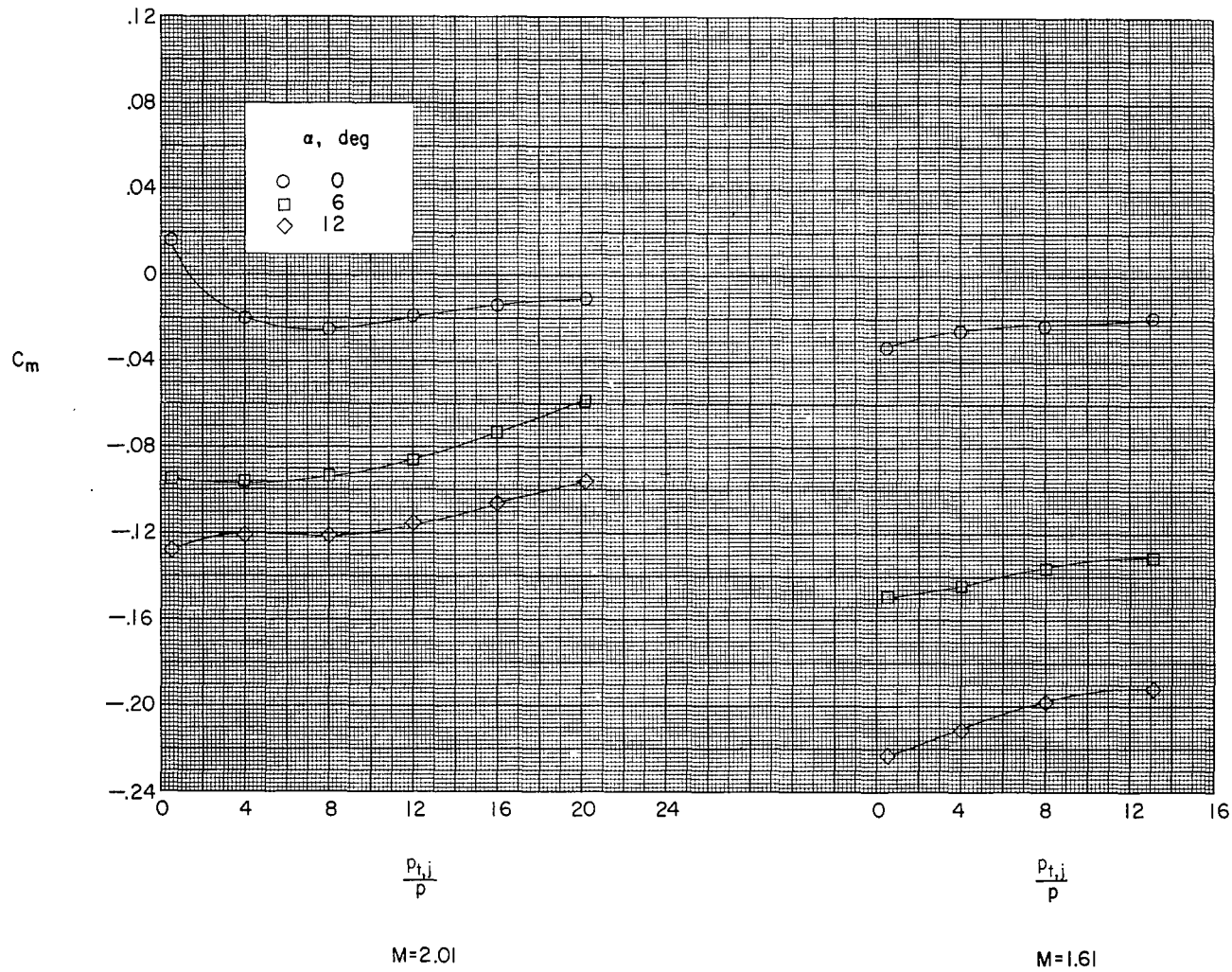
(c) Configuration 0151; small high tail.

Figure 6.- Continued.



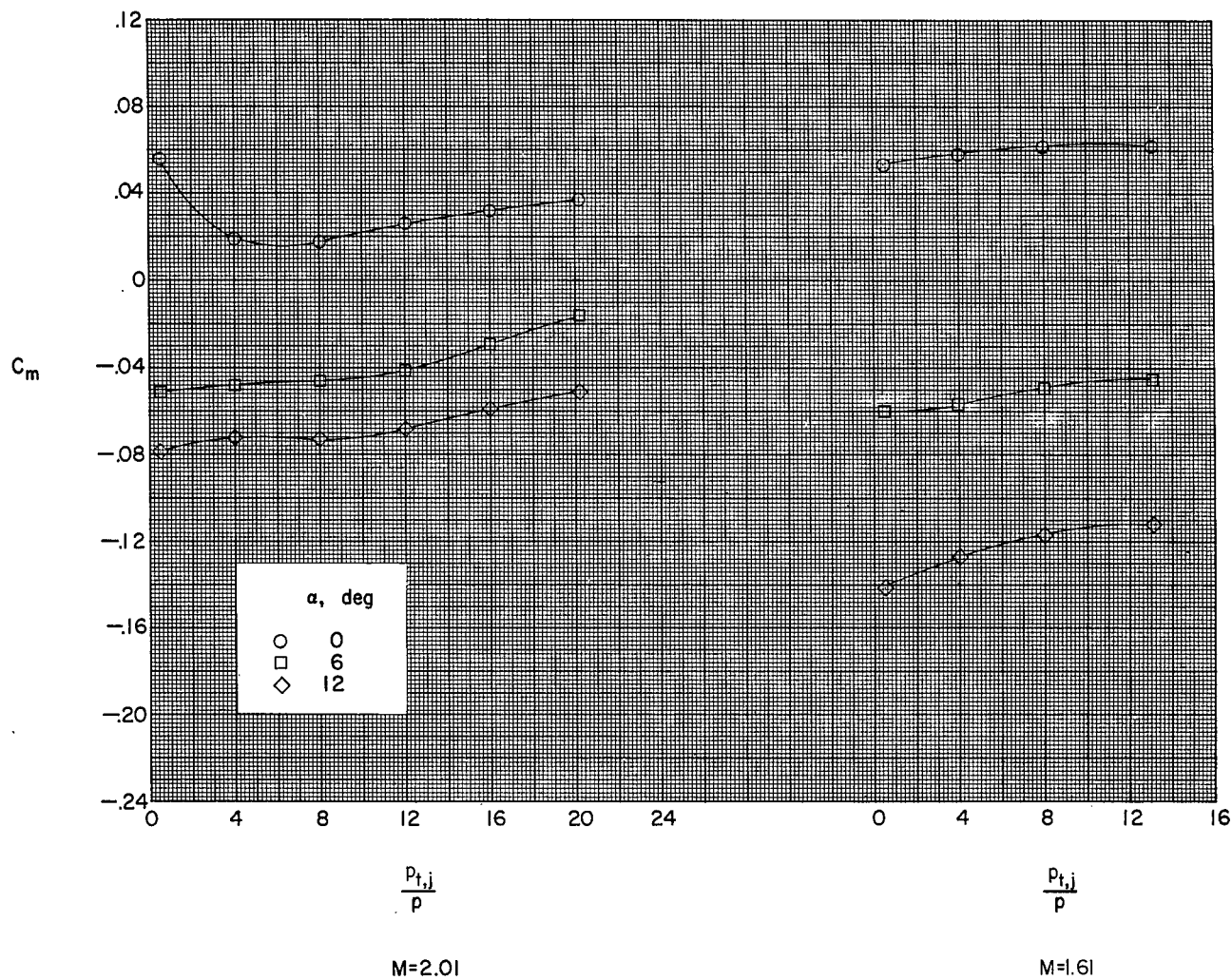
(d) Configuration 0051; no canopy; small high tail.

Figure 6.- Concluded.



(a) Configuration 0131; large high tail;  $i_t = 0^\circ$ .

Figure 7.- Variations of the semispan model pitching-moment coefficient with jet-pressure ratio.

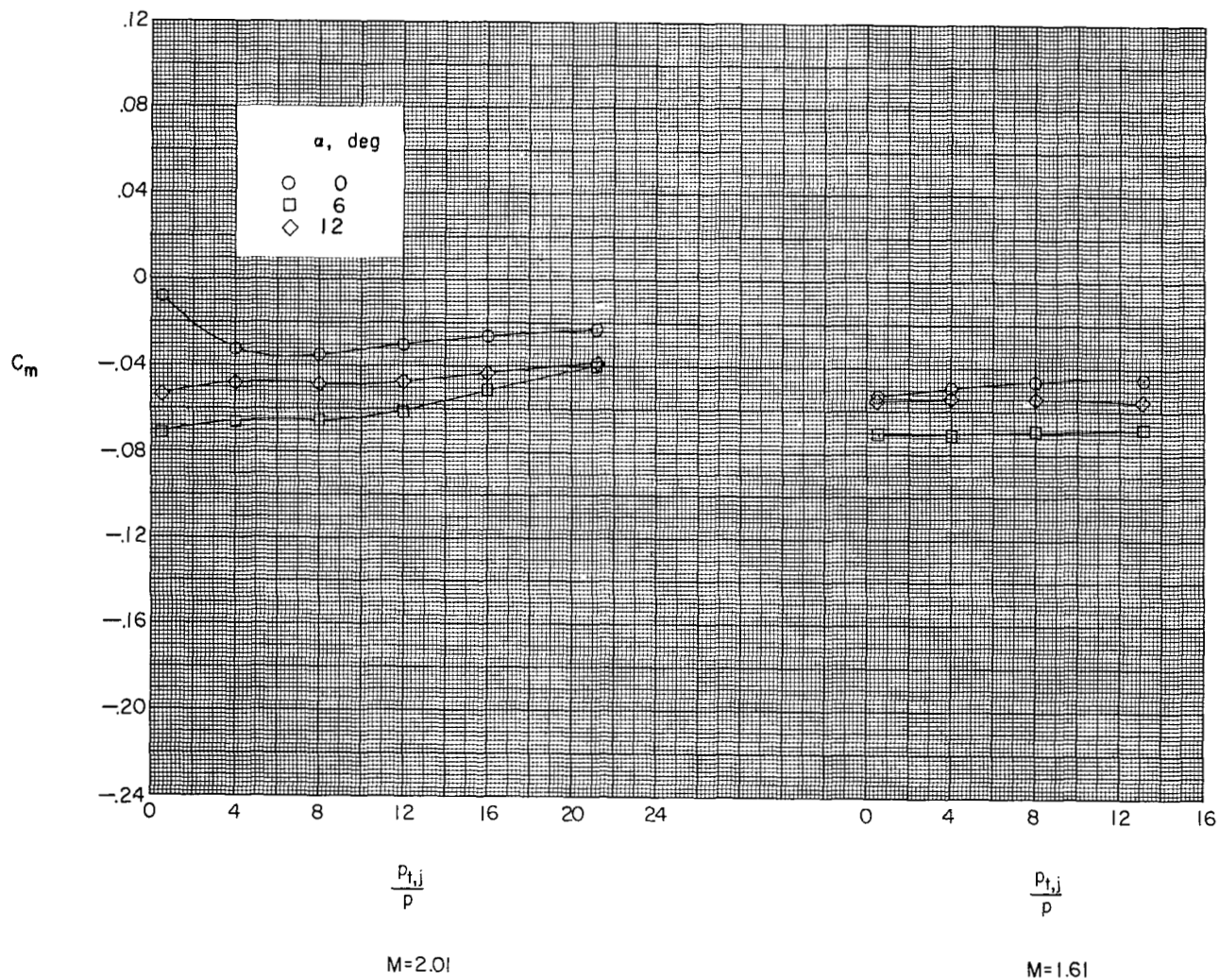


(b) Configuration 0141; large high tail;  $i_t = -3^\circ$ .

Figure 7.- Continued.

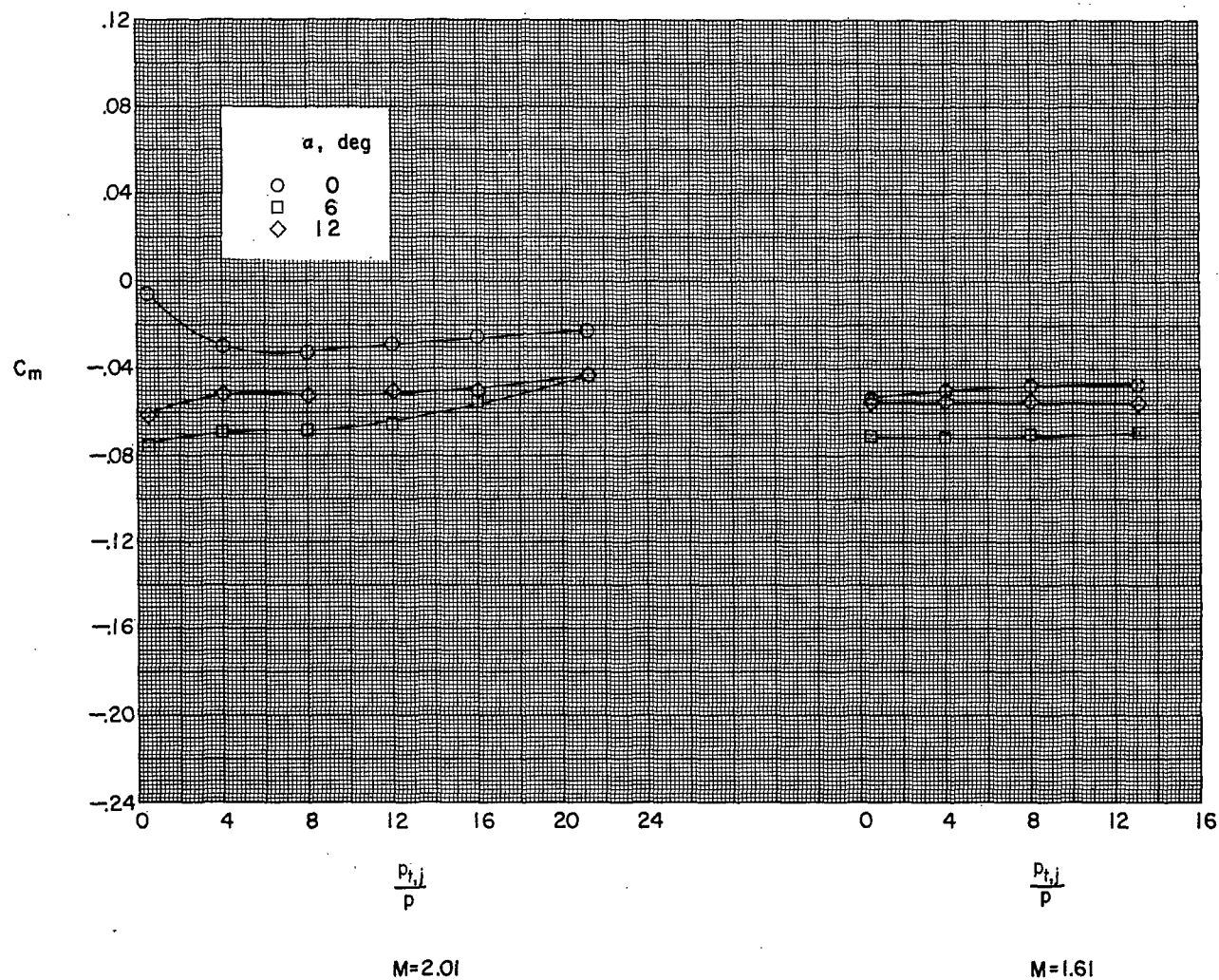


~~CONFIDENTIAL~~



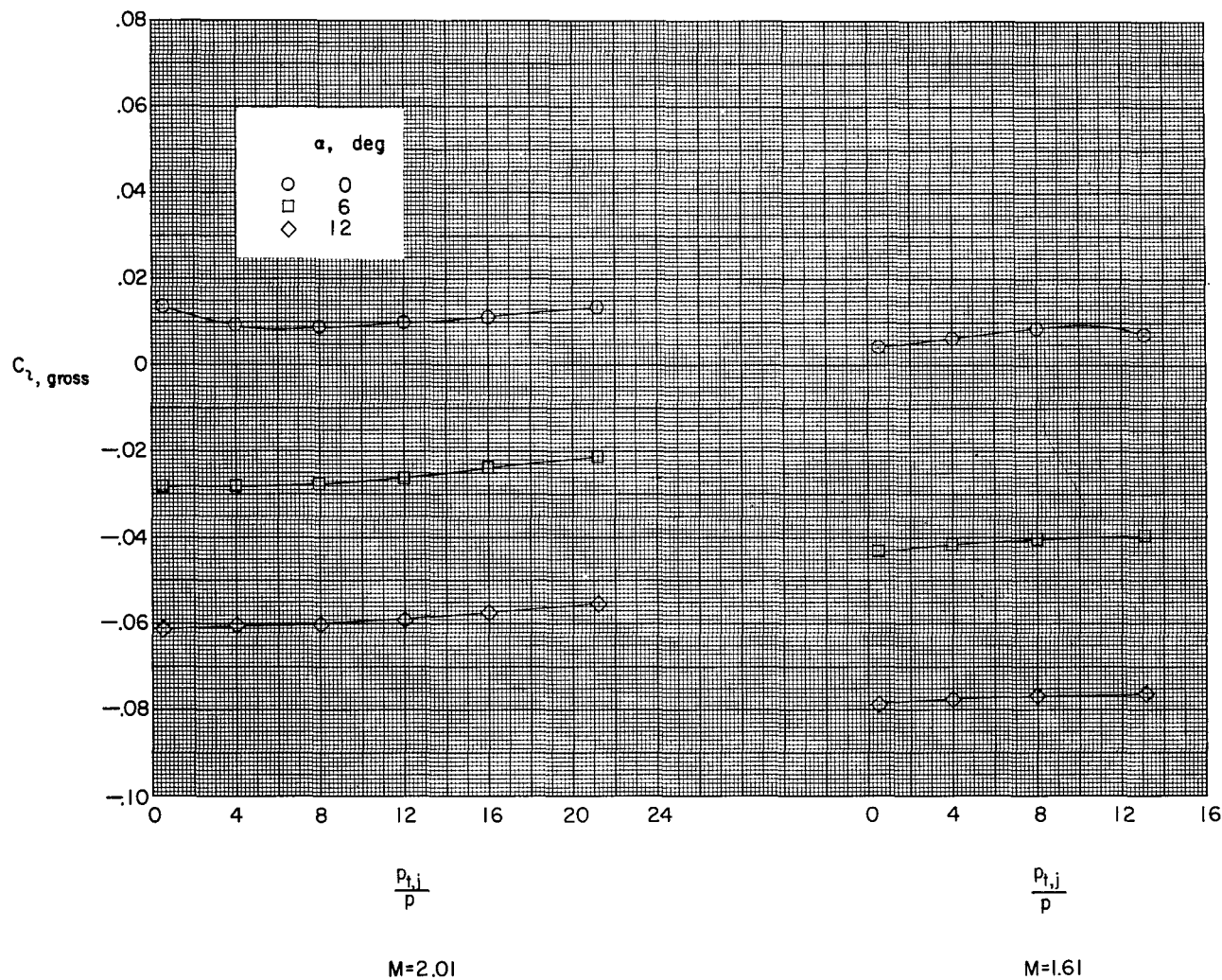
(c) Configuration 0151; small high tail.

Figure 7.- Continued.



(d) Configuration 0051; no canopy; small high tail.

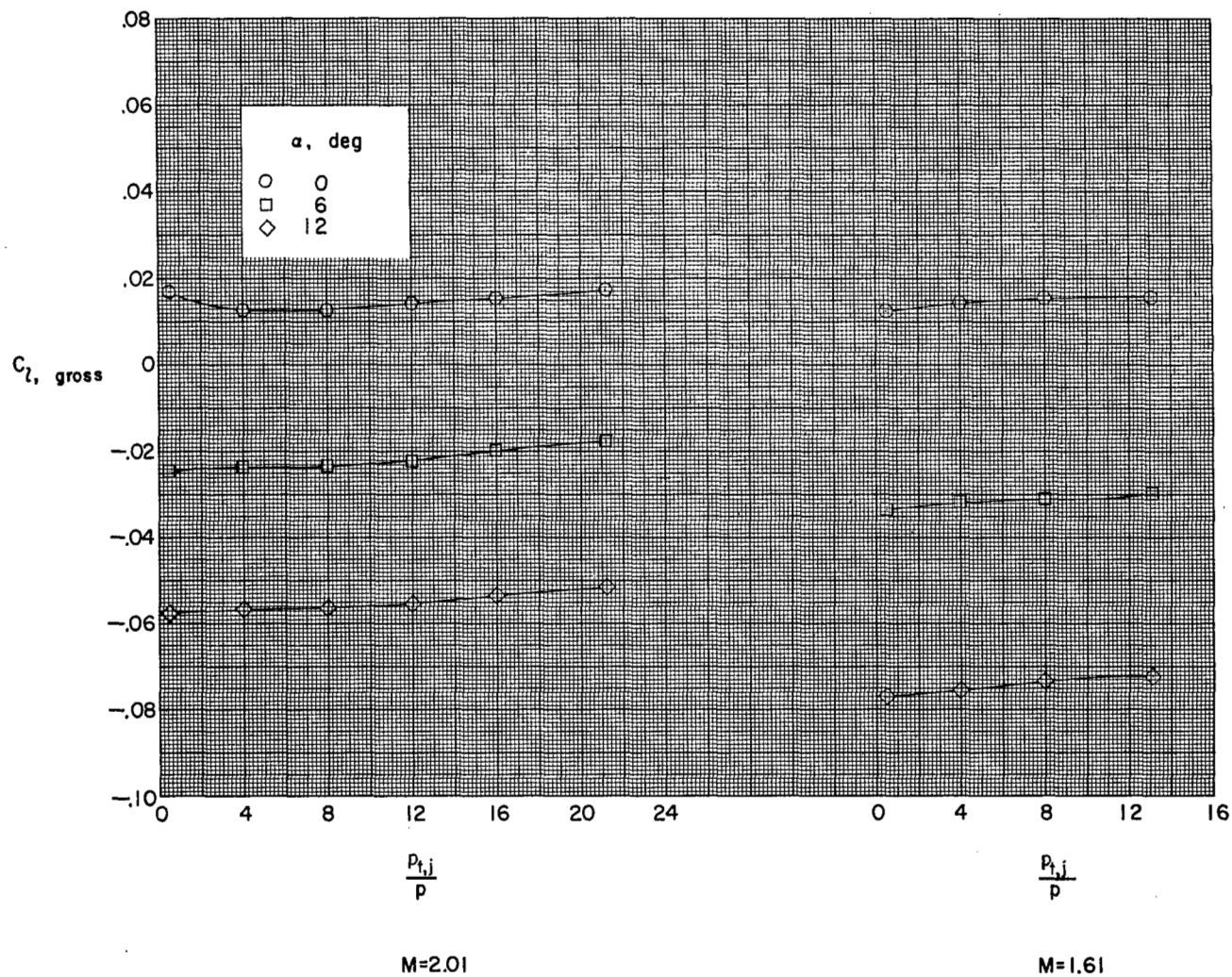
Figure 7.- Concluded.



(a) Configuration 0131; large high tail;  $i_t = 0^\circ$ .

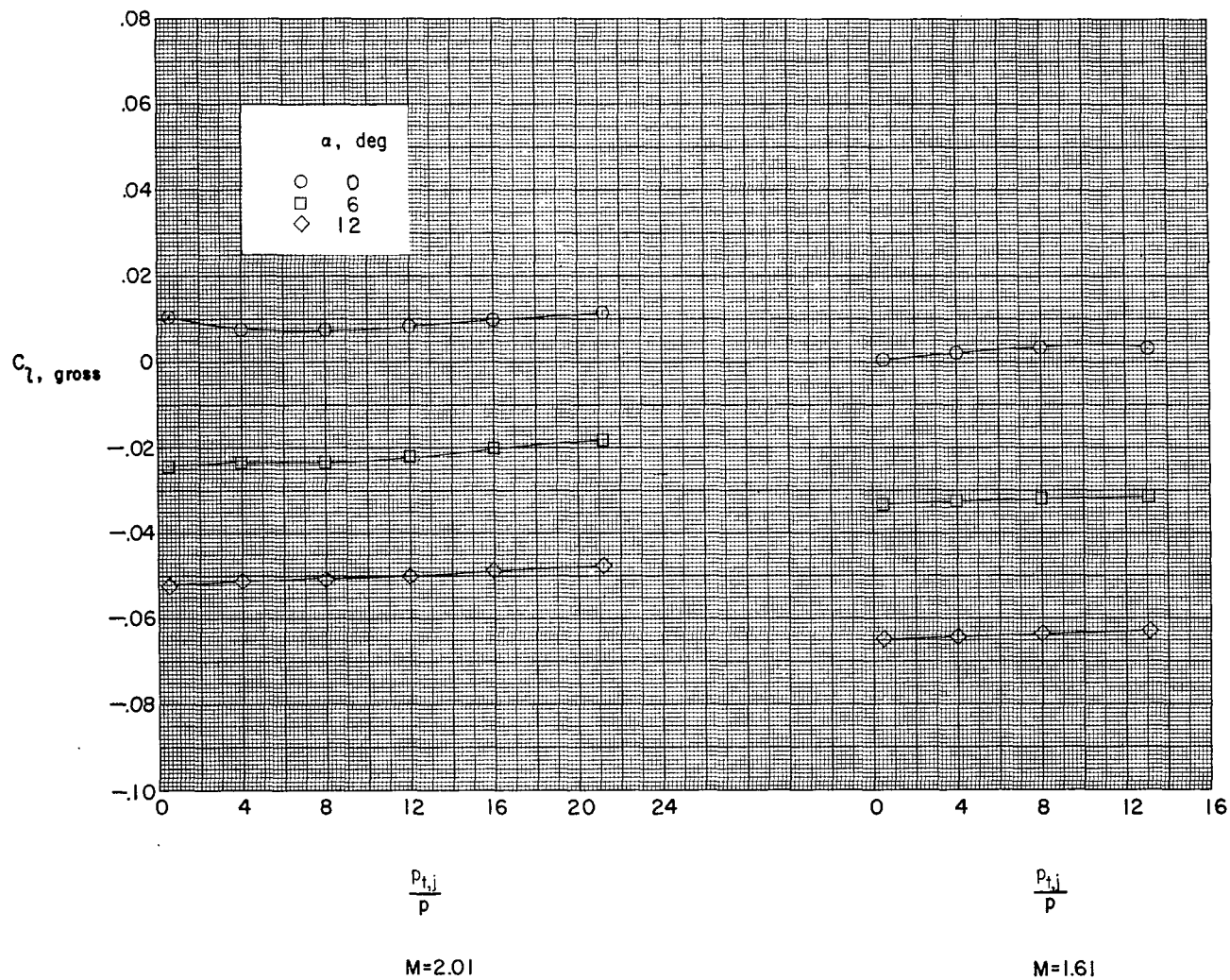
Figure 8.- Variations of the semispan model rolling-moment coefficient with jet-pressure ratio.





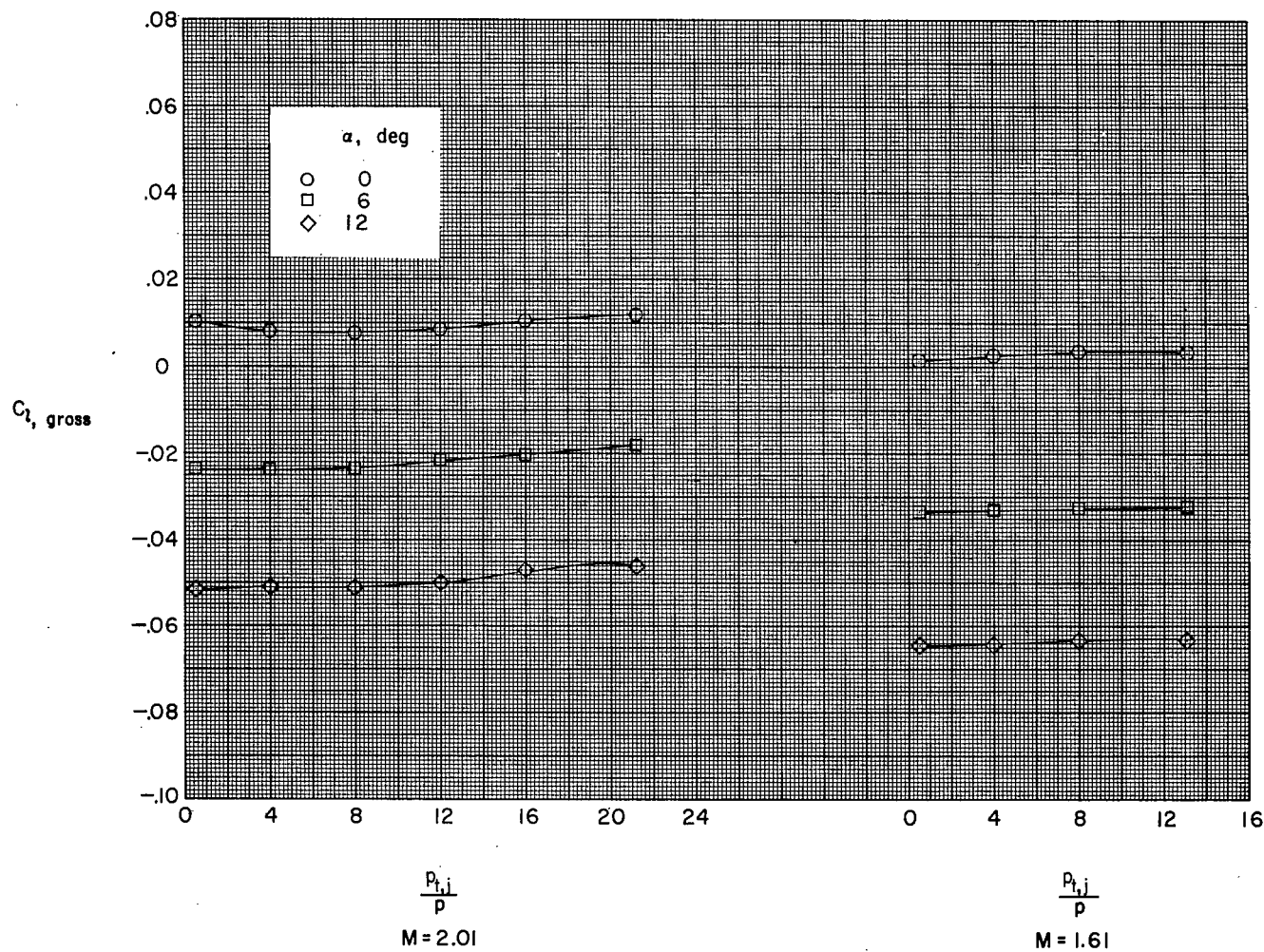
(b) Configuration 0141; large high tail;  $i_t = -3^\circ$ .

Figure 8.- Continued.



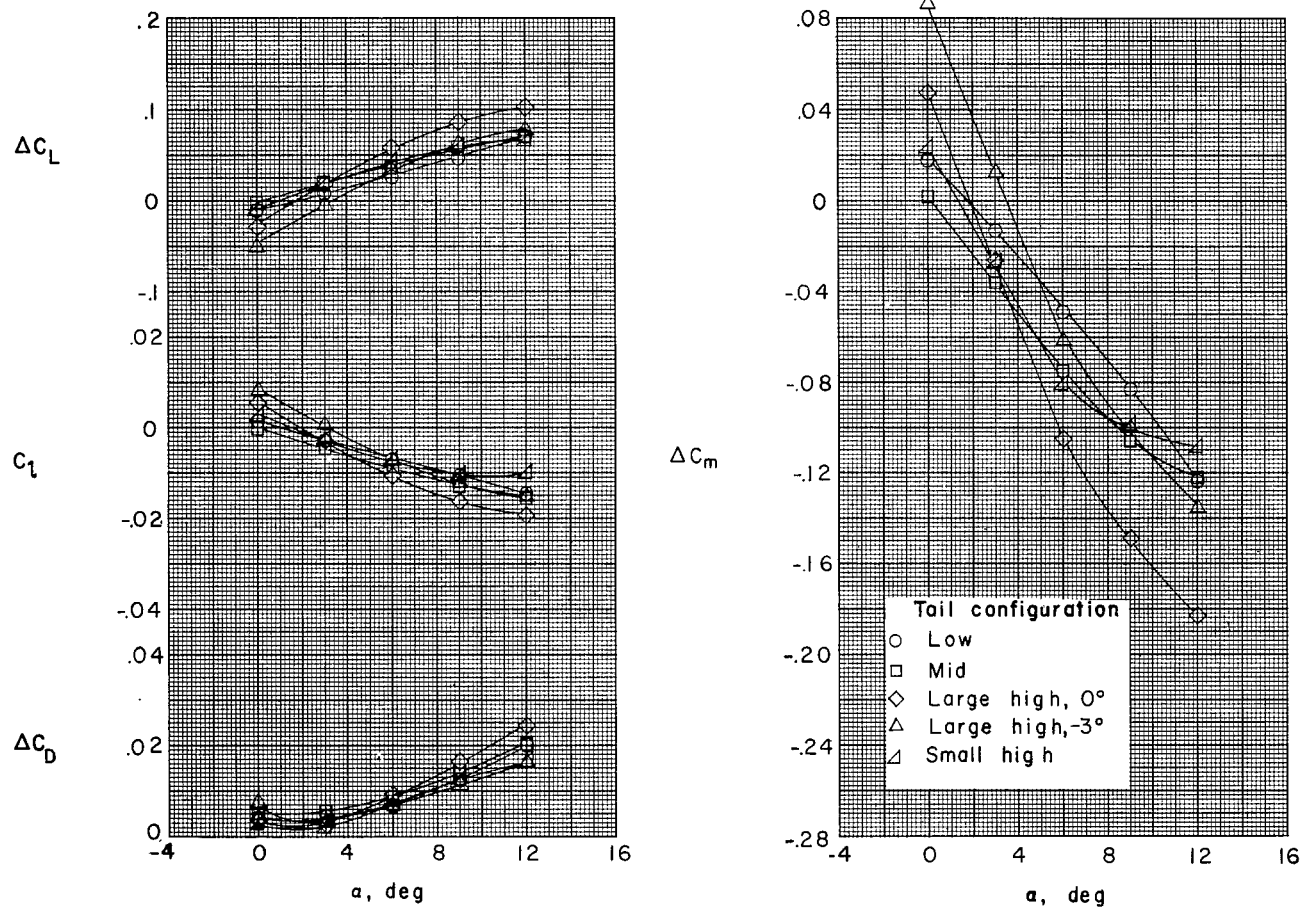
(c) Configuration 0151; small high tail.

Figure 8.- Continued.



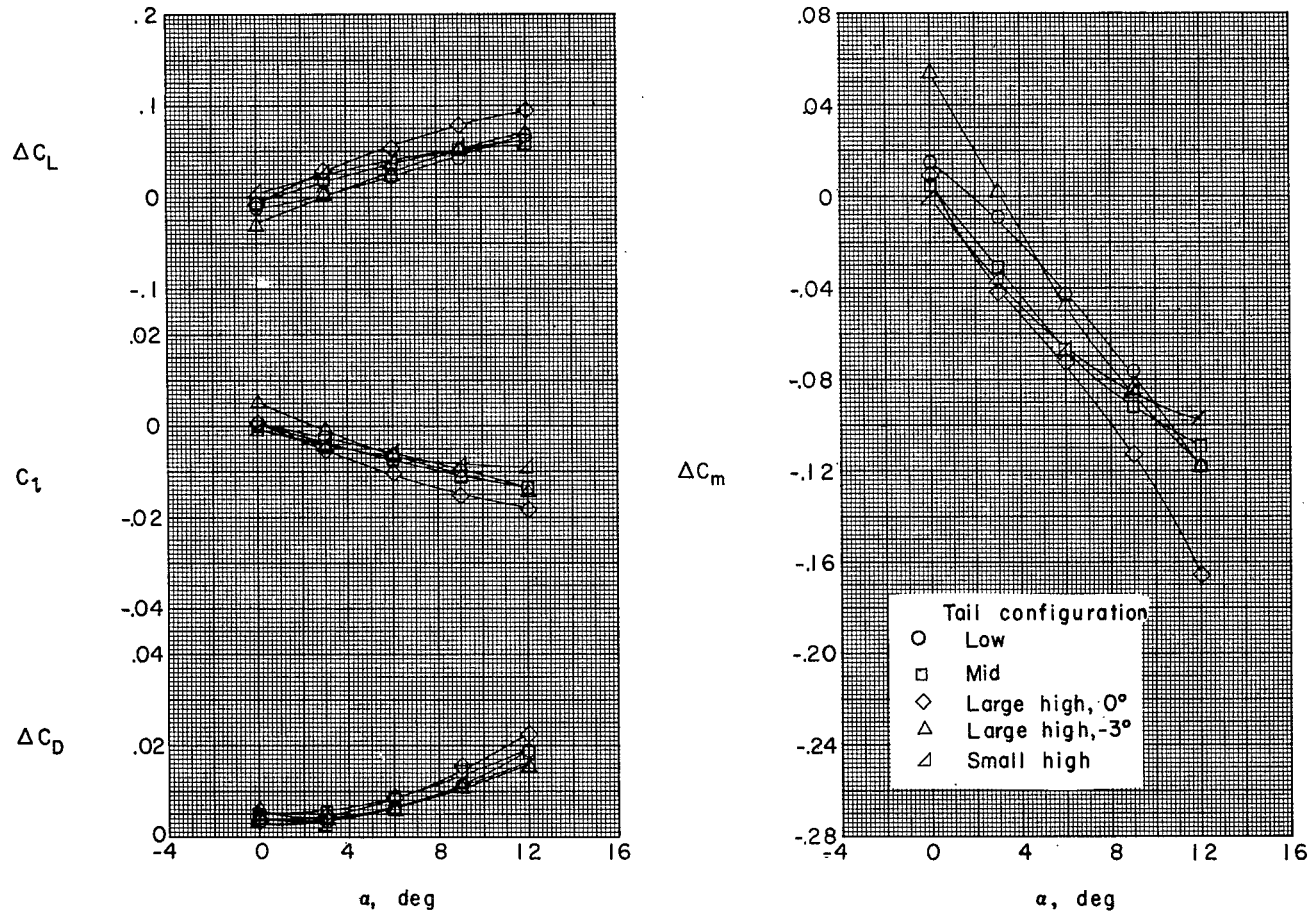
(d) Configuration 0051; no canopy; small high tail.

Figure 8.- Concluded.



(a)  $p_{t,j}/p = 0.5$ .

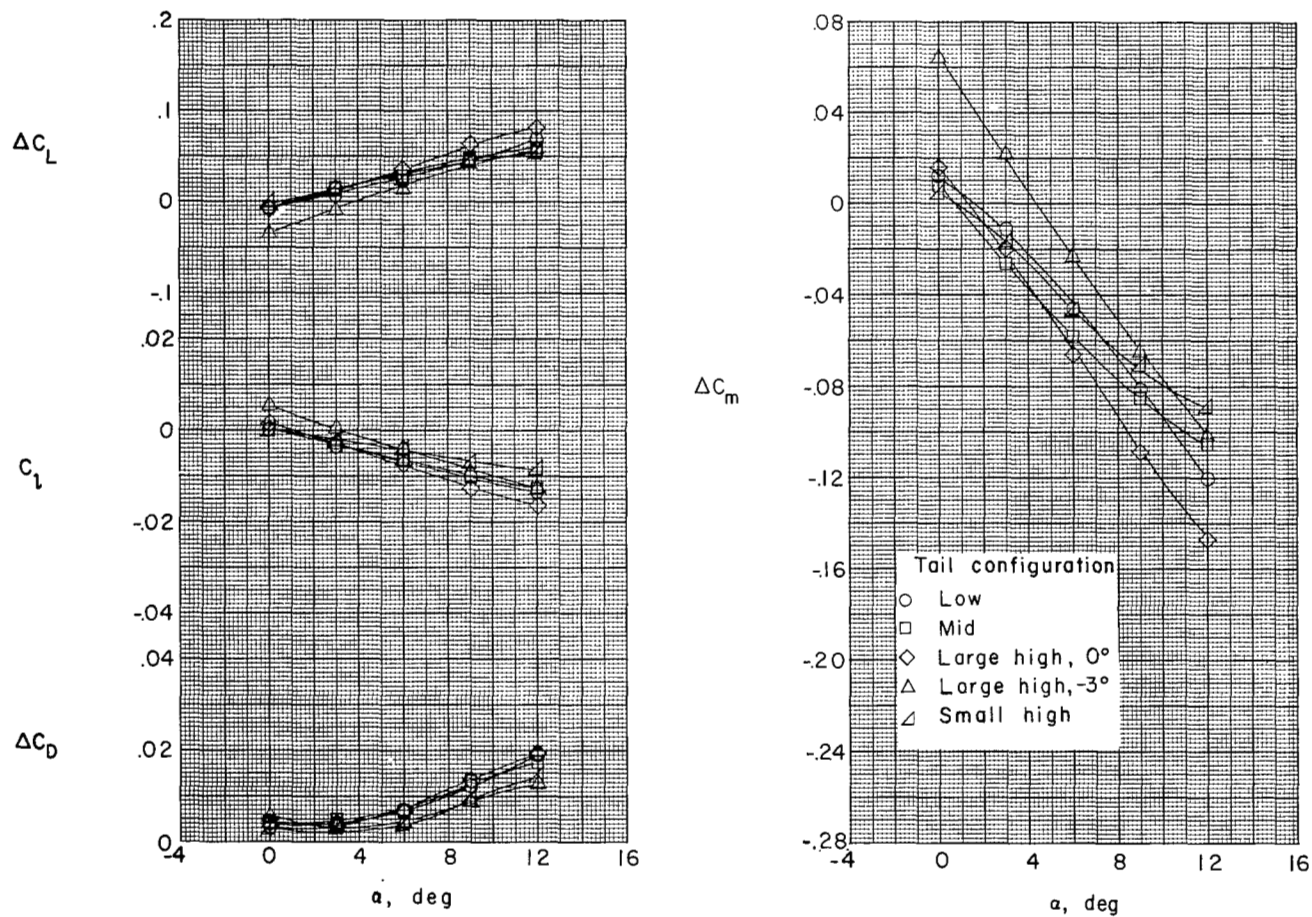
Figure 9.- Variations of the incremental coefficients due to the horizontal tail with angle of attack at  $M = 2.01$ .



(b)  $p_{t,j}/p = 12.0$ .

Figure 9.- Continued.

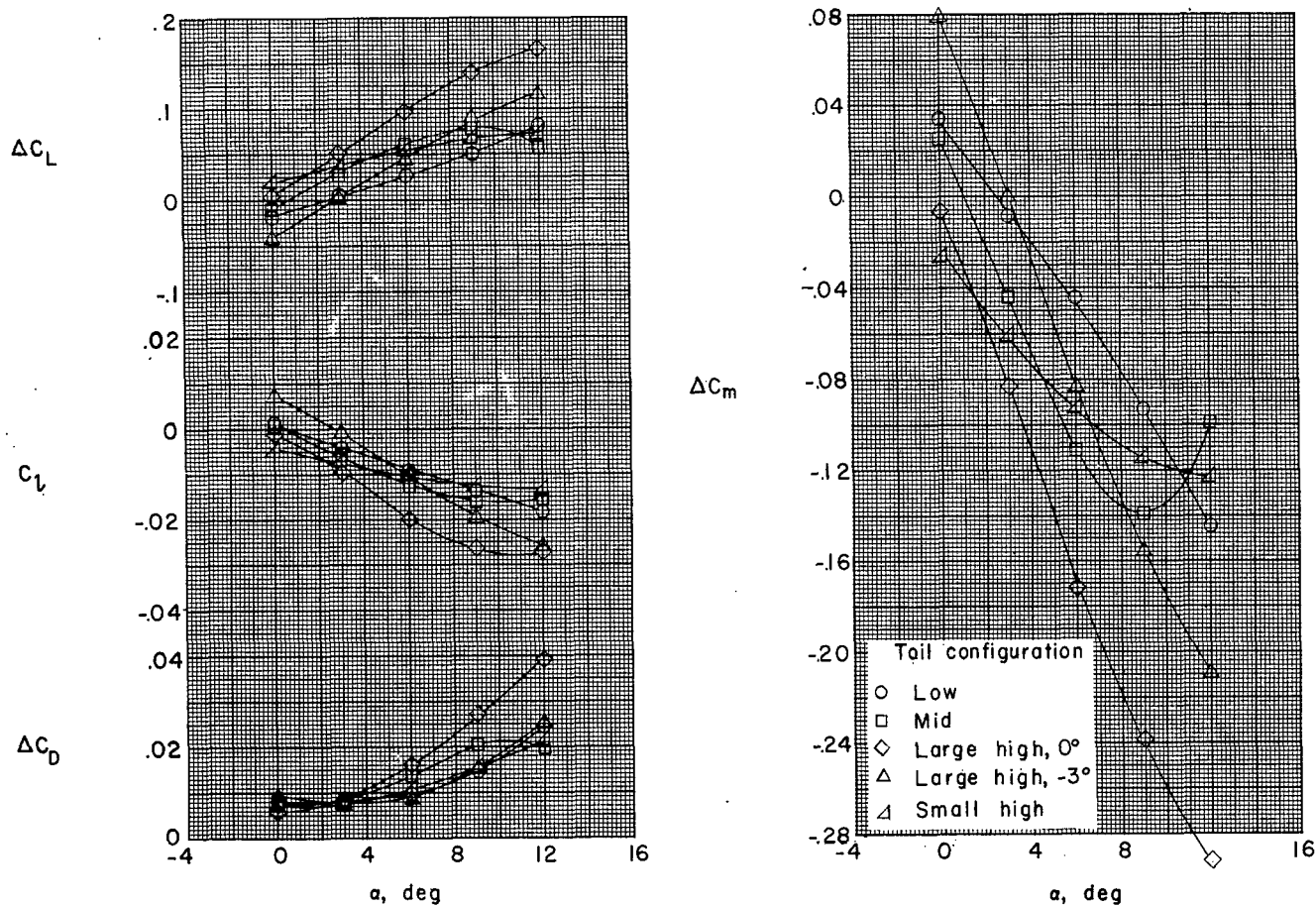
~~CONFIDENTIAL~~



(c)  $p_{t,j}/p = 21.2$ .

Figure 9.- Concluded.

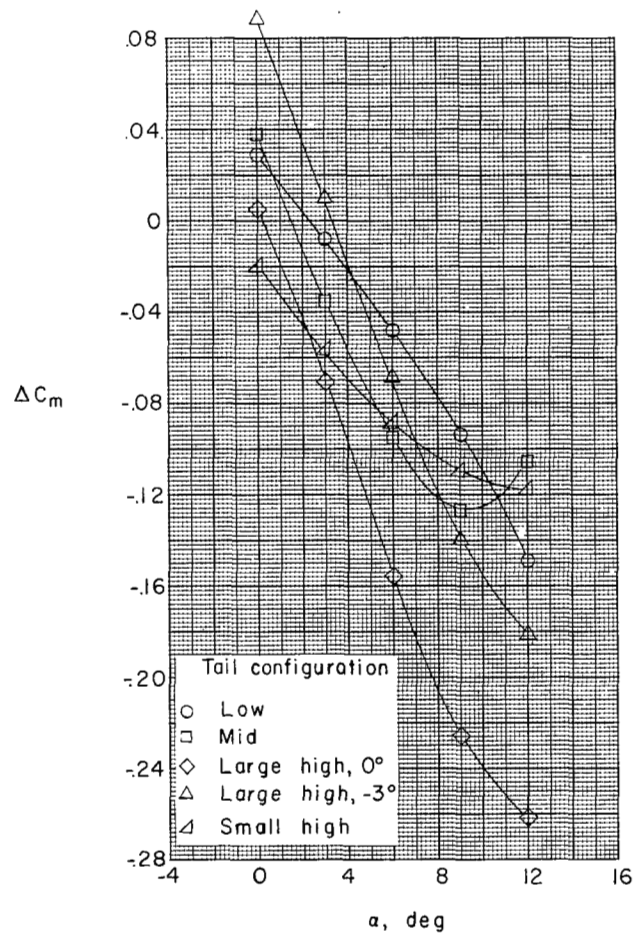
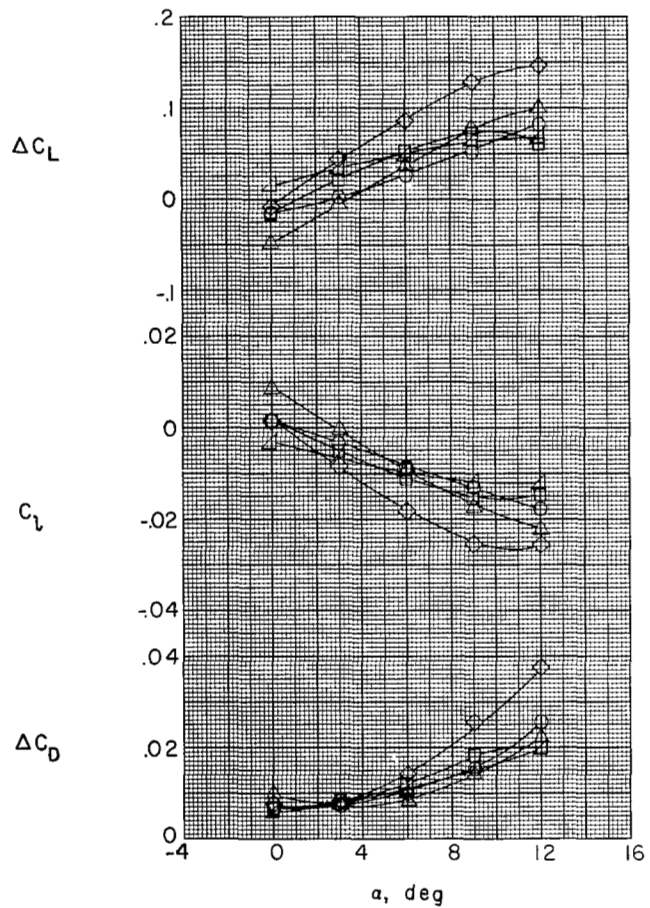




(a)  $p_{t,j}/p = 0.5$ .

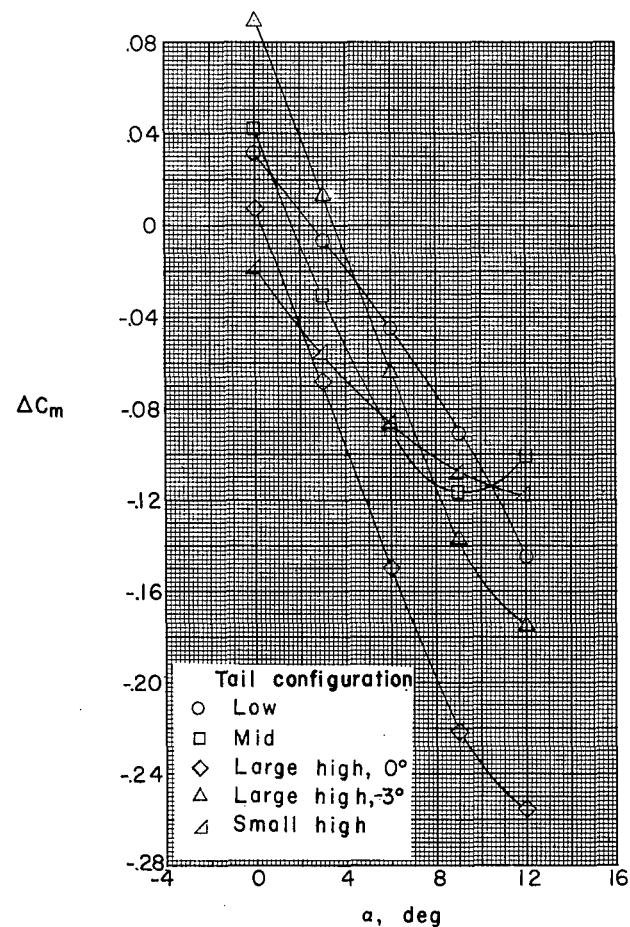
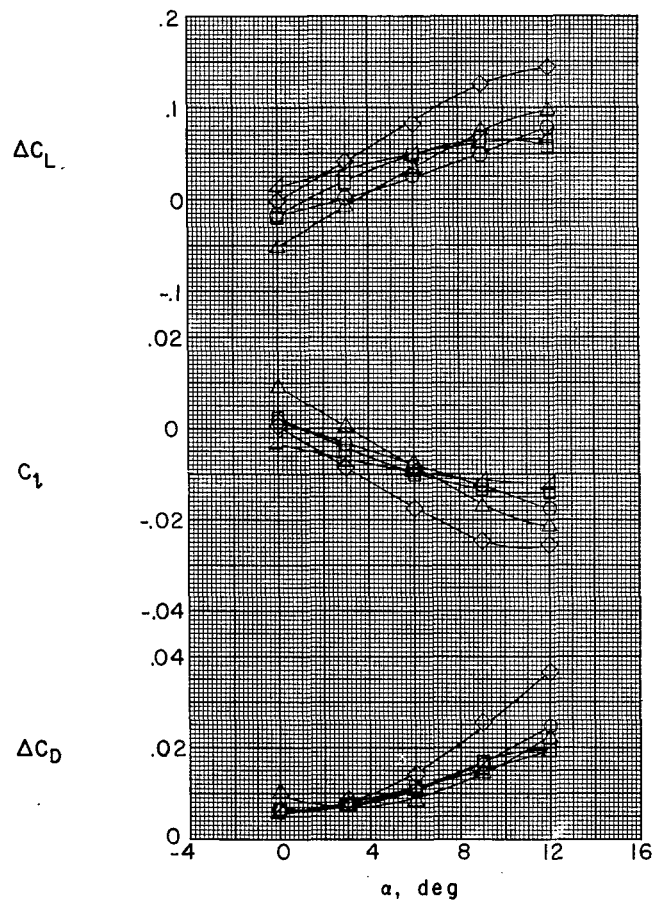
Figure 10.- Variations of the incremental coefficients due to the horizontal tail with angle of attack at  $M = 1.61$ .





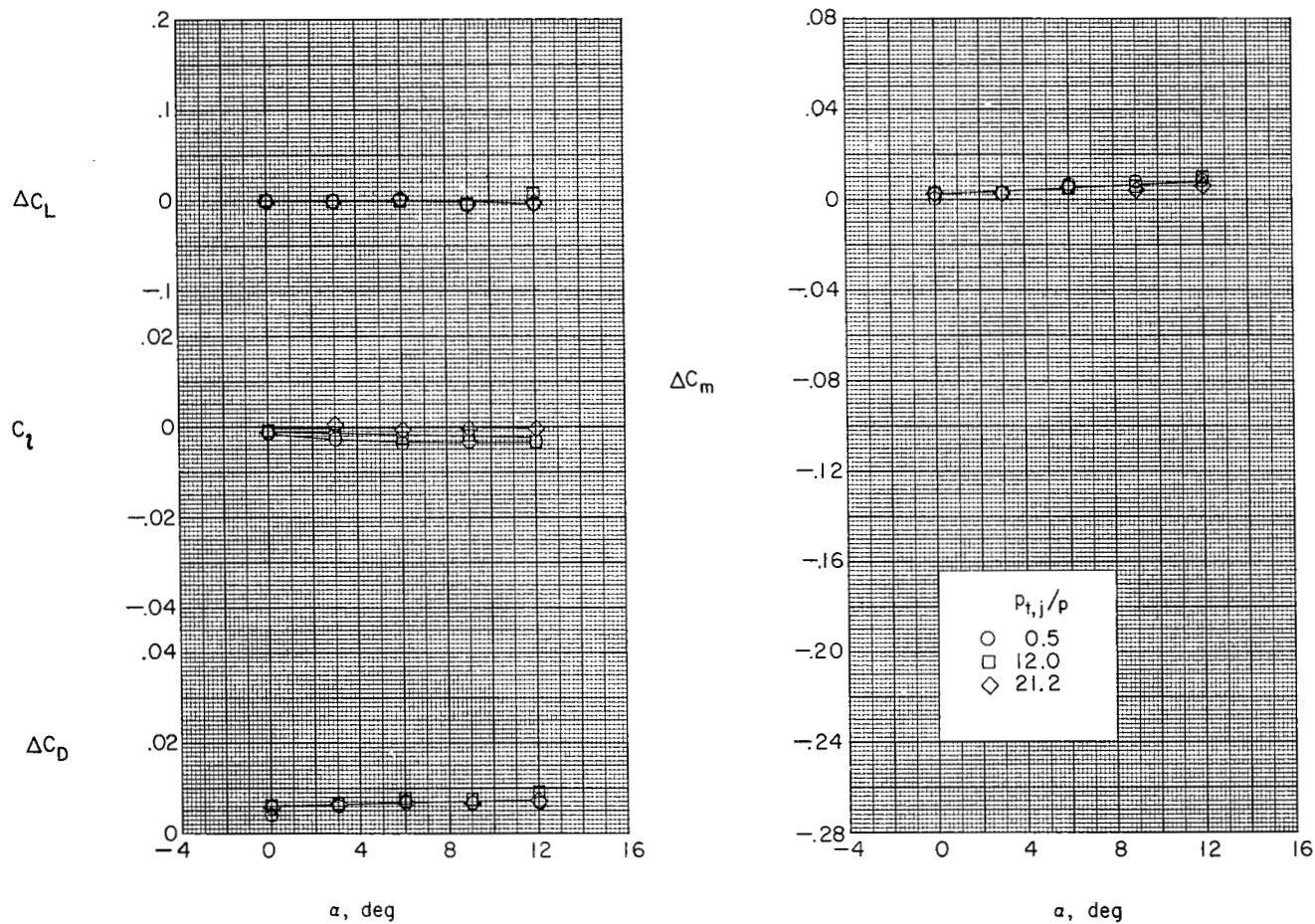
(b)  $P_{t,j}/P = 8.0$ .

Figure 10.- Continued.



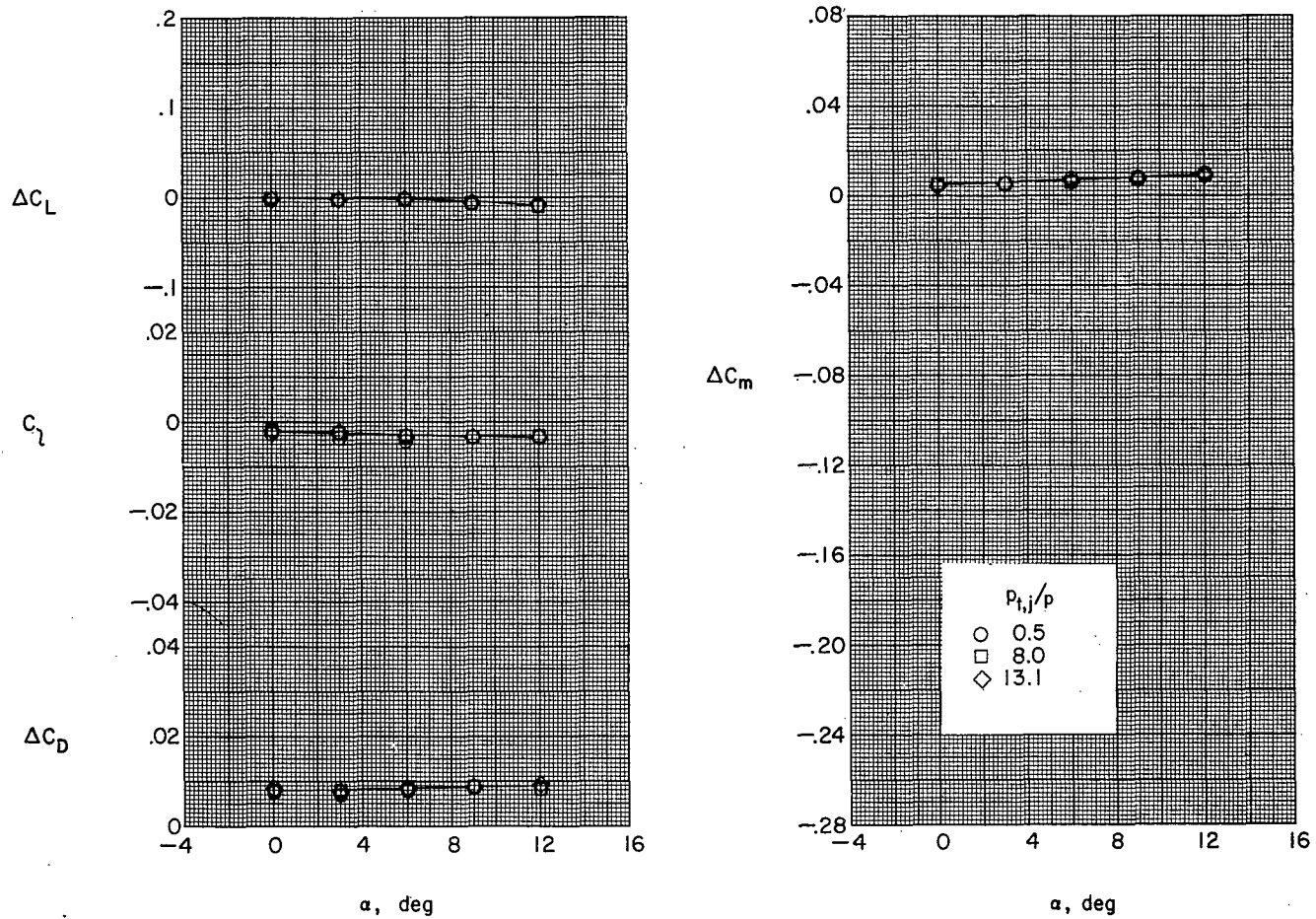
(c)  $p_{t,j}/p = 13.1$ .

Figure 10.- Concluded.



(a)  $M = 2.01$ .

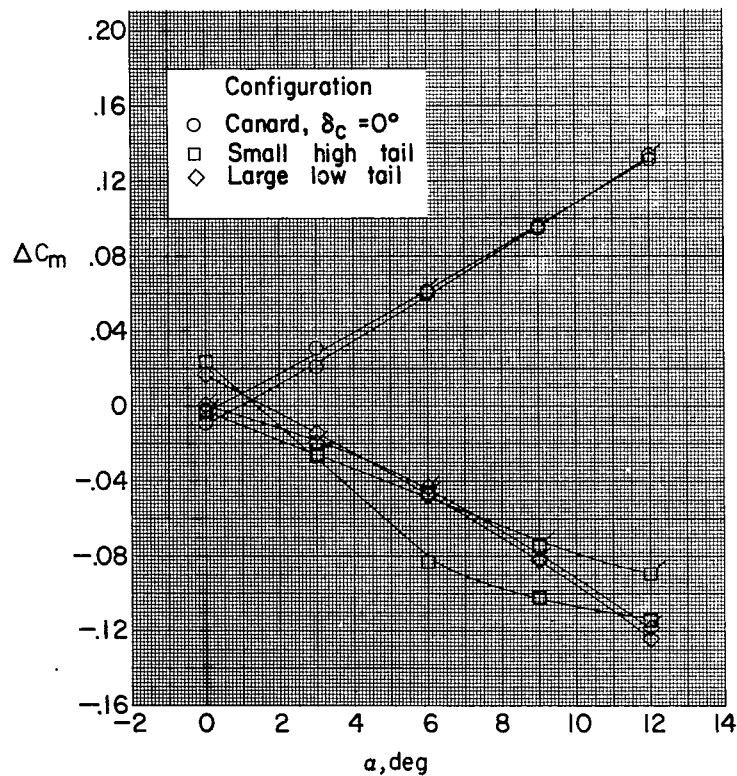
Figure 11.- Variations of the incremental coefficients due to the vertical tail with angle of attack.



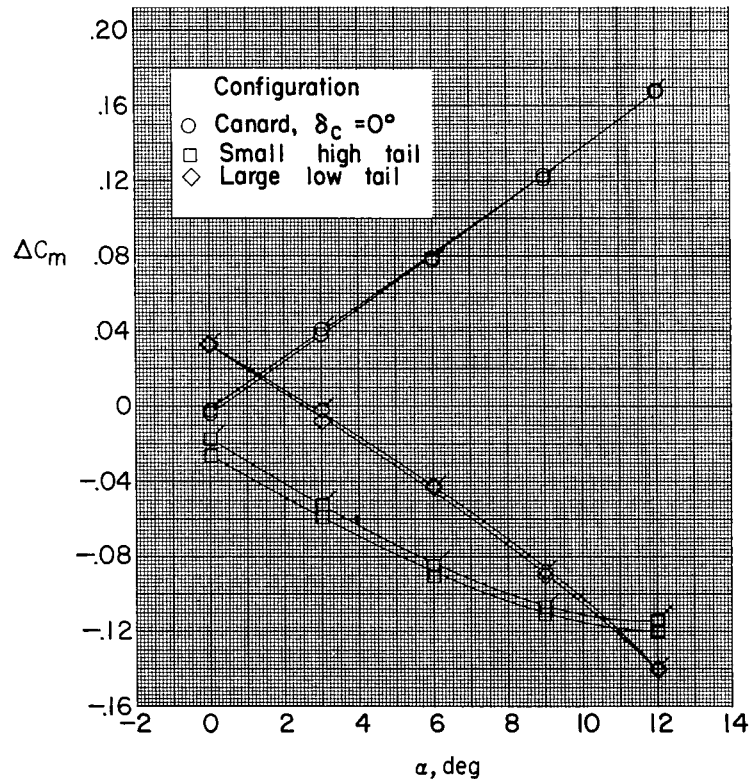
(b)  $M = 1.61$ .

Figure 11.- Concluded.

CONFIDENTIAL



$M=2.01$



$M=1.61$

Figure 12.- Comparison of the incremental pitching-moment coefficients with angle of attack for the canard configuration with those of two of the tail configurations. Plain symbols, jet off; flagged symbols, maximum jet pressure.

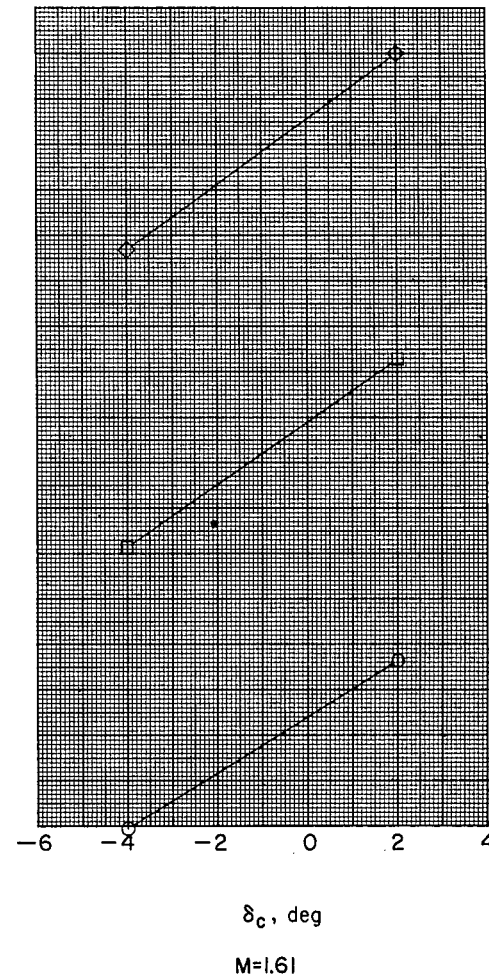
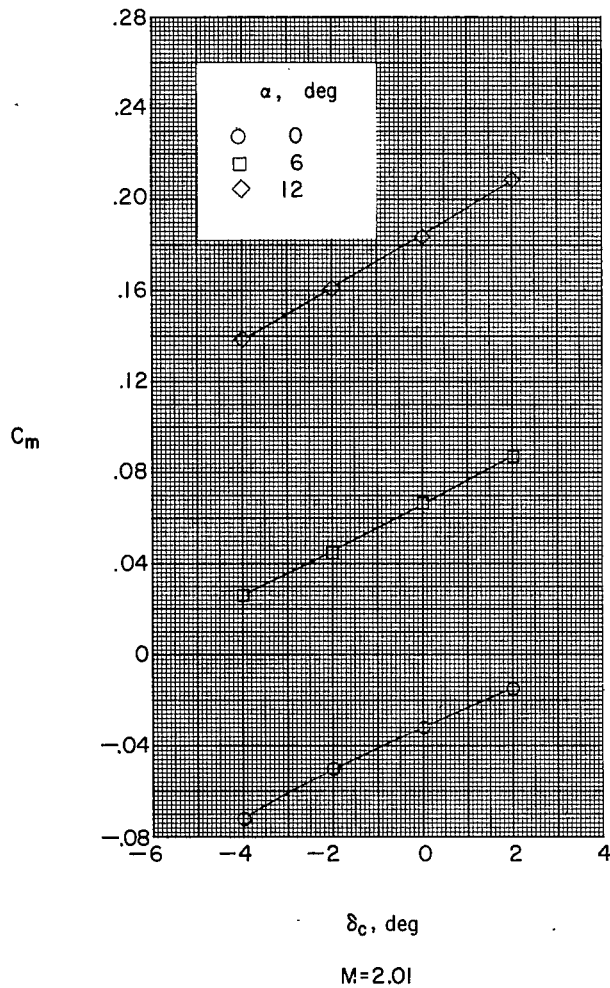


Figure 13.- Variation of the model pitching-moment coefficient with canard deflection. Jet off; no canopy; no horizontal tail.



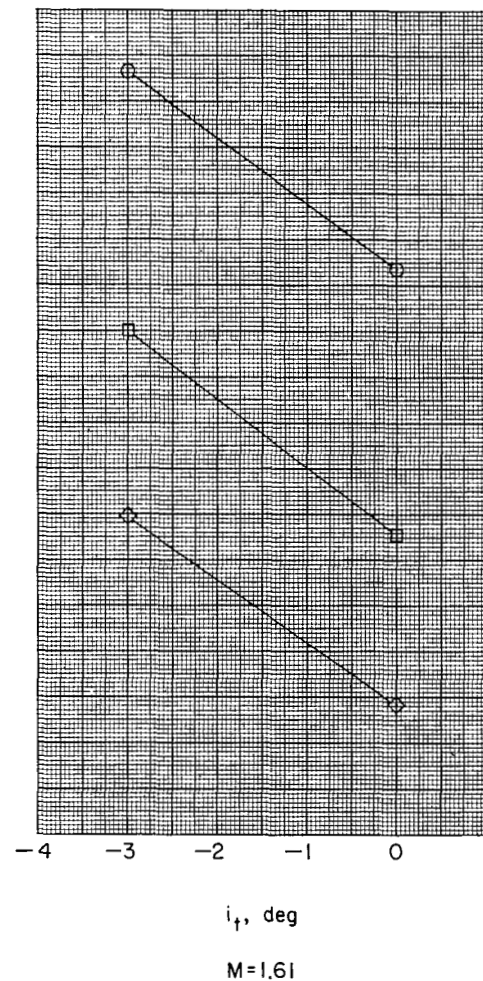
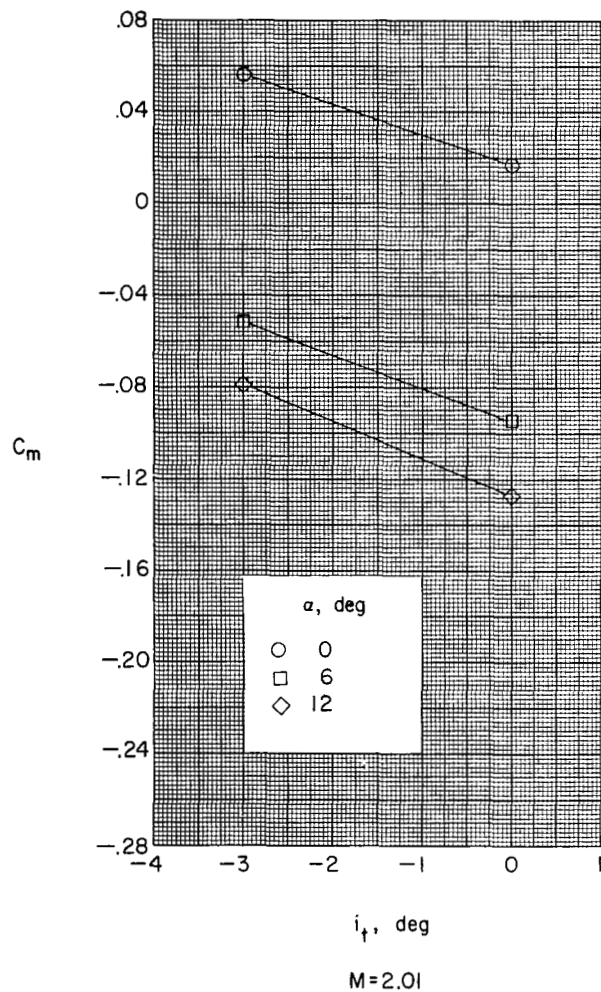


Figure 14.- Variation of the model pitching-moment coefficient with horizontal-tail deflection.  
Jet off; large high tail.

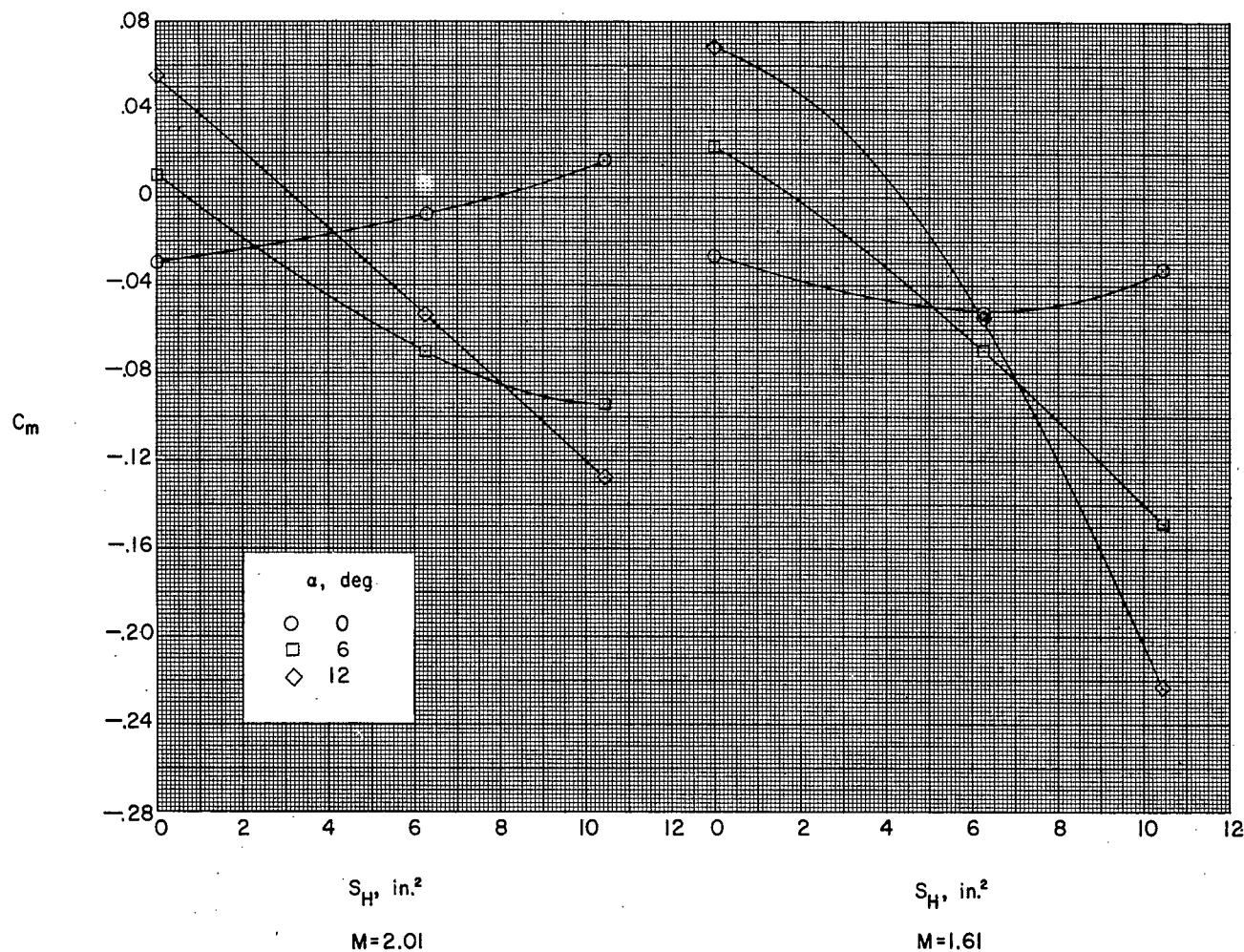
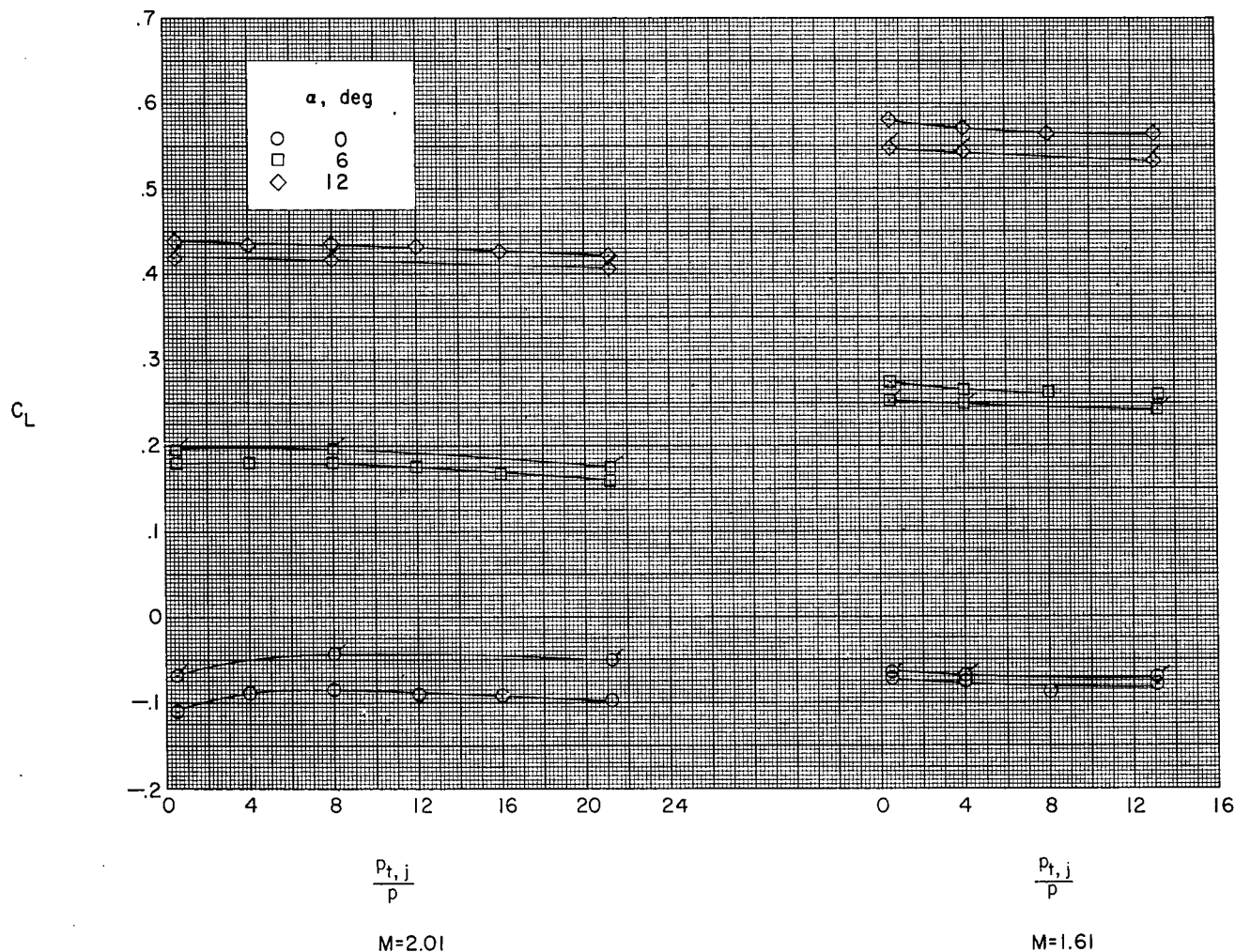
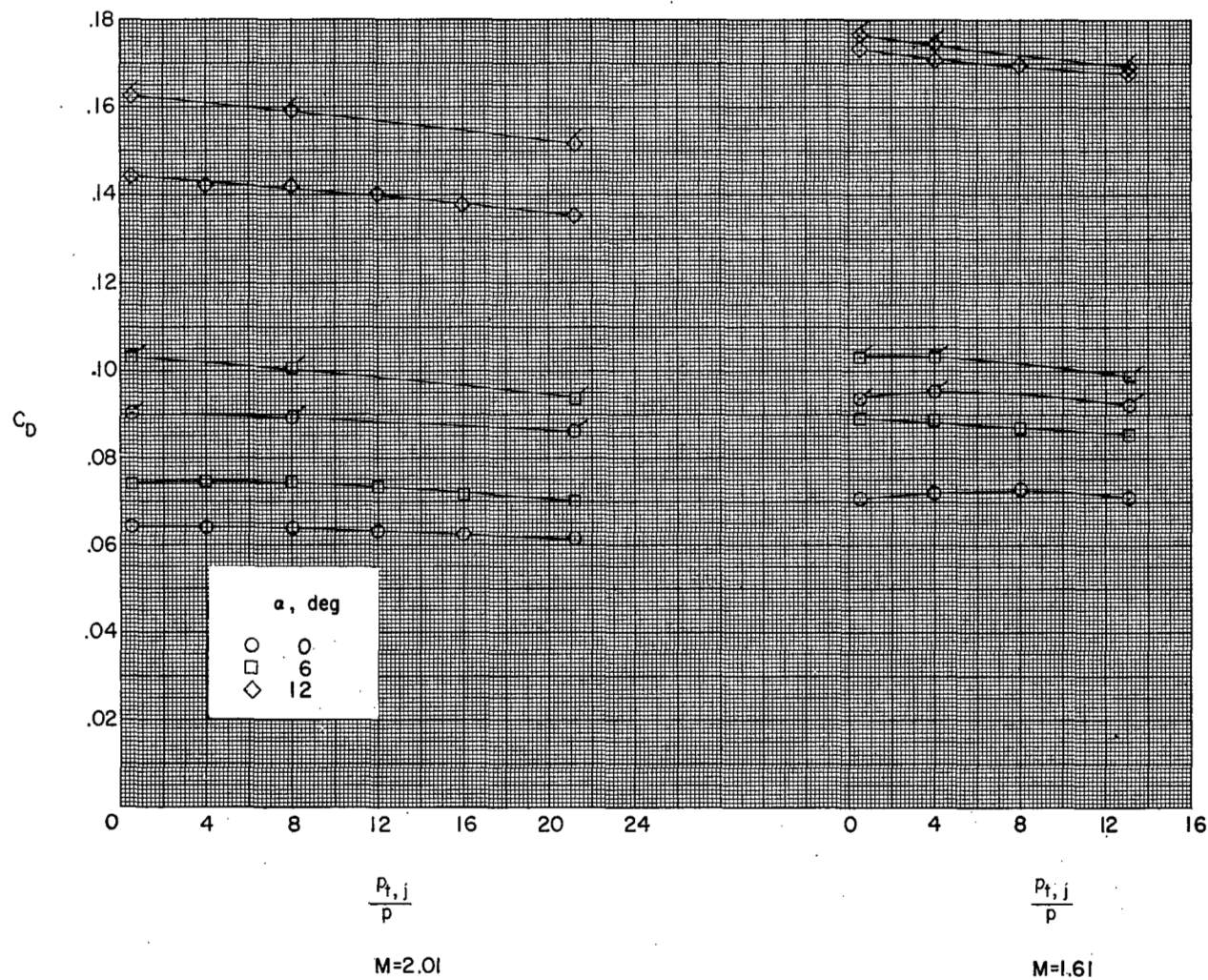


Figure 15.- Variation of the model pitching-moment coefficient with horizontal-tail area. Jet off; high tails;  $i_t = 0^\circ$ .



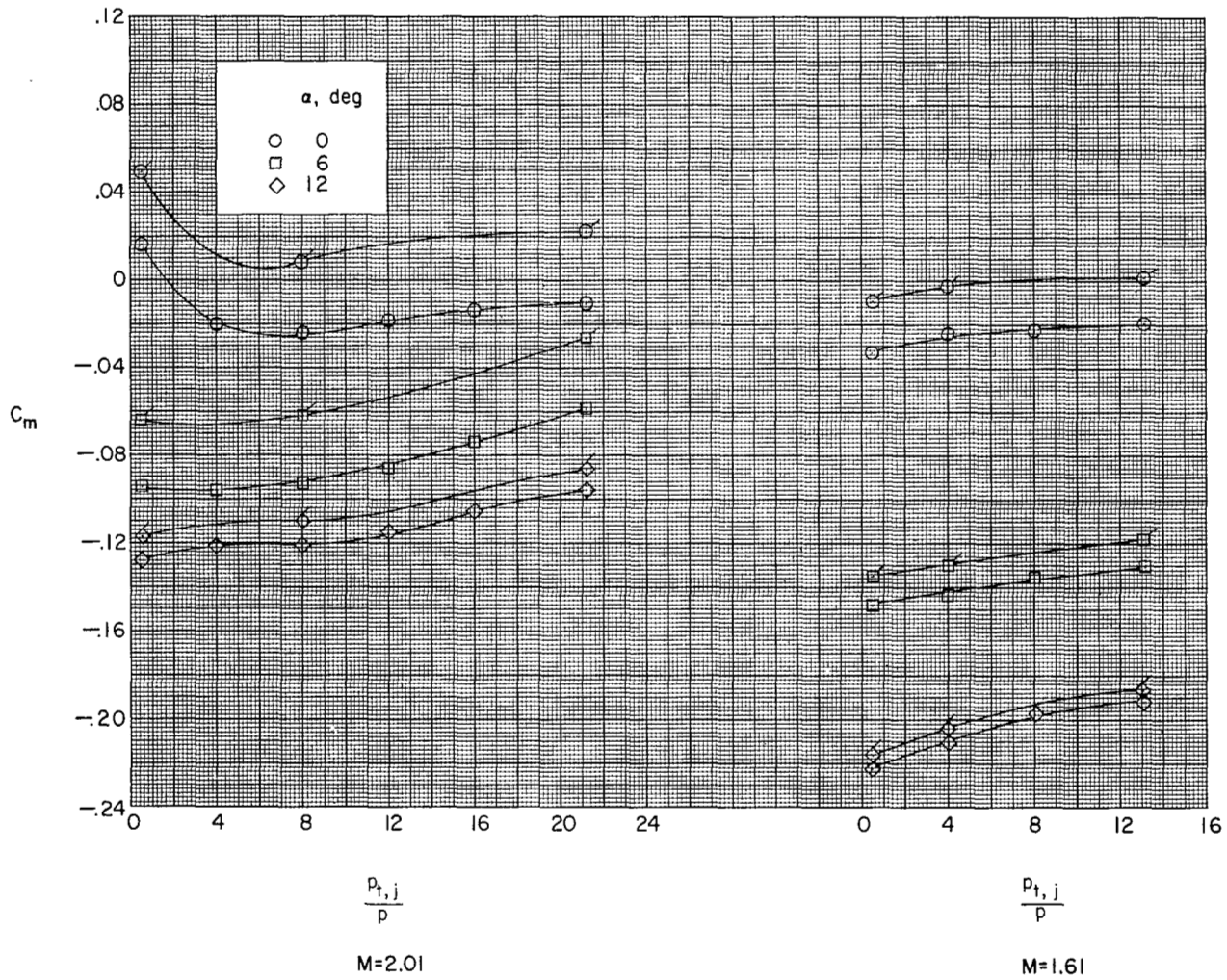
(a) Lift coefficient.

Figure 16.- Variation of the lift, drag, pitching-moment, and rolling-moment coefficients with jet-pressure ratio for configuration 0131 with and without inlet simulation. Flagged symbols indicate inlet closed.



(b) Drag coefficient.

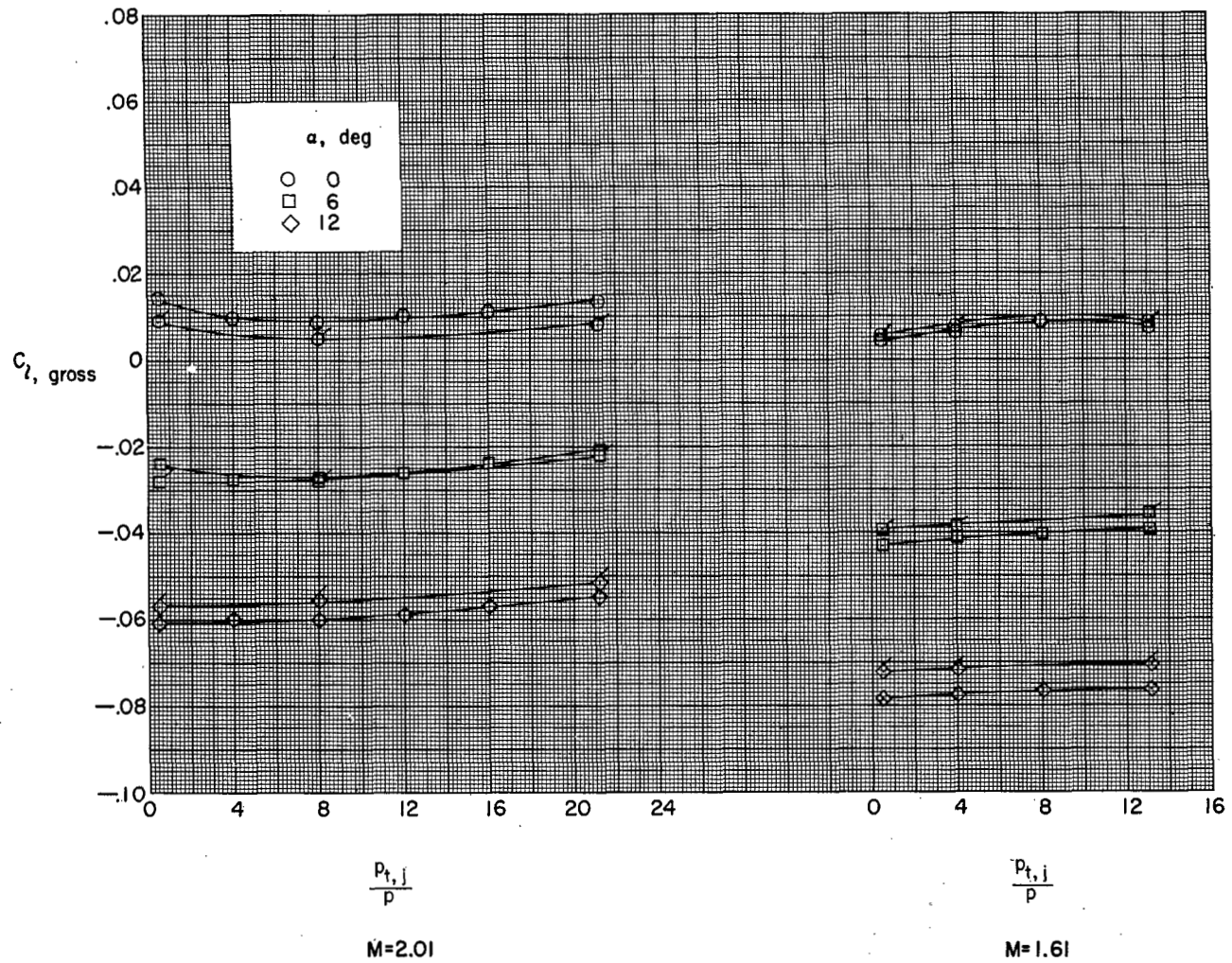
Figure 16.- Continued.



(c) Pitching-moment coefficient.

Figure 16.- Continued.

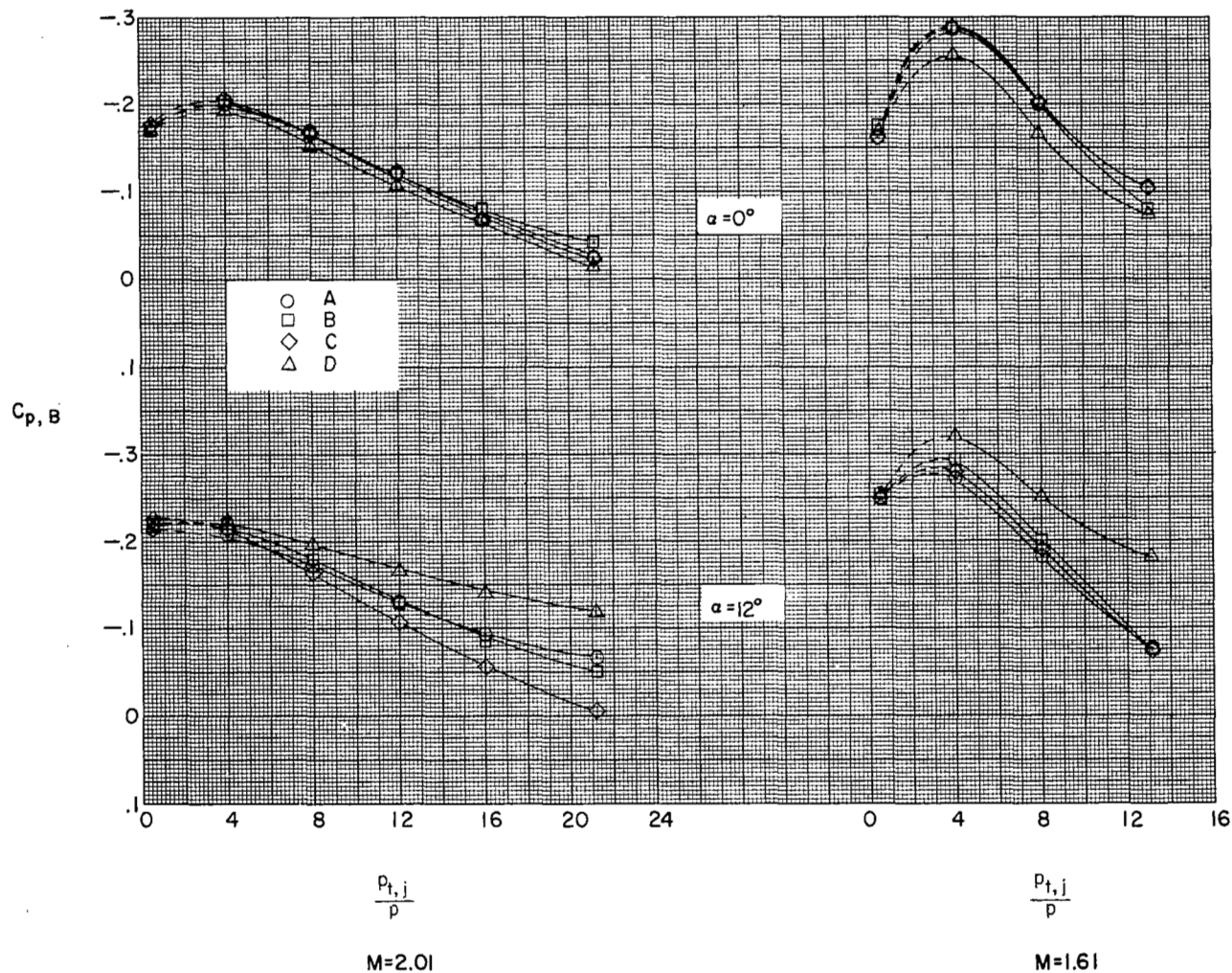




(d) Rolling-moment coefficient.

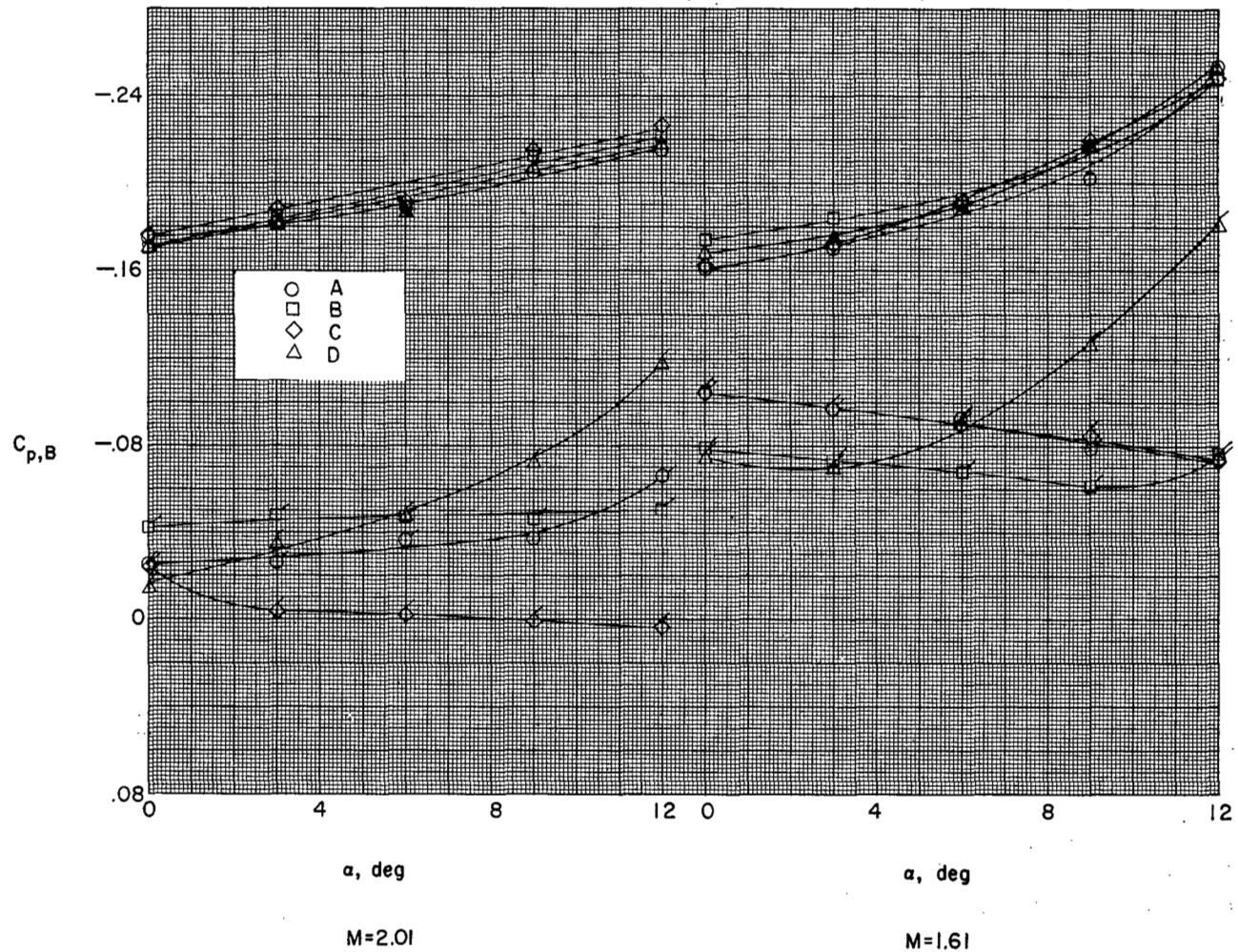
Figure 16.- Concluded.





(a) Variation with jet-pressure ratio.

Figure 17.- Variation of four average base pressure coefficients with jet-pressure ratio and angle of attack.



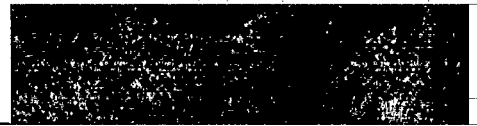
(b) Variation with angle of attack. Plain symbols, jet off; flagged symbols, maximum jet pressure.

Figure 17.- Concluded.

NASA Technical Library



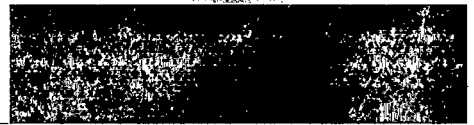
3 1176 01437 2610



**CONFIDENTIAL**



3 1176 01437 2610



**CONFIDENTIAL**